REACTION KINETICS AND MODELLING OF THE HYBRID SULFUR AMMONIA SOLAR THERMOCHEMICAL WATER-SPLITTING CYCLE IN AEROSOL PHASE

A Thesis

by

NAVAIRA FATHIMA

Submitted to the Office of Graduate and Professional Studies of
Texas A&M University
in partial fulfillment of the requirements for the degree of

MASTER OF SCIENCE

Chair of Committee,	Konstantinos Kakosimos
Committee Members,	Ahmed Abdala
	Mohammed Al-Hashimi
Head of Department,	Arul Jayaraman

December 2020

Major Subject: Chemical Engineering

ABSTRACT

The Hybrid Sulfur Ammonia Solar Thermochemical Water splitting cycle (HySA TCWSC) had proven to successfully split water to produce Hydrogen, the renewable source of energy. However, the process was found to be energy intensive in nature and the amount of molten salts produced by the conventional method were difficult to discard. Therefore, the possibility of the reaction being carried out in the aerosol phase rather than in molten state was considered as the aerosol reactor would require minimal amount of reactants to produce products. The behavior of the particles was studied. Therefore, a closer look at the reactions on particle level was considered. A mixture of ammonium sulfate (AS) and potassium sulfate (KS) was used for the reactions. The ratios 1 mol AS:0 mol KS, 1 mol AS:1 mol KS (stoichiometric ratio), 1 mol AS:2 mol KS were tested. The system was modelled using the heat transfer, mass transfer and reaction effects on the particle of AS in presence of KS. In order to model the particle, the reactions were confirmed using mass spectrometer (MS), Fourier Transformation Infrared (FT-IR) gas analyzer and Thermogravimetric Analysis (TGA) results for thermal decomposition of the prepared samples. Four reactions were concluded, and its kinetics were found using iso-conversional method. The first reaction was AS decomposition to ammonium pyrosulfate (APS), water (H_2O) and ammonia (NH_3). The reaction was of order 1.1 with activation energy 77 kJ/mol. The second reaction was APS conversion to NH_3, sulfur trioxide (SO_3) and H_2O in absence of KS. The reaction was of order 0.8 with activation energy of 102 kJ/mol. The third reaction was APS decomposition in presence of KS which converted to

potassium pyrosulfate (KPS). The reaction was of order 1.4 with activation energy 107 kJ/mol. Finally, the decomposition of KPS to KS and SO_3 took place which had order of reaction, 0.8 and activation energy 110 kJ/mol. The sample did not show much variation for small changes introduced. However, the increase in KS ratio delayed SO_3 produced and distinctly differentiated the NH_3 and SO_3 producing regions.

ACKNOWLEDGEMENTS

I would like to thank my committee chair, Dr. Konstantinos Kakosimos for giving me an opportunity to explore the topic. I am thankful to him for his guidance, support and understanding throughout my journey. I would like to extend my gratitude to my committee members, Dr. Ahmed Abdala and Dr. Mohammed Al-Hashimi who have actively been supportive during my journey.

I would like to thank my friends and colleagues at Texas A&M for a great experience in the university while performing my research. I would like to thank the Office of Graduate Studies (OGAPS) at Texas A&M for their active support and guidance.

Finally, I would like to thank my family and friends for being understanding, supportive and patient throughout my journey.

CONTRIBUTORS AND FUNDING SOURCES

This work was supervised by a thesis committee consisting of Dr. Konstantinos Kakosimos (chair), and evaluated by Dr. Ahmed Abdala (committee member) and Dr. Mohammed Al- Hashimi (committee member).

The data retrieved for SEM, PSA and XRD results were conducted in the Centeral Materials Laboratory at Texas A&M Qatar.

All other work conducted for the thesis was completed by the student independently under direct supervision of Dr. Konstantinos Kakosimos.

The research was possible due to the funding provided by the office of research at Texas A&M Qatar.

NOMENCLATURE

HySA	Hybrid Sulfur Ammonia
TCWSC	Thermochemical Water Splitting Cycle
NH_3	Ammonia
H_2O	Water
SO_3	Sulfur trioxide
SOx	Sulfur Oxides
NOx	Nitrogen Oxides
CO_2	Carbon dioxide
O_2	Oxygen
AS	Ammonium Sulfate
KS	Potassium Sulfate
AHS	Ammonium bisulfate
APS	Ammonium Pyrosulfate
KPS	Potassium Pyrosulfate
TGA	Thermogravimetric Analysis
SEM	Scanning Electron Microscopy
PSA	Particle Size Analysis
MS	Mass Spectrometer
XRD	X-Ray Diffraction

TABLE OF CONTENTS

Page

LIST OF FIGURES

Page

Page

Page

LIST OF TABLES

Page

CHAPTER I

INTRODUCTION

I.1 Background

Hydrogen, an alternative to the conventional fuels, has been focused on to reduce global issues. Usage of hydrogen as the energy storage and carrier medium flourished after the energy crisis in 1974 (Mazloomi & Gomes, 2012). The growth of usage of solar energy for most processes has increased over the years. Solar energy consumption growth has increased from small photovoltaic cells (PV) to large PVs and concentrated solar power (CSP) techniques with decreasing cost of operation (Timilsina, Kurdgelashvili, & Narbel, 2012). As a result, processes using solar energy are being studied actively using these techniques. Numerous methods of solar thermochemical water splitting cycle (TCWSCs) are explored to produce hydrogen. The abundance of renewable energy source, solar energy, is utilized efficiently in this process. The Hybrid Sulfur-Ammonia (HySA) TCWSC was proven to be one of the most efficient thermochemical water splitting cycles, due to the consumption of both, thermal and photochemical energy of the irradiant sunlight. The two techniques were used separately to split water non-biologically, however, the application of both in one cycle maximizes utilization of the resource (T-Raissi, Muradov, Huang, & Adebiyi, 2007). The HySA cycle consisted of molten salts which controlled the product formation and acted as a source for storing energy, and hence proved to be advantageous over the other TCWSCs. The ability to store energy, maximizes the capability of continuing the process in absence of the primary source. Different

reactors were explored to determine the best reactor for the solar thermochemical processes. Reactor design was tested for oxidizing different materials in a single cavity solar reactor (Felix Trombe, 1971). Another type of reactor, consisting of a rotating solar receiver was designed for ZnO dissociation (Steinfeld, 1999). Later, vortex cavity and double cavity reactors were tested to improve performance. The research based on different reactor setups continues to ensure efficient operation of the processes using solar energy.

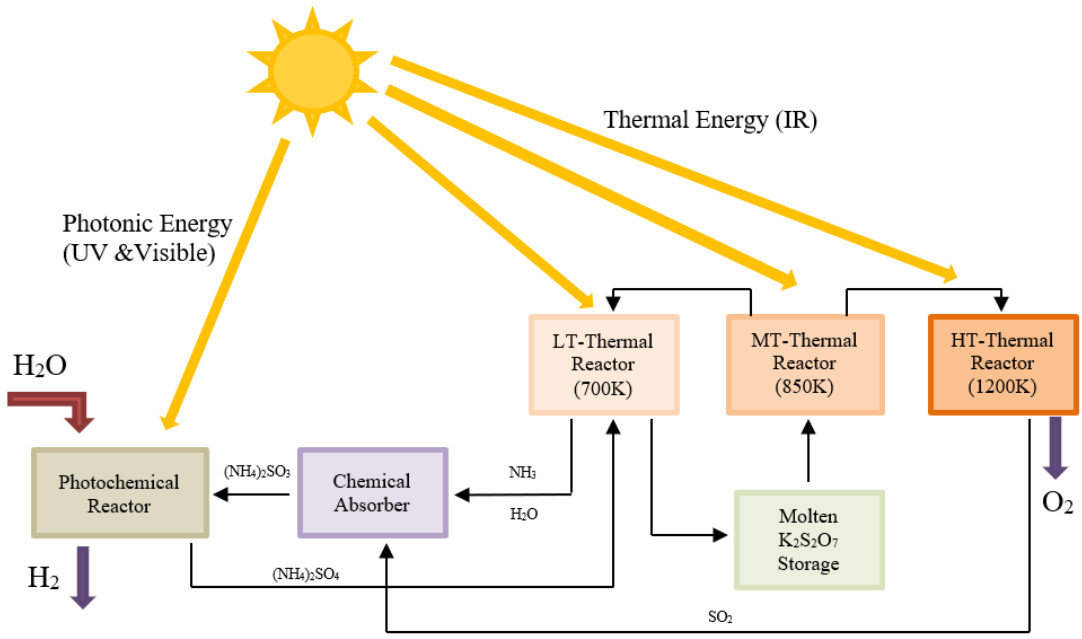

Figure 1: Hybrid Sulfur Ammonia Solar Thermochemical Water-splitting Cycle (Adapted from Kalyva, 2017)

The Hybrid Sulfur-Ammonia thermochemical water splitting cycle (HySA TCWSC) consisted of two sub cycles, Hydrogen production sub cycle and Oxygen production sub cycle (Figure 1). The O_2 production sub cycle consumed 80.9% of the irradiant energy while the rest (19.1%) is consumed by H_2 production sub cycle.

The reaction followed consisted of the steps (Kalyva, 2017):

$$SO_2 + 2NH_3 + H_2O \rightarrow (NH_4)_2SO_3 \quad (1)$$

$$(NH_4)_2SO_3 + H_2O \rightarrow (NH_4)_2SO_4 + H_2 \quad (2)$$

$$(NH_4)_2SO_4 + K_2SO_4 \rightarrow 2NH_3 + K_2S_2O_7 + H_2O \quad (3)$$

$$K_2S_2O_7 \rightarrow SO_3 + K_2SO_4 \quad (4)$$

$$SO_3 \rightarrow SO_2 + \frac{1}{2} O_2 \quad (5)$$

The first two reactions involve H_2 production. Step 3 onwards, O_2 sub-cycle was performed.

I.2 Motivation

The reactors studied posed particle deposition or sealing problems. Therefore, it was concluded that the aerosol reactor, consisting of an aerosol medium of reactants, minimized the problems faced by the other reactor types (Kalyva *et al.*, 2017). Moreover, the molten pyrosulfate salt state in HySA required large amount of solvent, which employed large process streams and higher heating requirements. The aerosol reactor minimized the energy requirements of this energy intensive process by decreasing the reactants used. However, the feasibility and performance of the process were to be determined. Therefore, combining the issues in place for splitting water using HySA solar thermo chemical water-splitting cycle, the objectives of the study were set.

I.3 Objectives

The study focused on a solution required to combat the problem created by large amount of hot solvents used in the second HySA sub-cycle. The major responses that tested the efficiency of the process were ammonia (NH_3) recovery and sulfur oxides (SOx)

recovery to ensure efficient self-driven nature of the cycle. The main goal of the study was to implement the cycle in aerosol phase. In order to do so, understanding of the particles, reactions and behavior of the particles was required. Hence, a few objectives were set in place. The main objectives of the study were:

1. *Characterization of the particle*

   The characterization of the particle was required to summarize and implement the behavior of the particle to the aerosol phase effectively. There were four steps of accurately characterizing and summarizing the behavior of the particles:

   i. Sample analysis

   Analyzing the sample structure, size and components ensured that the sample being used was accurately determined to implement the properties and compare the outcomes of initial reactants with the products. Moreover, different factors varied in the study determined the effect of each factor on the overall process.

   ii. Mechanism determination

   The mechanism for the reaction acted as the basis for the kinetic study. The process of the reactions explained in detail determined the stages and reaction steps that required determination of kinetic parameters.

   iii. Kinetics determination

   Determining the kinetics showed the rate at which the particle reacted. Moreover, it determined the activation energy required for the reaction to take place. The parameters obtained generalized the reaction even after scaling the process.

iv. Particle modelling

The heat and mass transfer effects combined with the kinetics described the whole process of reaction on a single particle. Assumptions and conditions necessary for the reaction were obtained by modelling the particle. Hence, providing parameters and means of comparisons for the experiments.

The desired outcome of this stage was a particle model defining the kinetics, mass transfer and heat transfer effects on the particle suspended in the aerosol. The outcome acts as a basis for further research carried out on this topic.

2. *Response of the reaction in aerosol phase*

The response of the particles in the given environment was essential to ensure that the reaction that was expected, took place and the parameters that were essential for the determination of efficiency of the reaction were detected by the equipment used. That is, the hypothesized assumption of the reaction behaving better in the aerosol phase instead of the molten salts phase can be tested after verifying that the reaction carried out in the aerosol phase produces products like the molten phase. Therefore, the objective of this study was to design the process of testing, calibrate (if necessary) and test the equipment required to study the responses of the reaction carried out in aerosol phase. NH_3 and SOx production and detection were the aimed outcomes of this stage.

CHAPTER II

LITERATURE REVIEW

II.1 Aerosol reactor

II.1.1 Particle preparation

The use of aerosol phase for production of desirable products has been scanty in the industry. However, the aerosol medium being a precursor for formation of essential components had drawn the focus of researchers to the aerosol reactor. The aerosol preparation method varies according to the process. The most used method consisted of dissolution of particles in a solution and recrystallization to form homogeneous compounds which were later crushed to the desired sizes. The samples were sieved according to the outcomes to work with the size range desired. Kanapilly *et al.* (Kanapilly, 1977b) showed the process of aerosol creation where the sample was first nebulized, and then dried to form ammonium sulfate particles. The sample was thermally decomposed, and the products were condensed to form aerosol particles of ammonium bisulfate. Hence, the products which required treatment were formed by condensation and the pure compounds were converted to aerosol by nebulizing and drying. After powder formation numerous authors have designed methods for aerosolization of the particles. Ding *et al.* (Ding & Riediker, 2016), proposed a novel idea to test the aerosolization of the particles in lab scale. The aerosolization of the particles was processed like fluidization of fluidized beds. Finally, the techniques of sample preparation and aerosolization were combined to produce suspended aerosol particles of desired sizes.

II.1.2 Reactor designs

An aerosol reactor was described as a reactor consisting of the components suspended in the aerosol phase using techniques suitable for the end results desired. According to Funke (Funke *et al*., 2008), Dow Chemical Company employed these types of reactors with small particles suspended in the gas phase of the reactor, producing tungsten carbide (Figure 2). Further researches were carried out in laboratories for production of ceramics and hydrogen (via methane decomposition).

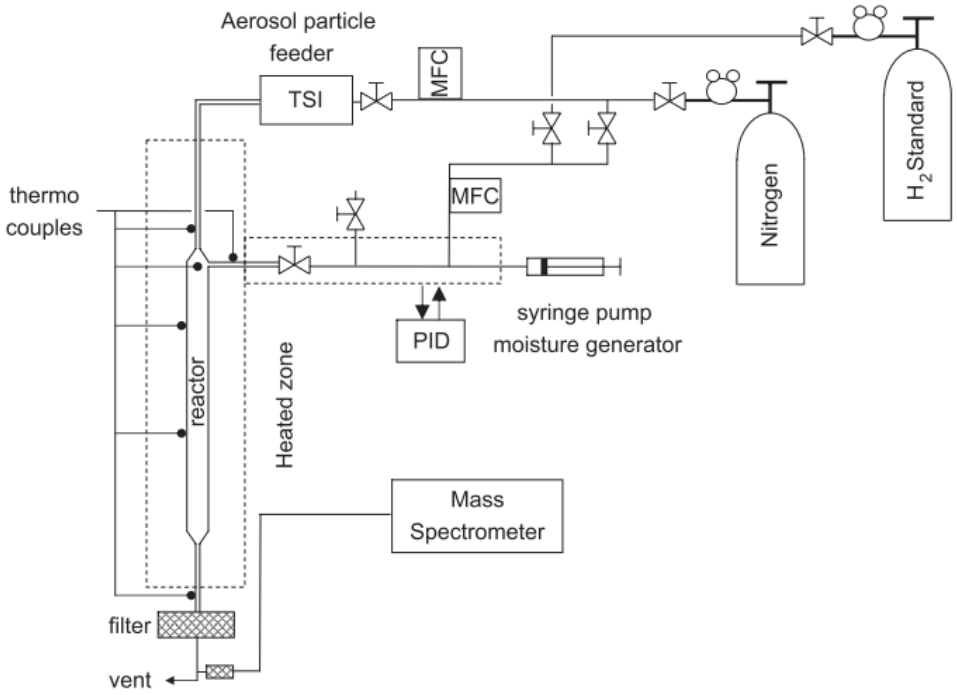

Figure 2: Aerosol Flow Reactor (Adapted from Funke, 2008)

Dahl *et al.* (Dahl *et al.*, 2004), proposed a solar reactor with vertical aerosol flow for methane decomposition. The reactor composed of a double tube with the outer tube containing a protective quartz medium and inner tube being the reactive graphite medium. The tubes were isolated using an inert gas (Argon). The presence of inert gas prevented

the decomposition of products on inner quartz wall which could damage the quartz medium. The secondary concentrator was used to concentrate sunlight on to the graphite via the quartz wall. Feed methane gas was introduced from the top of the reactor and the decomposed carbon particles were suspended in the aerosol phase, which could later be separated from hydrogen and collected. Similarly, Welte *et al.* (Welte, Barhoumi, Zbinden, Scheffe, & Steinfeld, 2016) explored the use of an aerosol reactor setup for thermochemical reduction of Ceria (Figure 3).

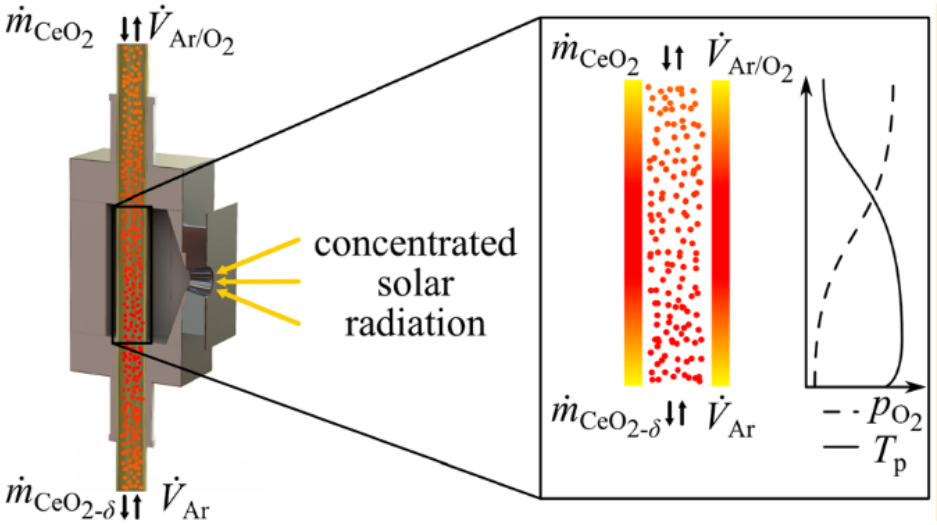

Figure 3: Vertical Flow Reactor with Temperature and Presuure variation Profile (Adapted from Welte, 2016)

Prior to the aerosol setup, the fluidized bed reactor, rotary type reactor and porous ceria lined cavity receivers were explored. However, due to the drawbacks presented by each setup, the concept of cavity receiver was further modified to introduce the aerosol reactor. A stream of inert gas was introduced into the reactor from the bottom and the small ceria particles were introduced from the top of the reactor. The particles were held in aerosol phase for the reaction to occur. The counter-current flow aided the separation

of gases from the Ceria particles, preventing recombination. High mass and heat transfer rates, and scalability were the other advantages of the aerosol reactor setup. In another research, Perkins *et al.* (Perkins, Lichty, & Weimer, 2007) explored the application of an aerosol reactor for thermal ZnO dissociation. The reactor consisted of particles suspended in a gaseous medium acting as a carrier transporting the particles to the reactive site. The small particles increased heat and mass transfer rates which were essential for converting the system to chemically controlled system. The studies conducted proved to be beneficial on switching the reaction medium from conventional to aerosol phase mediums. However, concerns regarding high temperatures in aerosol phase and the material of the reactor in use have been raised in these studies. Nevertheless, Scheffe *et al.* (Scheffe, Welte, & Steinfeld, 2014) concluded that the aerosol medium has proven to be advantageous for many organizations, leading to growth of research in this direction.

As an extension of the previously explored idea of application of aerosol reactors to HySA cycle, the efficiency of aerosol reactors as compared to conventional methods for HySA O_2 sub-cycle was to be explored in this study. However, to understand the behavior of the particles in aerosol phase, the reaction mechanism, thermodynamics, and reaction kinetics of this reaction were to be determined. Kalyva *et al.* (Kalyva *et al.*, 2017) performed Thermogravimetric Analysis (TGA) and Differential Scanning (DSC) experiments on aerosol particles to verify the thermodynamic calculations done by FactSage©. The results revealed variation in reaction temperature ranges as compared to the temperatures shown by the software. It was concluded that the variation in temperature ranges resulted from the different reaction paths and intermediate products that could be

present in achieving the final product. Therefore, the reaction kinetics were to be studied before introducing the reactants to the aerosol reactor.

II.2 Kinetics determination

The kinetics study is essential as it generalizes the behavior of the reactions regardless of the quantities present. However, the reaction steps were essential to determine the kinetic parameters. The previous studies showed conflicts in studies used and intermediate products formed. In order to accurately determine the kinetics, the previous conclusions were summarized according to the conditions present.

Numerous studies have been conducted in literature, to study the reaction mechanisms and reaction kinetics of reactions in aerosol medium using TGA initially. According to Brown (Brown, 2004), the kinetic analysis for solid decomposition usually starts within the faults and grows out forming another solid product and some gases. The kinetic determination using TGA involved either isothermal or non-isothermal methods. Brown (Brown, 1998) stated that the application of isothermal and non-isothermal methods for determining the reaction depended on the reaction. However, it was commonly seen that non-isothermal method of determining kinetics have been more reliable for reactions involving decomposition. Non-isothermal tests covered a wider range of temperatures as compared to isothermal tests. The discrepancies in determining the kinetic parameters from non – isothermal experiments were reduced by operating at slow heating rates. The kinetic study was either a function of time or temperature depending on the reaction under consideration. The methods to calculate the kinetic parameters were divided into two sets. The first being model based methods and second

being model free methods (iso-conversional). The model defined the process taking place and summarizing the overall conclusion of the process. One dimensional non-isothermal model was developed by Sanchez *et al.* (Sánchez, Méndez, & Bautista, 2014) for the decomposition of methane. Perkins *et al.* (Perkins *et al.*, 2007) explored the isothermal and non-isothermal reaction kinetic parameters for ZnO decomposition while Funke *et al.* (Funke *et al.*, 2008) explored the non-isothermal iso-conversional (varying heating rates to determine model free parameters) kinetic parameters for hydrolysis of Zn. These models were summarized by different authors to generalize the models. Fedunik (Fedunik-Hofman, Bayon, & Donne, 2019) summarized the models and tested them for carbon looping systems. The non-isothermal methods were focused on in this study. Kinetic parameter determination in each method depended on the fractional conversion given as α. The models presented were either in their differential form ($f(\alpha)$) or integral form ($g(\alpha)$). Khawam (Ammar Khawam, 2006) and Jiang *et al.* (Jiang *et al.*, 2020) defined the total reaction rate depending on a function of the differential form of the model containing fractional conversion. The two forms were converted from one to another depending on the application. These methods were further incorporated by other authors to determine the kinetic parameters of reactions consisting of decomposition of ammonium sulfate.

The decomposition of ammonium sulfate (AS) was studied, and the kinetic parameters were determined by using isothermal methods. The experiments were carried out in a TGA for determining the reactions and kinetic parameters (Urano, 1970). Further researches explored the kinetics of ammonium bisulfate (AHS) reaction with potassium sulfate (KS) using isothermal experiments. AHS converted to ammonium pyrosulfate

(APS) before reaction with KS to form NH_3, water (H_2O) and SOx (Wentworth, 1992). Recent studies shifted their focus from isothermal to non-isothermal iso-conversional methods as the conditions present are suitable for thermochemical decomposition reactions. Therefore, Song *et al.* (Song, Zhao, Li, Sun, & Yu, 2013) used Kissinger's method incorporating an approximation for accurate results to determine the kinetics of AS decomposition with ferric oxide. The results presented contained a complete picture of the pre-exponential factor, activation energy and the model followed by each stage in the experiment. The iso-conversional method was initially used to calculate the activation energy. The model most appropriate to the system was used alongside the activation energy to determine the pre-exponential factor. The kinetic parameters determined were employed in the reaction rate to generalize the model of the reaction. The HySA cycle best fits the scenario of non-isothermal iso-conversional method for determining the kinetic parameters. Hence, TGA was used to determine the kinetic parameters by non-isothermal iso-conversional method.

II.3 Particle modelling

The particles participating in the reaction were small spherical particles. The behavior of the particle depended on the heat transfer, mass transfer, kinetics and phase change. Studies have been presented to develop models based on the size of the particles, shape of the particles, surrounding medium of the particle and phase change in the particle. Angelopoulos *et al.* modelled the dehydration of red mud using a cylindrical symmetry for the particles (Angelopoulos, Balomenos, & Taxiarchou, 2016) while 1-D model considering the cross-sectional area of the TGA instead of a single particle was studied by

Samdani (G. Samdani, 2012) for gasification of char. However, the generalization ignored the behavior at particle level which would be required for aerosol consideration. Most other researches focused on spherical structure of the particle as the grains present in the system incorporated a spherical shape. Coulson and Richardson *et al.* (Sinnott, 2017) proposed two models for non-catalytic solid-gas reactions, shrinking core model (SCM) and progressive conversion reaction model. The SCM proposed that the reaction first takes place at the surface of the particle, progressively moving towards the core. As the reaction takes place, either the size of the particle remains constant with one solid particle being converted to another or the particle shrinks in size due to disintegration of the particle during the reaction. The progressive conversion model assumed that the reaction takes place in the whole particle at the same time. Levenspiel (Levenspiel, 1999) further explained the two models and presented the estimated time required for the particle to disappear under SCM.

Hofman *et al.* (Fedunik-Hofman et al., 2019) briefly summarized the different models present, SCM, pore model, nucleation model and apparent model. The SCM assumed a non-porous particle while the pore model considered a porous particle. The nucleation model focused on the accumulation and growth of the particle and the apparent model provided apparent kinetics for the models.

Researches conducted have incorporated diffusion. Babinski (Babinski, Sciazko, & Ksepko, 2017) considered a fluidized bed with internal and molecular diffusion. The equations given for molecular diffusion and internal diffusion have been adapted from Bird *et al.* (Bird, Stewart, & Lightfoot, 2007). Saxena (Saxena, 1976) stated that model of

a particle predicts the behavior of the whole bed. The effects of diffusion were summarized in a study by Anabel *et al.* (Anabel, Celia, Germán, & Rosa, 2018) using the Jander's equation. The equation was modified to calculate the effective diffusivity.

Amiri *et al.* (Amiri, Bekker, Ingram, Livk, & Maynard, 2013) presented a 1-D model for dehydration of a spherical gibbsite particle. The effects of heat transfer and reaction kinetics on the concentration of the particle were studied. The distributed model which is an extension of the SCM was applied (Figure 4). The state functions vary with the radius of the particle according to the distributed model. Furthermore, the effects of particle size, diffusion and external factors affecting the environment were studied. The model was created as a continuation of the work presented by Amiri (Amiri, Ingram, Bekker, Livk, & Maynard, 2013) and (Amiri, Ingram, Maynard, Livk, & Bekker, 2014) which considered the solid-liquid-gas transformation of the particle using SCM previously.

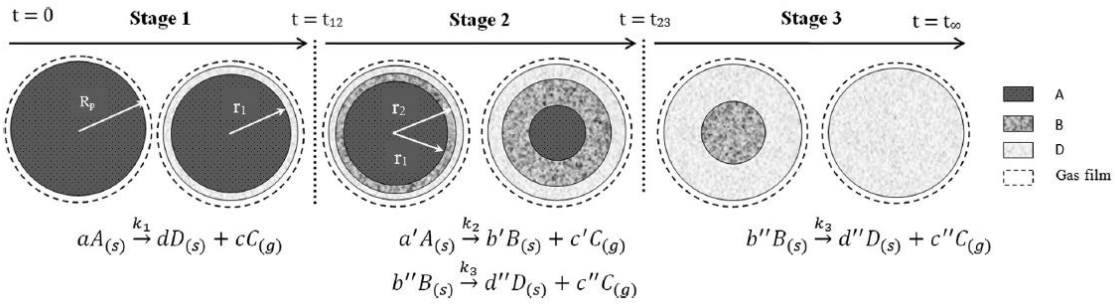

Figure 4: Reaction Modelling of Alumina Particle (Adapted from Amiri, 2013)

The first paper concentrated on the particle exposed to isothermal conditions while the latter studied performance of the particle under non-isothermal conditions. Similarly, Marin (Marin, Wang, Naterer, & Gabriel, 2012b) considered a particle immersed in liquid

for modelling. Later, Marin (Marin, Wang, Naterer, & Gabriel, 2012a) studied the behavior of a particle with a film of liquid instead of immersion of solid particle in the liquid. A moving boundary model describing the behavior of the particle was formulated. Later, a non-isothermal model incorporating radiative force was suggested by Nakhaei *et al.* (Nakhaei *et al.*, 2018) for the decomposition of a plastic particle.

All the researches carried out started with the basic model of defining the reaction rates first. Later, the heat transfer equation was determined using basic equation of heat transfer defined by Bird *et al.* (Bird *et al.*, 2007). The mass transfer equation was defined using the equation of continuity mentioned by the same author and other similar transport phenomenon books. All these equations were combined with the assumptions and modified to develop the model for the particle.

CHAPTER III

THEORY AND METHODOLOGY

III.1 Sample setup

III.1.1 Sample preparation

The HySA thermochemical water splitting cycle comprised of AS decomposition in the presence of KS on being exposed to solar radiation. Theoretically, 1 mol of AS and 1 mol of KS were needed for the complete reaction. However, the absence of KS and excess KS presence was tested to determine the effect of KS on the experiment. Therefore, samples of three ratios, 1AS:0KS (deficient of KS), 1AS:1KS and 1AS:2KS (excess KS) were prepared for the experiments.

During the preparation of the samples different factors were tested to determine the impact of the factors on sample making procedure. The resultant samples were tested using different methods.

The factors tested while preparing the sample were:

i. Effect of stirring the sample while drying using scanning electron microscopy (SEM) for testing homogeneity.
ii. Effect of heating the sample while drying using SEM for homogeneity test.
iii. Effect of crushing samples directly without dissolving in water.

The sample formed was tested using X-Ray Diffraction (XRD) and SEM to determine the solid formed and homogeneity of the sample.

The three ratios were prepared by dissolving the desired amounts in distilled water and drying the sample in air over a few days to ensure homogeneity of the ions present. The dried samples were crushed to different sizes using mortar and pestle. The resultant sample was tested for Particle Size Analysis (PSA) and SEM to determine the distribution of particles and the size range of particles formed. Based on the PSA, the particles were sieved to ensure the range of size of particles used in the experiments are known.

Figure 5 shows the standard procedure followed for sample preparation.

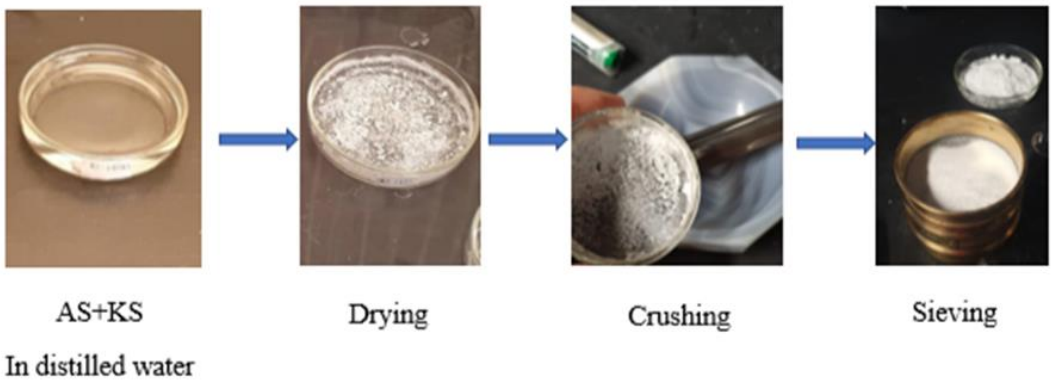

Figure 5: Sample Preparation

The sample collected after sieving was stored in vials using proper labels to be used in further experiments as shown in Figure 6.

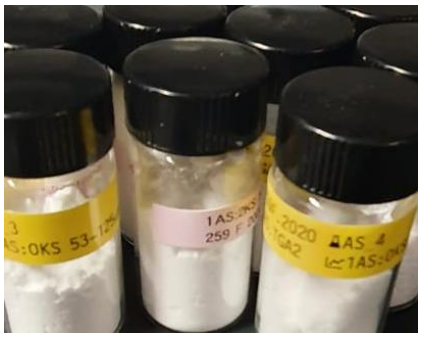

Figure 6: Samples Formed and Bottled

The list of samples prepared were as given in Table 1 and Table 2. Ammonium sulfate (AS), Potassium Sulfate (KS), Ammonium bisulfate (AHS) and Potassium pyrosulfate (KPS) were the basis of the samples.

Table 1: List of Samples Prepared

Sample ID	Description	Purpose
AS_01	1AS:0KS sample prepared by dissolving in water, recrystallizing, crushing and sieving to size 53-125 µm.	To conduct kinetic analysis and solar reactor experiments.
AS_02	1AS:0KS sample prepared by crushing the sample without dissolving in liquid and sieving to < 53 µm.	For comparison with dissolved and crushed sample and comparison of results based on different sizes.
AS_03	1AS:0KS sample prepared by crushing the sample without dissolving in liquid and sieving to 53-125 µm.	For comparison with dissolved and crushed sample and comparison of results based on different sizes.
AS_04	1AS:0KS sample prepared by crushing the sample without dissolving in liquid and sieving to > 125 µm.	For comparison with dissolved and crushed sample and comparison of results based on different sizes.
KS_01	0AS:1KS sample prepared by dissolving in water, recrystallization, and crushing.	For testing the initial reactant.

Table 2: Table 1 Continued

Sample ID	Description	Purpose
KPS_00	0AS:1KPS sample prepared by dissolving in water, recrystallization, and crushing.	For testing the decomposition of intermediate.
AHS_01	1AHS:0KS sample prepared by dissolving in water, recrystallization, and crushing.	For testing the decomposition of intermediate.
ASKS_01	1AS:1KS sample prepared by dissolving in water, recrystallizing, crushing and sieving to size 53-125 µm.	To conduct kinetic analysis and solar reactor experiments.
ASKS_02	1AS:2KS sample prepared by dissolving in water, recrystallizing, crushing and sieving to size 53-125 µm.	To conduct kinetic analysis and solar reactor experiments.
ASKS_03	1AS:1KS sample prepared by crushing the sample without dissolving in liquid and sieving to <125 µm.	For comparison with dissolved and crushed sample.
CSH	$CuSO_4.5H_2O$ powder provided by SETARAM.	For calibrating MS and FT-IR for Sulfur Oxides.
AC_01	Pure $(NH_4)_2CO_3$.	For calibrating MS and FT-IR for Ammonia.

III.1.2 Introduction of sample in the reactor as an aerosol

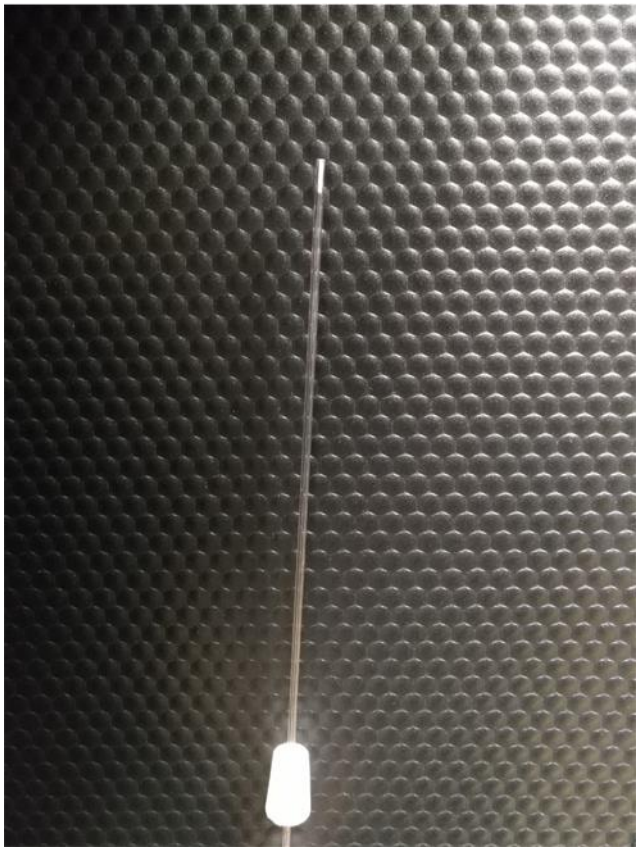

Figure 7: Sample Placed in a Capillary

The sample prepared was used in determining the kinetics as well as for the solar experiments. To expose the sample to the radiant flux, a capillary of 0.5mm inner diameter was used. The capillary was used to replicate the form present in an aerosol phase where the particles are exposed to light particle by particle. The sample held in place using the capillary as shown in Figure 7 behaved as a particle by particle system where the particles were homogeneously distributed and the effects of non-homogenous flow of particles was neglected. The particles at the back end of the capillary behaved as the particles shadowed

by other particles in the aerosol phase. Therefore, the aerosol phase was replicated using a controlled capillary environment.

The sample in the capillary was seen as a compressed version of the particles that would be present in the actual aerosol reactor. The particles on the circumference of the capillary acted as the particles directly exposed to radiation in the real setup, while the particles in the center of the capillary acted as the particles in the aerosol reactor shadowed by the particle in front. Moreover, the gradual increase in temperature replicated the process a particle in aerosol reactor will be exposed to. However, in this scenario, the other effects of an unstable system were eliminated. The change in mass and evolution of gases was used to monitor the reaction taking place. Therefore, the ideal scenario that acted as a basis of design for actual aerosol reactor was formed.

III.2 Kinetics determination using thermal analysis

III.2.1 Thermogravimetric analysis (TGA)

Figure 8: Thermogravimetric Analyzer

The TGA (Figure 8), SETSYS by SETARAM© was connected and controlled using the Calisto Software. The system was switched on and connected to the software for type B thermocouple. The PIDU values were specified based on the standard values for type S thermocouple as the sampling thermocouple was of type S. The system was calibrated using metals and blanks. The metals were introduced into 100 µL alumina crucible. Each metal has a set melting temperature. The system was set to ramp up the temperature till melting point of the metal was reached at heating rate of 5 °C/min. Argon was used as the carrier and protective gas in the system. The flow of Argon was taken as 36 mL/min which was split into two inlets, one from the top of the furnace and other from the bottom of the furnace (15+21 mL/min). The weight of the sample was tared before

ramping up of the system to obtain the mass loss by the end of the experiment. After reaching the melting temperature, the system was set to an isotherm of 10 mins before cooling it down to room temperature at 30 °C/min. These calibration standards were used for temperature correction that was applied in the experiments. In addition to the metal calibrations for temperature corrections, references were run for each experiment conditions using a blank crucible.

After the metal calibration, a list of experiments was designed to test the outputs using TGA. A blank was run for each experimental condition and was subtracted from the results of the actual experiments. Each experiment was run until 800 ºC at different heating rates and an isotherm of 10 minutes was set after reaching 800 ºC. The list of TGA Experiments and its purpose is given in Table 3, Table 4 and Table 5.

Table 3: TGA Experiments

ID	Sample	Mass (mg)	Heating Rate	Purpose
AS Experiments				
TGA2_09	AS_01	14	5	Kinetics
TGA2_10	AS_01	14	4	Kinetics
TGA2_11	AS_01	14.2	2	Kinetics
TGA2_12	AS_01	14.5	8	Kinetics
TGA2_13	AS_01	16.7	6	Kinetics

Table 4: Table 3 Continued - 1

ID	Sample	Mass (mg)	Heating Rate	Purpose
AS Experiments				
TGA2_22	AS_01	17.2	2	Comparison with TGA2_11 for effects of change in mass of sample.
TGA2_28	AS_01	19.1	8	Comparison with TGA2_12 for effects of change in mass of sample.
TGA2_42	AS_03	15.5	5	Comparison with TGA2_09 for change in preparation method
TGA2_43	AS_02	12.3	5	Comparison with TGA2_42 for effect of different size of particles
AS-KS Experiments				
TGA2_14	ASKS_01	14.5	2	Kinetics
TGA2_15	ASKS_01	16.6	8	Kinetics
TGA2_16	ASKS_01	15.3	4	Kinetics
TGA2_17	ASKS_01	14.1	5	Kinetics
TGA2_29	ASKS_01	14.6	6	Kinetics
TGA2_31	ASKS_01	16.5	3	Kinetics
TGA2_32	ASKS_01	14.7	2.5	Kinetics
TGA2_33	ASKS_01	14.8	1.5	Kinetics
TGA2_37	ASKS_03	13.4	5	Comparing with TGA2_17

Table 5: Table 3 Continued - 2

ID	Sample	Mass (mg)	Heating Rate	Purpose
AS-2KS Experiments				
TGA2_30	ASKS_02	15.3	4	Comparison with AS-KS experiments (TGA2_17) for effect of ratio change.
TGA2_38	ASKS_02	14.8	5	Comparison with AS-KS experiments (TGA2_16) for confirming effect of ratio change.
Other Tests				
TGA2_18	KPS_00	24.5	2	Determining the decomposition of intermediate product formed.
TGA2_40	KS_01	14.4	5	Determining decomposition of KS by itself.

The other TGA experiments that were carried out consisted of CSH and AC for calibration of the equipment for SOx, H_2O and NH_3.

III.2.2 Mass Spectrometer analysis (MS)

Figure 9: MS Setup

The MS as shown in Figure 9 was connected to the PC through MASsoft software. The gases expected alongside the molecular weights were specified in the system. The system collected the data of the gases reaching the equipment according to their molecular weights and reported them as partial pressures in the system. However, these molecular weights might not be representative of the actual components and hence, correction for partial pressures of each component using the relative sensitivities and signal strength of each component at that molecular weight was essential. The actual partial pressures were converted to concentrations in terms of ppm to compare results of the MS with the FT-IR for kinetics-based experiments and gas analyzer in the solar experiments (explained later).

III.2.3 Fourier Transformation Infrared gas analysis (FT-IR)

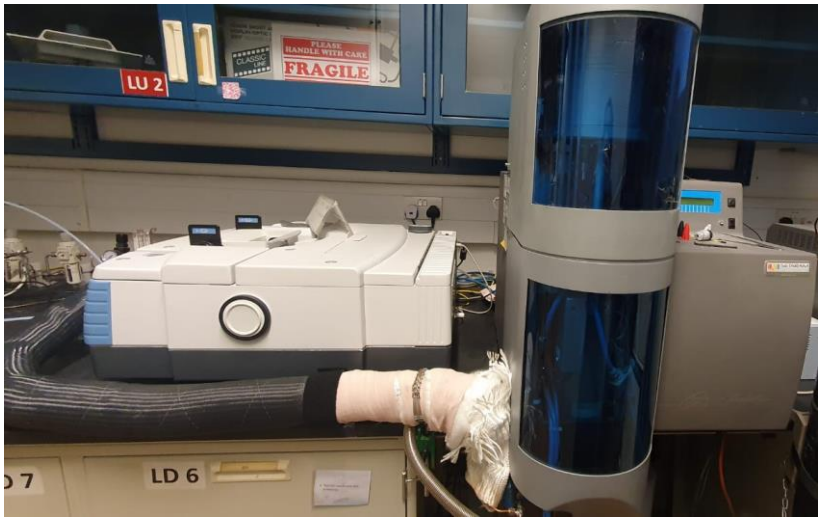

Figure 10: FT-IR Setup Connected to TGA

The FT-IR (Figure 10) by Nicolet© is a unit that consists of different attachments for sampling. The gases were sampled using the gas analyzer which was connected to the TGA via a pressure valve and heated gas line. The gases from the TGA flowed to the bottom and through the heated line to the gas chamber. The gas analyzer was switched on and set to 200 °C to bake (removal of moisture) for 5 hours. The temperature was decreased to 80 °C after 5 hours to ensure that the gas travelling to the gas chamber does not condense in the pathway. Moreover, the gas line was insulated to avoid heat losses.

OMINIC was used to control the system through the PC. Infrared passes through the gas reading the signal for each type of gas present. The results were presented by the series collection which runs through the course of the TGA experiment. The gases estimated from the reactions were mainly NH_3, H_2O and SOx. Therefore, ammonium carbonate and copper sulfate, completely dissociating chemicals producing the required gases were used for calibration of the gas analyzer.

III.2.4 Kinetic parameters

The first step to determining the kinetics was to confirm the reaction mechanism in place. In order to determine the reactions, the set of AS and KS experiments in place were tested for the responses. The experiment was run in the TGA connected to FT-IR and MS. The FT-IR and MS took in the gas stream from the experiment and analyzed the data. According to the literature, the possible gaseous and solid products were predicted. The predicted gases were fed for detection in the MS. After the reaction the experiment was split into different steps based on the change in slope of the graph as shown in the example of Figure 11.

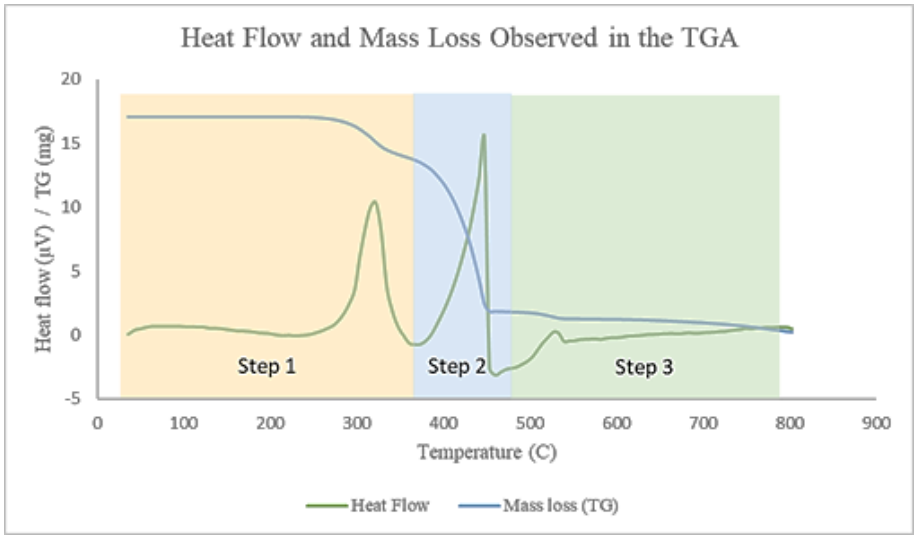

Figure 11: Example of Steps Determination for an Experiment.

The reactions were determined for each step. Based on the results obtained from the MS, the qualitative analysis of the gases was done to determine the gases present in the system at different points in the experiment. According to the results, the reactions consisting of gases that were not detected were eliminated. Depending on the reactions

after elimination of the reactions that were not possible, the TGA mass balance was carried out. The estimated amount of solid that should be left in the system due to the assumed reaction was calculated and compared with the mass left in the system after the stage. The goal seek feature on Microsoft Excel© was used to solve for the conversion of solid left and calculated theoretically to be equal. Based on the conversion, the amount of theoretical gases that should have been released with the given ratios were calculated and compared with the total mass of gases that were released. The confirmation between the theoretical and experimental values showed the dependency of the reactions assumed. The reactions in place were concluded and the FT-IR data was analyzed to verify the ratio of gases estimated to be released. The FT-IR calibration factor was used to convert the area under the curves to mass of each gas released during each stage. The summarized reactions were used in the kinetics determination study.

The kinetic parameters pertaining to the reactions were obtained by non-isothermal iso-conventional method. Since the system operated under non-isothermal conditions the kinetics are determined accordingly. The rate of reaction was written based on equation 6. The function and kinetic parameters were determined by the methods mentioned next.

$$r = \frac{d\alpha}{dt} = k\, f(\alpha) = Ae^{-\frac{E_a}{RT}} f(\alpha) \quad (6)$$

Where,

$$\alpha = \frac{m_i - m_o}{m_f - m_o} \quad (7)$$

$$f(\alpha) = (1-\alpha)^n \text{ for reaction order n} \quad (8)$$

The function f(α) changes depending on the mechanism followed by each stage. The list of common mechanisms and their functions were mentioned in Appendix.

$$k = A\ e^{\frac{-E_a}{R\,T_0}} \quad (9)$$

m_i = instantaneous mass in mg, m_o = initial mass in mg, m_f = final mass in mg

β = heating rate in °C/min, E_a = activation energy in J/mol, A = pre-exponential factor, R = gas constant (8.314 J/mol K), T = temperature in K, n = order of the reaction.

The two ways to determine the kinetics, model-based and iso-conversional methods were tested. Each model was tested in the model-based case to give the best fit possible. The model with the best fit was used to calculate the kinetic parameters.

The general equation linking the rate of conversion to the model was rearranged in the form of equation 10 and the left side of the equation was plotted with respect to 1/T to give a linear plot from which kinetic parameters were determined. This method was backed up by Perkins (Perkins *et al.*, 2007).

$$\ln\left[\frac{\left(\frac{d\alpha}{dT}\right)\beta}{f(\alpha)}\right] = \ln A - \frac{E_a}{R}\left(\frac{1}{T} - \frac{1}{T_0}\right) \quad (10)$$

The equation was rearranged (equation 11) in the integral form and plotted to give the best fit for different models. This model was backed up by Hofman *et. al* (Fedunik-Hofman *et al.*, 2019).

$$\ln\left[\frac{g(\alpha)}{T^2}\right] = -\left(\frac{E_a}{R}\right)\left(\frac{1}{T}\right) + \ln\left[\frac{AR}{E_a\beta}\right]\left(1 - \frac{2RT_{av}}{E_a}\right) \quad (11)$$

Therefore, the integral as well as differential form of the function were used separately to determine the kinetics.

The second method involving model free approaches was known to be more robust as the model does not have to be known to determine the activation energy. However, later, the model had to be defined to determine the pre-exponential factor. The same

equation 6 was rearranged and modified for the function to be a constant when the conversion varied. The equation was written using the integral (equation 12) and differential form (equation 13) of the model.

$$\ln\left(\beta \frac{d\alpha}{dT}\right) = \ln[f(\alpha)A] - \frac{E_a}{R\,T} \quad (12)$$

However, an approximation using Kissinger's method modified the equation and accounted for the discrepancies. The approximation was given by equation 14 which was confirmed by Song (Song *et al.,* 2013) and Hofman (Fedunik-Hofman *et al.,* 2019). The approximation was usually used as the authors have specified high accuracy of results with the mentioned Q(u) approximation.

$$\ln\left[\frac{\beta}{Q(u)T^2}\right] = \ln\left[\frac{A\,R}{E_a\,G(\alpha)}\right] - \frac{E_a}{RT} \quad (13)$$

$$Q(u) = \frac{u^4+18u^3+88u^2+96u}{u^4+20u^3+120u^2+240u+120} \quad (14)$$

Where,

$$u = \frac{E_a}{RT} \quad (15)$$

The experiments performed for AS and AS-KS ratios at different heating rates was used in determining the kinetics. The E_a value was deduced by taking the temperature for 80% conversion at different heating rates in the first stage. Equation 13 was plotted to determine the value from the slope of the graph. Later, equation 13 was modified to determine the value of A from the intercept as shown in equation 16.

$$\ln[G(\alpha)] = -\ln\beta + \ln[Q(u)T^2] + \ln\frac{AR}{E_a} - \frac{E_a}{RT} \quad (16)$$

The conversion for different heating rates at a set temperature was tabulated and a graph was plotted for each model. The integral of the model was plotted corresponding to

lnβ. The graph with slope close to -1 and R^2 close to 1 was selected as the model and justified for that step in the experiment.

The diffusion parameter (D_e) was calculated by equation 17 which was backed by Segal (Segal, 2011).

$$(1-(1-\alpha)^{\frac{1}{3}})^2 = \frac{2\,k_0 D_e}{r^2}\,t \qquad (17)$$

III.3 Modelling of particle

III.3.1 Mathematical equations

A particle was modelled mathematically by defining and specifying the effects that the particle was exposed to during the reaction. Firstly, the particle's shape and size were determined. Secondly, the environment to which the particle was exposed was defined. A particle undergoing a reaction may or may not change its phase. The phase of the product and the products were defined for the particle. The heat and mass transfer effects combined with the kinetics described the whole process of reaction on a single particle.

In order to account for heat transfer, the basic energy equation (equation 18) in polar coordinates acted as the elementary step.

$$\rho C_p\left(\frac{\partial T}{\partial t}+ v_r\frac{\partial T}{\partial r}+\frac{v_\theta}{r}\frac{\partial T}{\partial \theta}+\frac{v_\varphi}{r\sin\theta}\frac{\partial T}{\partial \varphi}\right)= k\left[\frac{1}{r^2}\frac{\partial}{\partial r}\left(r^2\frac{\partial T}{\partial r}\right)+\frac{1}{r^2\sin\theta}\frac{\partial}{\partial \theta}\left(\sin\theta\frac{\partial T}{\partial \theta}\right)+\frac{1}{r^2\sin^2\theta}\frac{\partial^2 T}{\partial \varphi}\right]+\mu\Phi_v+\Delta H\,(r_a) \qquad (18)$$

The equation of continuity defined was given by equation 19.

$$\varepsilon C\left(\frac{\partial x_A}{\partial t}+ v_r\frac{\partial x_A}{\partial r}+\frac{v_\theta}{r}\frac{\partial x_A}{\partial \theta}+\frac{v_\varphi}{r\sin\theta}\frac{\partial x_A}{\partial \varphi}\right)= C\,D_{AB}\left[\frac{1}{r^2}\frac{\partial}{\partial r}\left(r^2\frac{\partial x_A}{\partial r}\right)+\frac{1}{r^2\sin\theta}\frac{\partial}{\partial \theta}\left(\sin\theta\frac{\partial x_A}{\partial \theta}\right)+\frac{1}{r^2\sin^2\theta}\frac{\partial^2 x_A}{\partial \varphi}\right]+ar_a \qquad (19)$$

These equations were further modified according to the assumptions (mentioned in the next section) to determine the equations for the model. These equations were combined with the rate of reaction to replicate the reaction taking place in the particle.

III.3.2 Assumptions

- A spherical particle of AS with homogeneous structure was considered.
- The concentration was set to change radially.
- Effects of reaction, diffusion, heat transfer and mass transfer were considered.
- Thermodynamic properties were assumed to remain constant throughout.
- Multiple step reaction was considered.
- The reaction was non-catalytic in nature (only thermal energy acted as the driving force).
- The size of the particle remains constant during the reaction.
- Transport resistances other than heat transport and diffusion were ignored.
- Ammonia production rate was set as the basis for the decomposition of the reactant.
- All heat transfer was coupled as conductive heat transfer.
- The particle decomposition followed the shrinking core model

III.3.2 Matlab solver

The Matlab solver was used to solve the heat transfer, mass transfer and reaction equations simultaneously to determine the fractional conversion of the particle over time and the temperature of the particle over time. First the partial differential equations present were converted to ordinary differential equations using numerical methods of lines. The function ode23s in Matlab was used to solve the differential equations formed. The end results were plotted and compared to experimental data obtained from TGA.

III.4 Solar reactor experiments

III.4.1 Setup

Figure 12: Xenon Arc Lamps Concentrating Light

Seven Xenon arc lamps (Figure 12) of 240 V each were used in the system to concentrate light onto the target location. Each lamp was separately controlled to move left, right, front and back using the LabView software.

The optimal position for lamp 4 (used in the study) was set and the lamp was moved front or back to focus and defocus the light concentrated at the target.

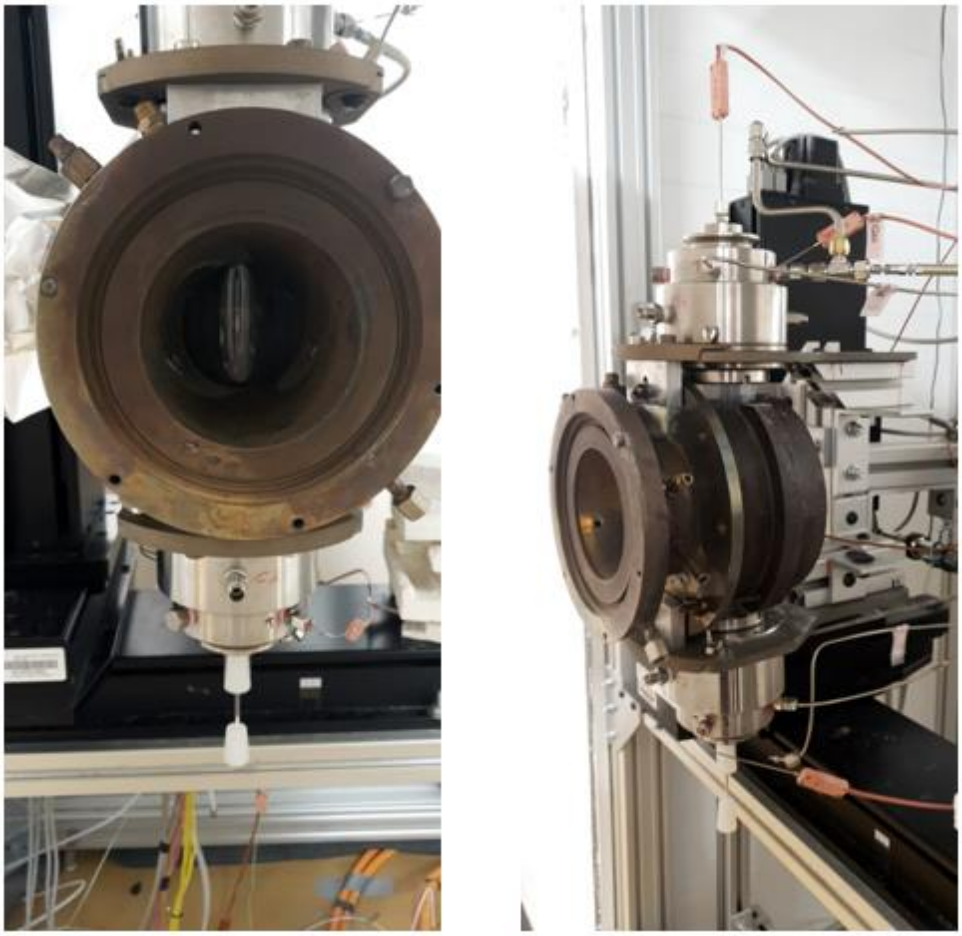

Figure 13: Front View and Side View of the Reactor

The reactor (Figure 13) consisted of a glass tube sealed on the upper and lower end. The lower end consisted of a gas inlet and glass tube of smaller diameter. The sample was placed in a capillary and sealed into the glass tube using a rubber stopper. A rubber stopper was used at the other end of the capillary to avoid the sample from moving downwards. In addition to the rubber stopper, quartz wool was placed before placing the sample to ensure that the sample does not move. The size of the capillary was determined after confirming the point of focus when the Xenon arc lamps were switched on. A

thermocouple was placed right above the point of capillary to measure the temperature of the sample.

The top of the reactor was connected to the MS and Gas Analyzer as the gas outlets. Thermocouples were connected to the top and bottom flange to measure the temperatures. Moreover, a concave metal concentrator encompassed the glass tube to ensure that the deviated light and heat was concentrated to the target by reflection and radiation. Thermocouples were placed on the front and back of the concentrator.

The temperatures, pressure and flowrate were monitored using LabView. LabView was used to specify the inlet flowrate of gas in the system (Argon).

III.4.2 Equipment preparation

III.4.2.1 Mass spectrometer setup (MS)

The MS was setup as defined in previously. The exist stream from the top of the reactor acted as the inlet for the MS.

III.4.2.2 Gas analyzer setup

The gas analyzer was connected to the PC by LabView. The gas analyzer was calibrated to detect NH_3, NOx, CO_2 and O_2. It collected the data for NOx and NH_3 in terms of ppm. The gas outlet from the reactor reached the inlet of the gas analyzer through a flexible pipe. A filter blocked out the residue and allowed just gas to enter the gas analyzer.

III.4.2.3 Attenuated Total Reflector (ATR)

Figure 14: ATR Accessory of the FT-IR Module

The ATR is one of the accessories of the FT-IR module that works on the principle of reflection for solids and liquids. The equipment consists of a diamond crystal through which the light reaches the sample. The sample is locked in place using the blue screw shown in Figure 14. The sample pressed between the diamond crystal and the metal head was tested. Depending on the reflection of the beam, the sensor creates a profile of absorption or transmission for the sample placed, on OMINIC. The setup was cleaned using ethanol.

The system was prepared and calibrated before the experiments to ensure that the components present in the sample were tested accurately. The software's experimental setup was specified, and a blank was collected before starting the experiment as the background. Certain components were expected during the conversion of the sample. AS,

KS, Ammonium bisulfate (AHS) and Potassium pyrosulfate (KPS) were the components which were expected to remain in the solid after the reaction. Therefore, a series of samples with different ratios of AS, KS, AHS and KPS were taken. The spectra for different combination of samples prepared was collected and fed into the software. A known sample of certain ratio between AS, KS, AHS and KPS was prepared and tested to check if the system accurately determines the ratio between the components. The remaining sample from the experiments was tested in the ATR.

III.4.3 Procedure

The original aerosol reactor design consists of sample trickling down through the reactor. The sample is exposed to radiation and as it travels down the system, it absorbs the heat, increases in temperature and undergoes the reaction proposed. By this concept, the temperature of the particle increases gradually and reaches the temperature required. The same concept was applied in the setup prepared where the heat flux given to the sample was constant, however, the temperature gradually increases as seen in the Figure 15. Once the required temperature is reached, the lamp was switched off.

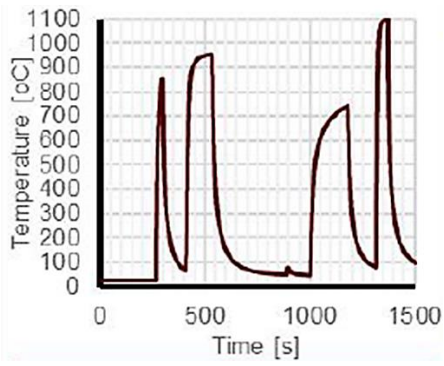

Figure 15: Temperature of the Sample at 4 Different Heat Fluxes Provided

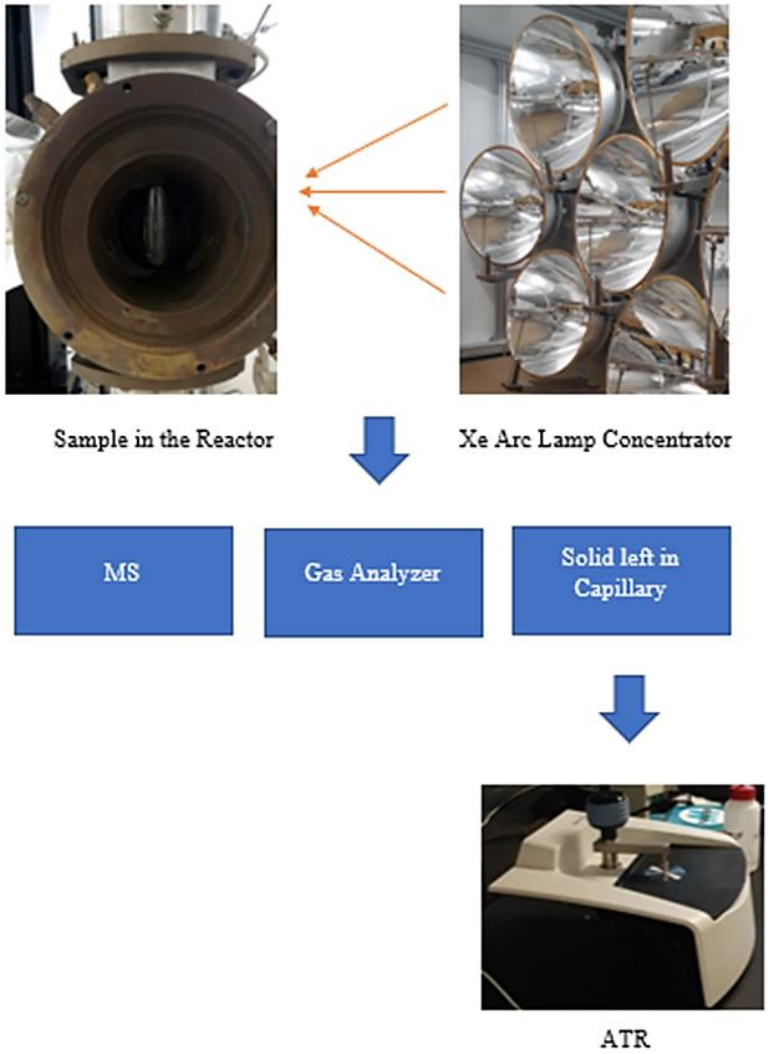

Figure 16: Experimental Procedure for the Solar Reactor Experiments

The setup (Figure 16) was preheated by increasing the temperature of the system to make sure that the delay in heating up of the system does not affect the reaction. Meanwhile, the sample was prepared in the capillary. After preheating, the sample was inserted, and argon flow was introduced to the system at 200 mL/min. The gases present in the system were read using MASsoft©. The argon gas purged out all the other gases. The lamp was switched on after all the gases were purged out. For each ratio of sample

placed, two variables temperature and flux were varied. One variable was kept constant while the other was varied. The flux was varied by moving the lamp forward or backwards. The system was shut at the specified temperature and time required for the system to reach the temperature was calculated. After the experiments, the flux received by the sample was calculated in addition to the concentration of gases in the system. The remaining sample was tested on the ATR for the components present and converted during the reaction.

CHAPTER IV

RESULTS AND DISCUSSION

IV.1 Sample characterization

The samples prepared were characterized based on different tests depending on the effects to be tested.

IV.1.1 Effect of not dissolving the sample in water and recrystallizing

The samples which were crushed without dissolving in water were tested using XRD for the initial reactants present. The AS_01 (crystallized particles of ratio 1AS:0KS), AS_03 (crushed particles of ratio 1AS:0KS) samples showed similar behavior with presence of just AS with or without recrystallization as seen in Appendix. The mixtures were tested under the XRD, ASKS_03 (crushed particles of ratio 1AS:1KS).

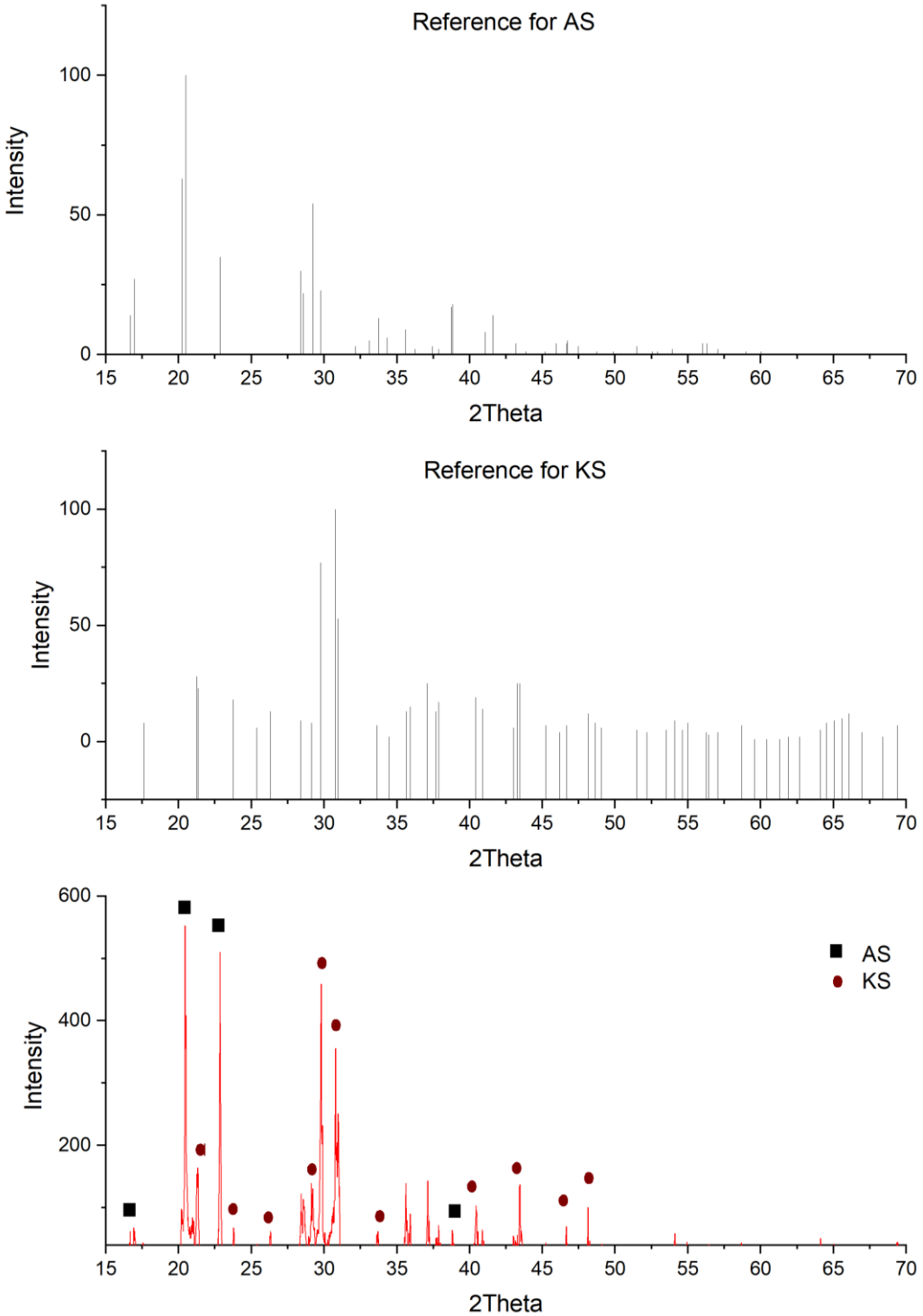

Figure 17: XRD Analysis for ASKS_03

Figure 17 showed that the peaks of the sample obtained by directly crushing the AS and KS samples together were identical to the peaks formed by AS and KS separately. Therefore, the sample stayed as a mixture of AS and KS upon not dissolving in water.

SEM/EDS was performed to further study the crushed sample. The samples studied were AS_03 (crushed particles with ratio 1AS:0KS) and ASKS_03 (crushed particles with ratio 1AS:1KS).

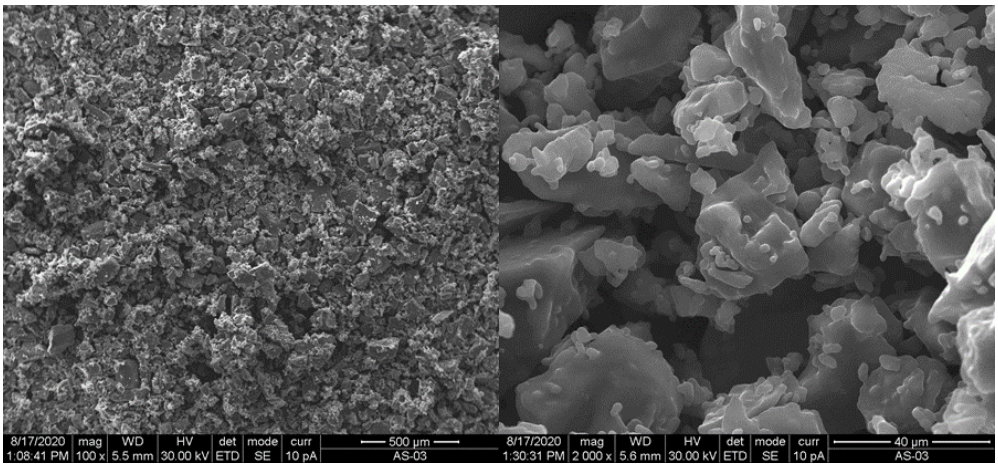

Figure 18: SEM Image for AS_03

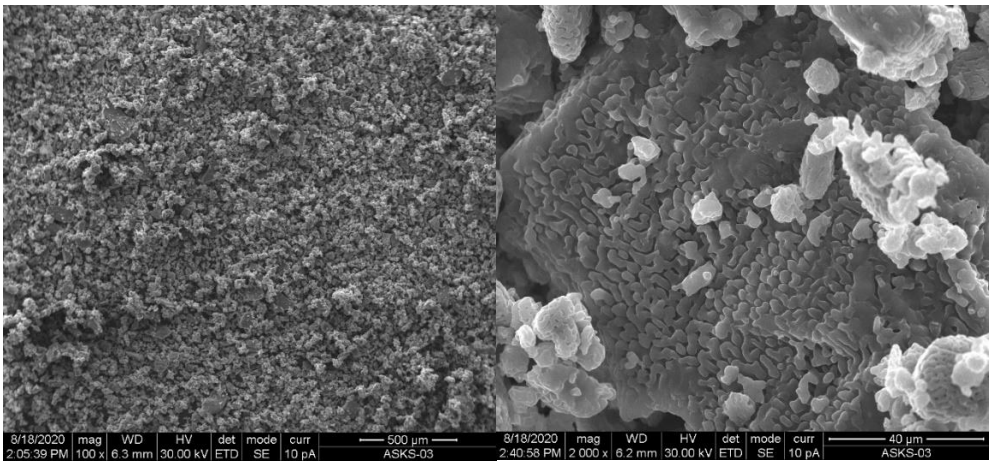

Figure 19: SEM Image for ASKS_03

Figure 18 and Figure 19 showed that the crushed particles consisted of a porous particle. A large particle with small grains agglomerated on top was formed. The porosity of the particle was larger in ASKS_03 as compared to AS_03.

IV.1.2 Effect of dissolving the sample in water and recrystallizing

The samples prepared by recrystallization were tested using XRD analysis for the components present, ASKS_01 (recrystallized sample of ratio 1AS:1KS) and ASKS_02 (recrystallized sample of ratio 1AS:2KS)

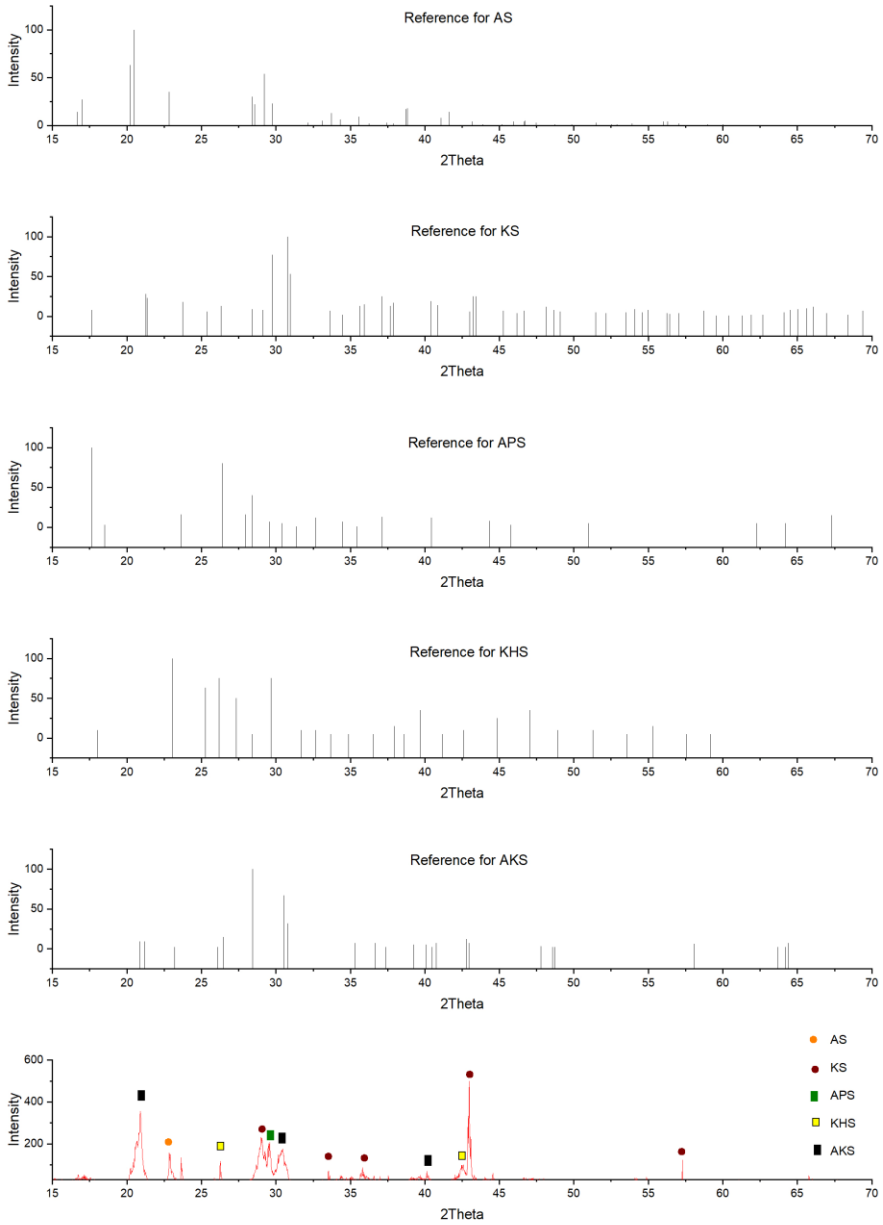

Figure 20: XRD Analysis for ASKS_01

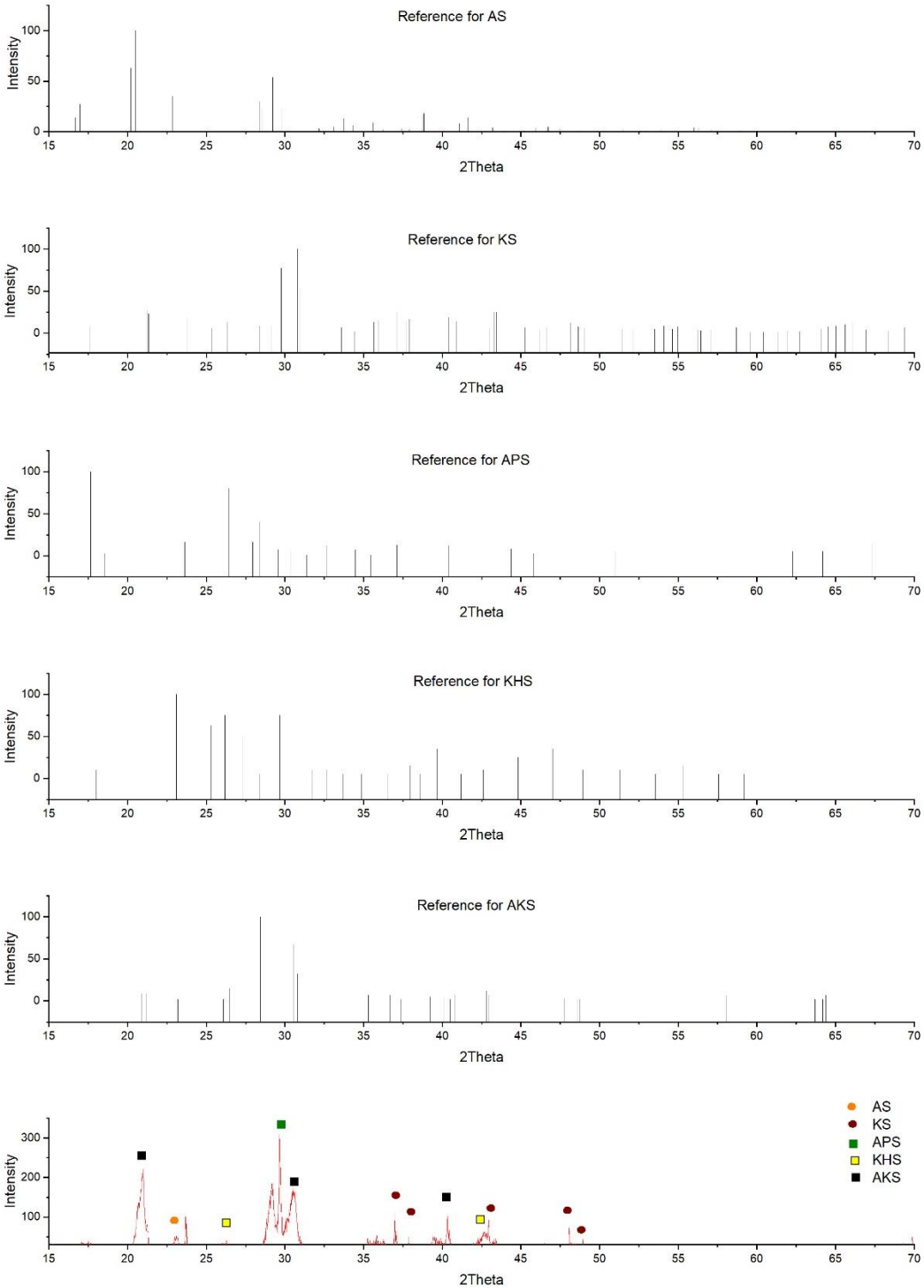

Figure 21: XRD Analysis for ASKS_02

Figure 20 and Figure 21 showed that contrary to the expected components present in the sample, dissolving in water and recrystallizing leads to formation of new products. The sample turned out to be a combination of AS, KS, Potassium ammonium Sulfate (AKS) and traces of APS and KHS. Further tests are required for determination of the composition of each component in the solids.

SEM/EDS was performed for further understanding of the samples. The samples showed similar behavior to the samples that were not dissolved (Figure 18 and Figure 19). However, on dissolving the particles and recrystallizing, the porosity decreased as seen in Figure 22, and Figure 23. The grains decreased in number and the particles became less porous. Increase in KS ratio however increased the number of grains and made the sample more brittle as seen from Figure 24, where the size of the grains was smaller and the particle was less porous. The approximate grain size from the SEM results was seen to be 5-15 µm.

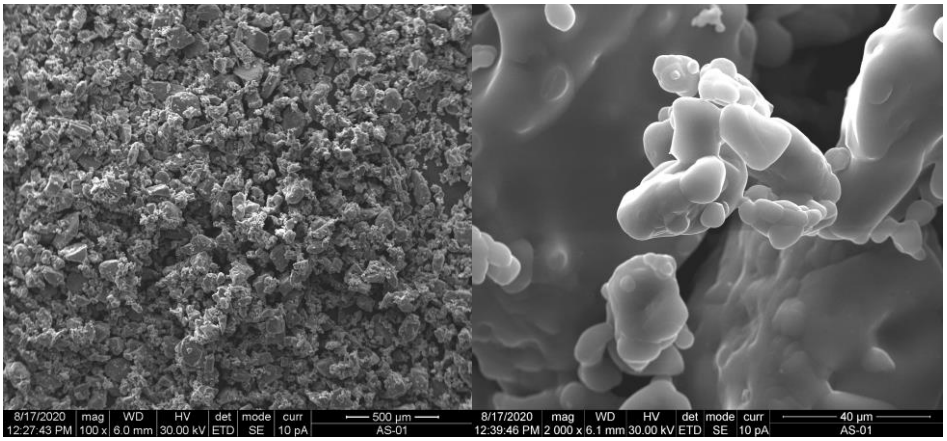

Figure 22: SEM Image for AS_01

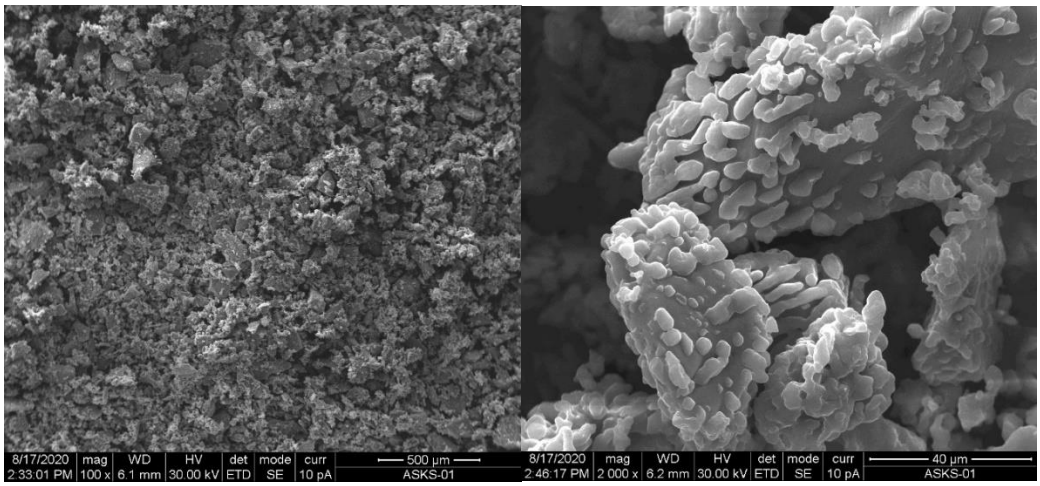

Figure 23: SEM Image for ASKS_01

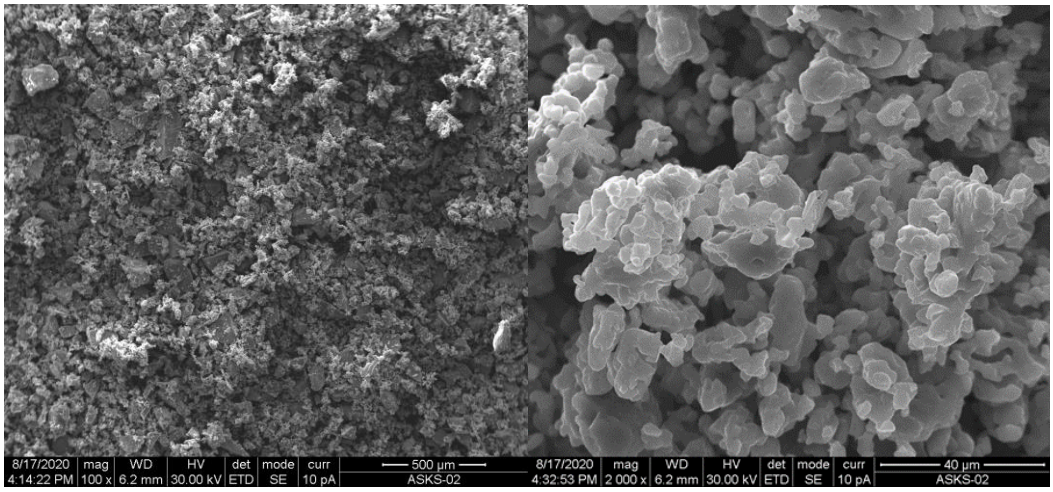

Figure 24: SEM Image for ASKS_02 at 100x Magnification

Therefore, the differences between the crystallized and crushed particles showed that new compounds were formed during recrystallization. However, further analysis of the compositions will be required to determine its effects on the model.

IV.1.3 Effect of different crushing speeds

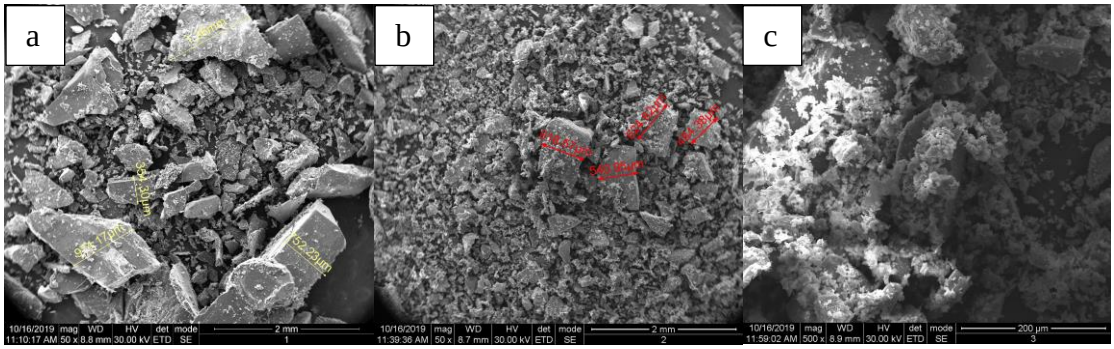

Figure 25: SEM Results for Large (a), Medium (b) and Small Particles (c)

The sample, ASKS_01 was crushed to different particle sizes and tested under the SEM. The samples were categorized as crushing speeds for small, medium and large particles. The results showed that, even though the crushing speeds were varied, the sample consisted of a mixture of particles with different size ranges in micrometer. Moreover, the sample consisted of the same structure with a grain and agglomerated small grains. As seen in Figure 25 c, the particles were more homogeneously sized than the ones seen in Figure 25 a and b. However, the range of particles was greater in lower crushing speeds. Therefore, higher crushing speeds were used in order to reduce the variability of sizes of the particles under study.

IV.1.4 Effect of different ratios

The PSA analysis conducted for AS_01, ASKS_01 and ASKS_02 consisting of different ratios of KS in the sample showed the effect of ratios on the particle sizes.

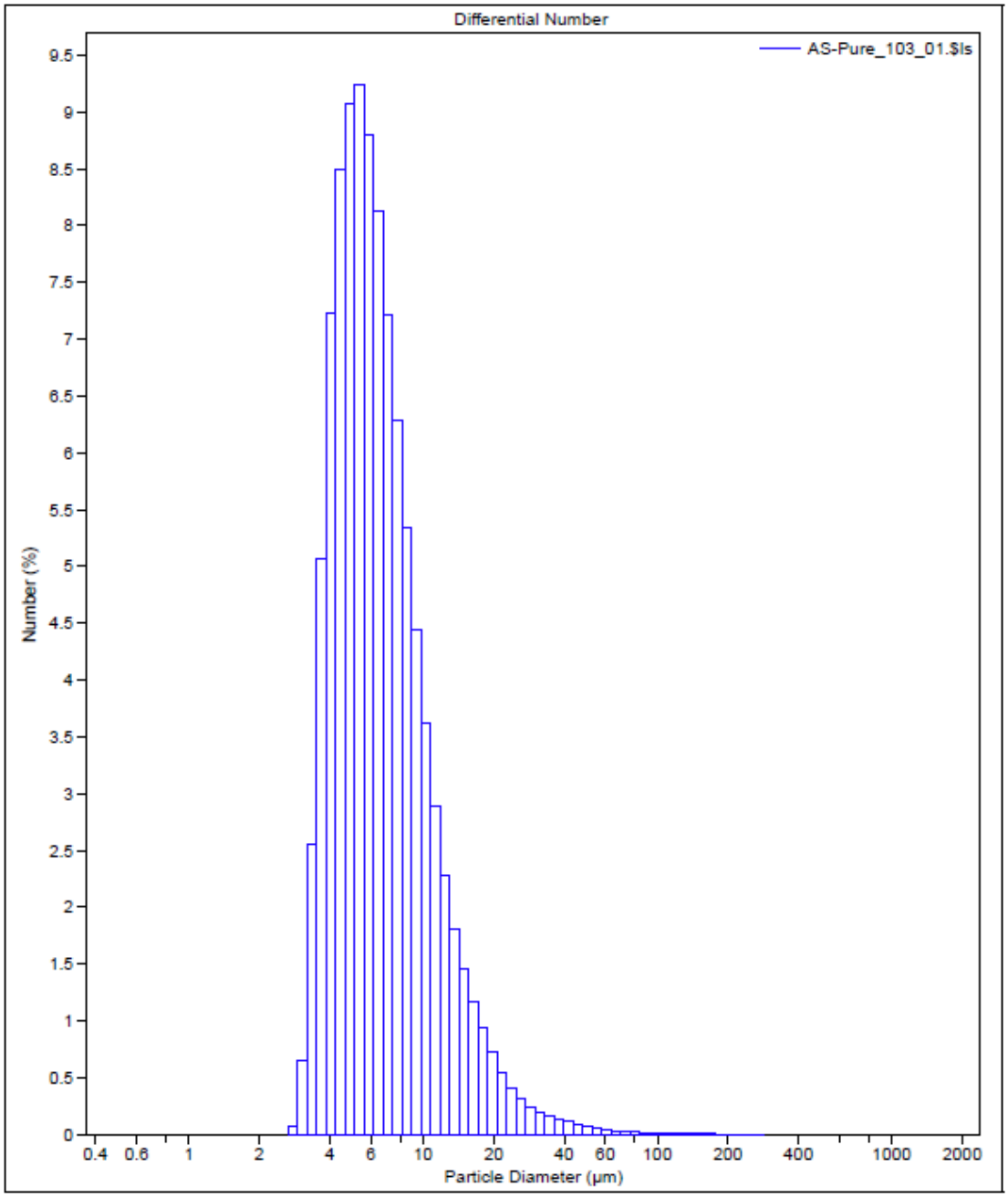

Figure 26: PSA for 1AS:0KS

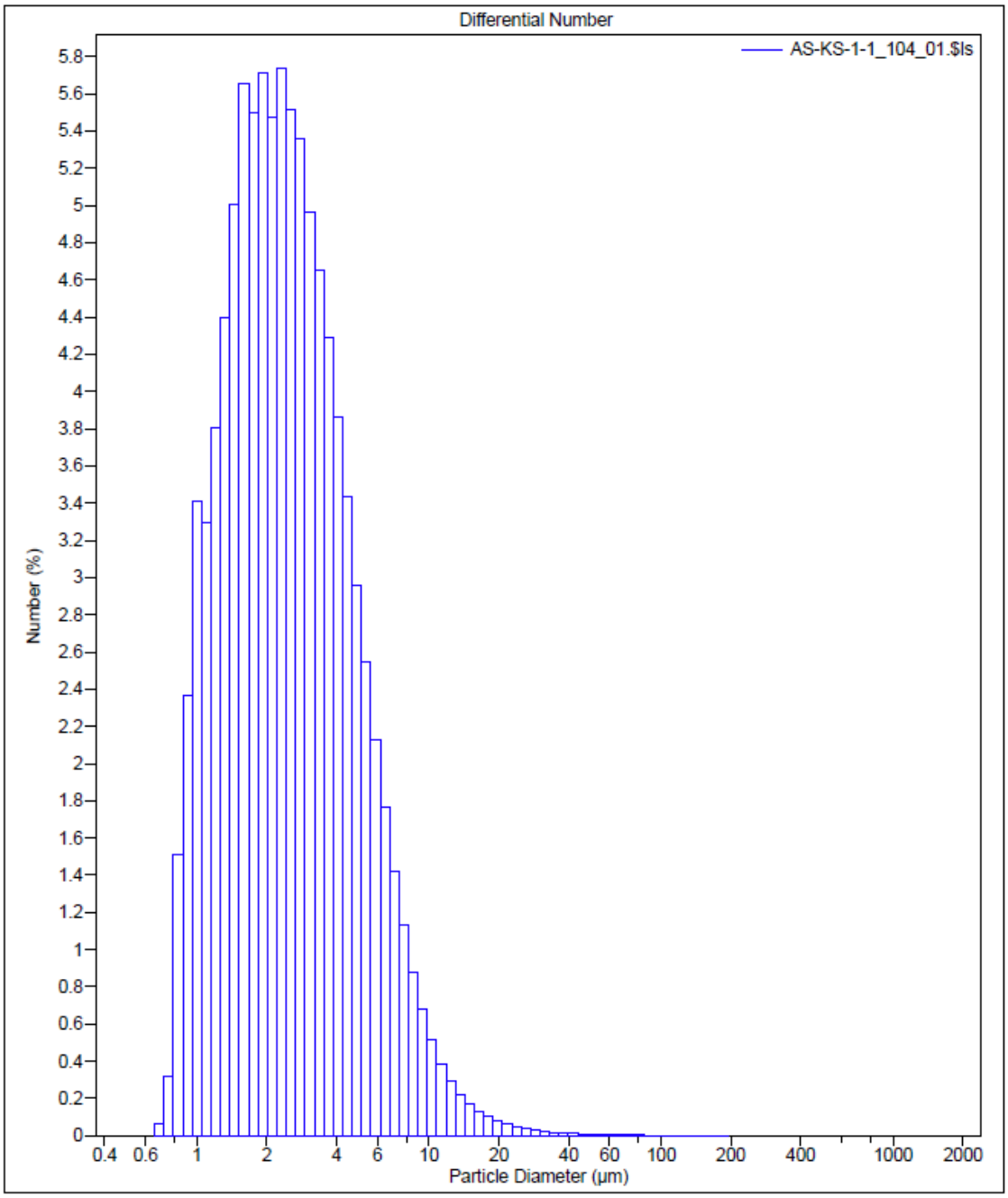

Figure 27: PSA for 1AS:1KS

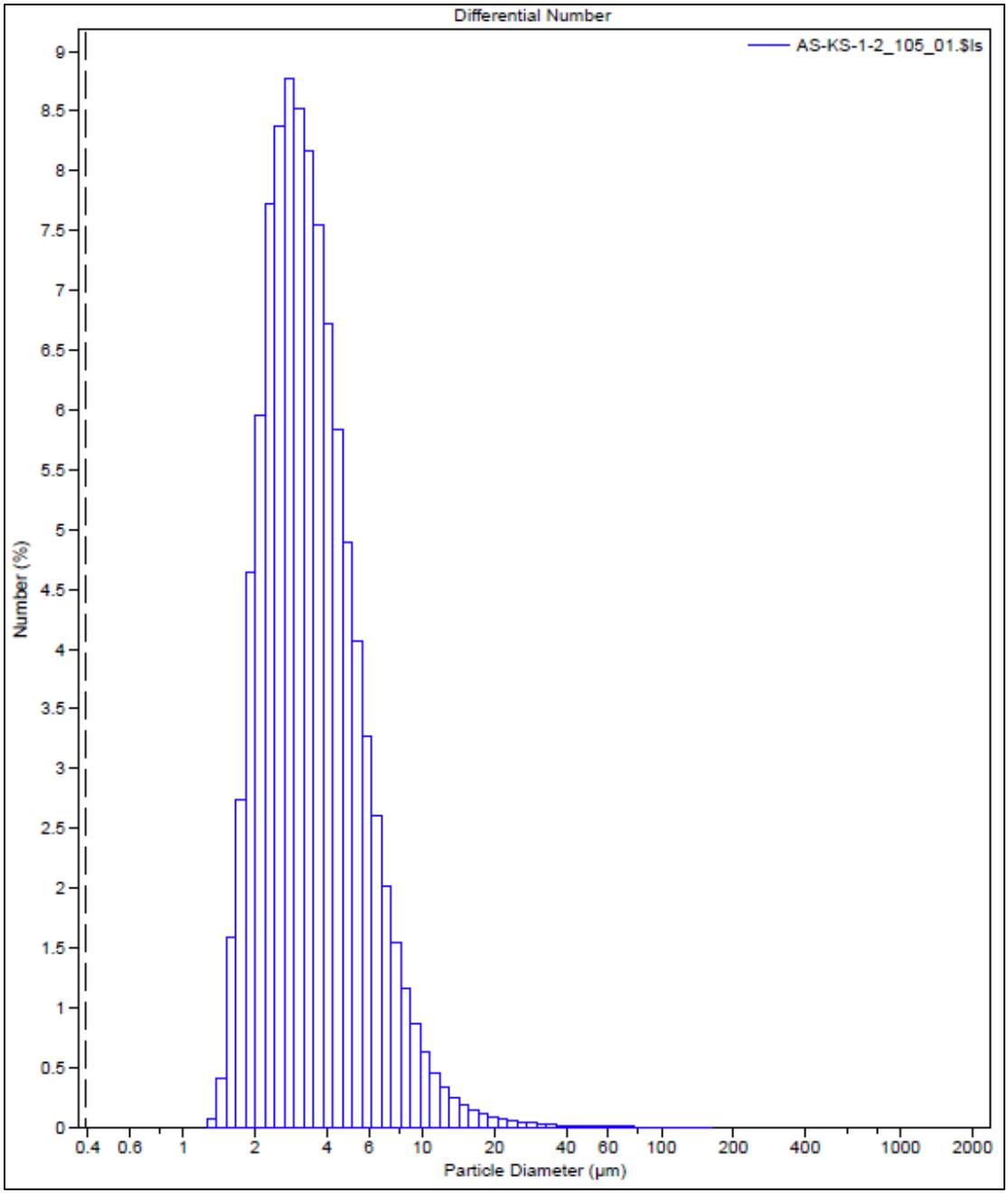

Figure 28: PSA for 1AS:2KS

Figure 26, Figure 27, and Figure 28 show that the samples consisted of particles of size range 1-200 µm. It was seen that the density of particles increased with smaller

particle size increased as the ratio of KS increased. However, the particles in all the three ratios fall between 1 to 200 µm.

Moreover, the PSA analysis was conducted on samples directly crushed without crystallization.

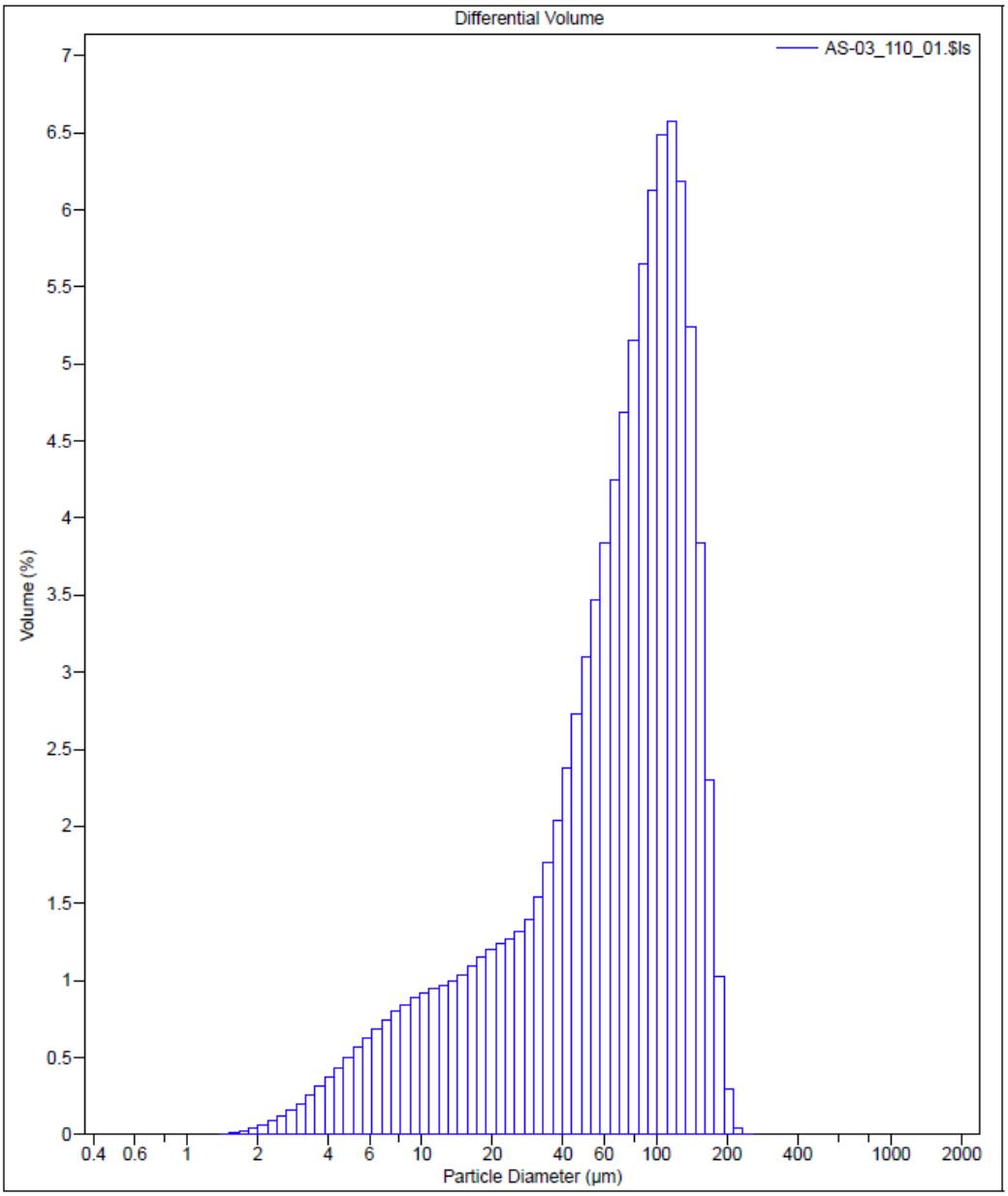

Figure 29: PSA for 1AS:0KS Crushed (AS_03)

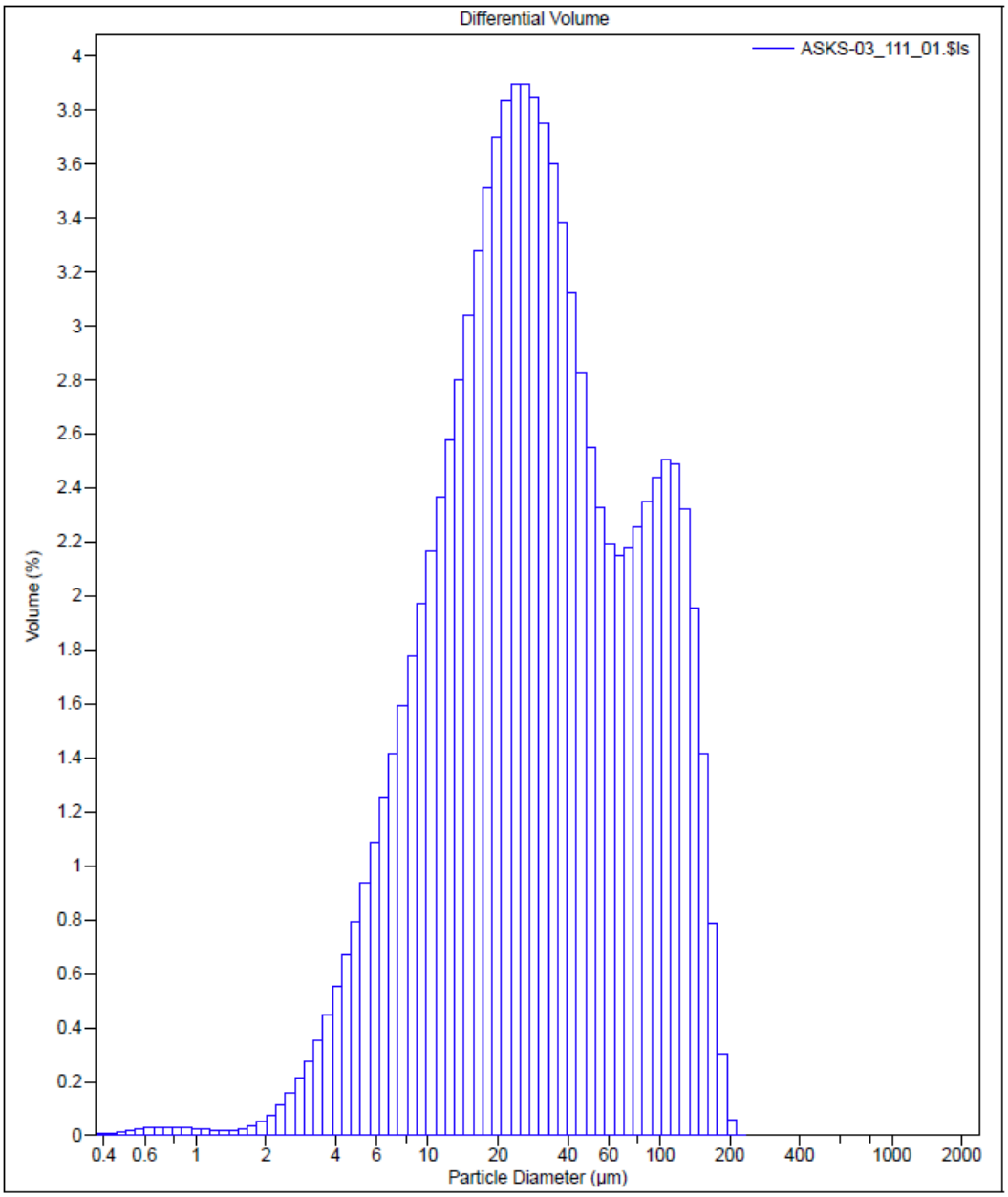

Figure 30: PSA for 1AS:1KS Crushed (ASKS_03)

Figure 29 and Figure 30 showed that when the samples were crushed directly without recrystallization, the size of the particles were close to 150 µm for just AS and appeared with double peak for the AS-KS mixture. Therefore, the AS particles were the bigger particles while KS particles were the smaller particles with size around 20 µm.

Therefore, the samples prepared were sieved to ensure that the size range of the particles was known. The size range of 53-125 μm was chosen as the medium range for the samples.

IV.1.5 Effect of decomposition of different samples

The components present in the end solids of experiments TGA2_17 (ASKS_01 at heating rate 5 ℃/min), TGA2_18 (ASKS_01 at 2 ℃/min) and TGA2_38 (ASKS_02 at 5 ℃/min) were analyzed using XRD while the end solids in TGA2_14 (ASKS_01 at 2 ℃/min), TGA2_15 (ASKS_01 at 8 ℃/min) and TGA2_30 (ASKS_02 at 4 ℃/min) were analyzed using SEM/EDS.

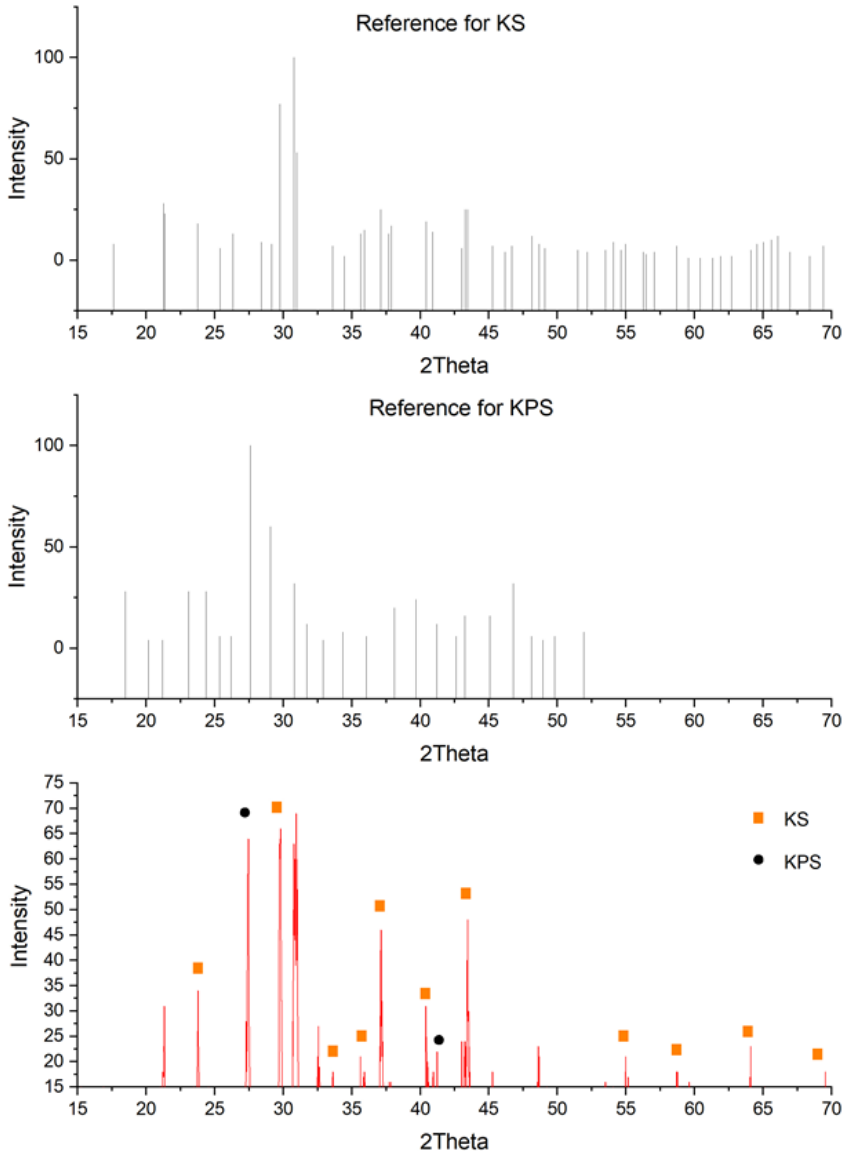

Figure 31: XRD Analysis for TGA2_18

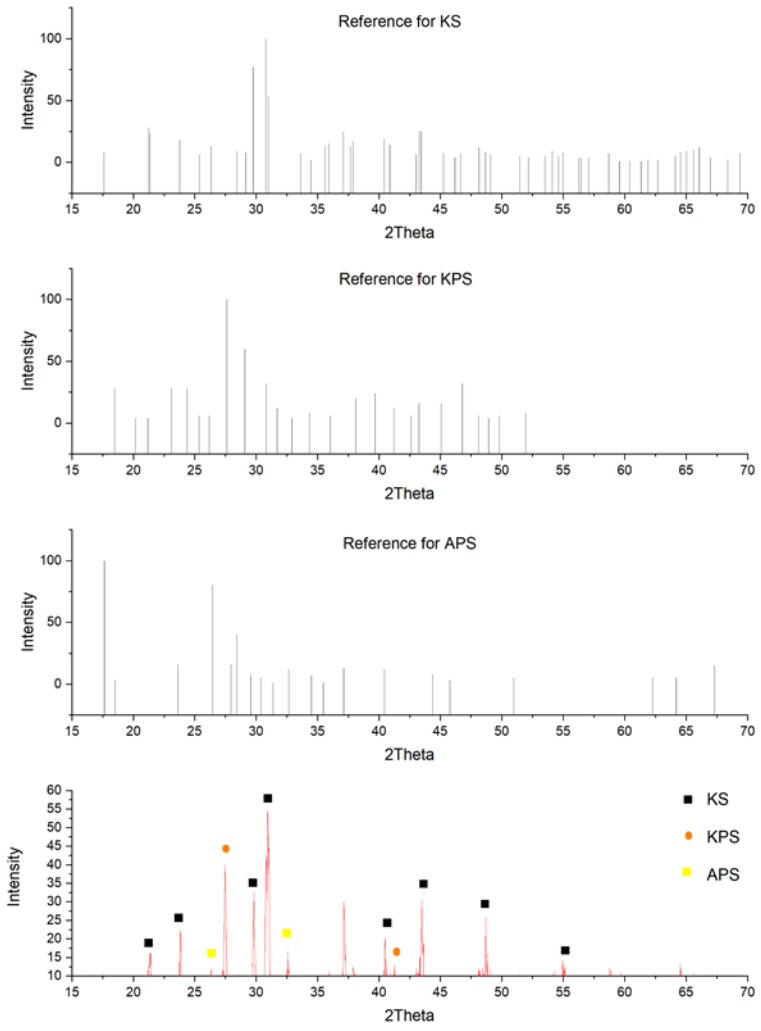

Figure 32: XRD Analysis for TGA2_17

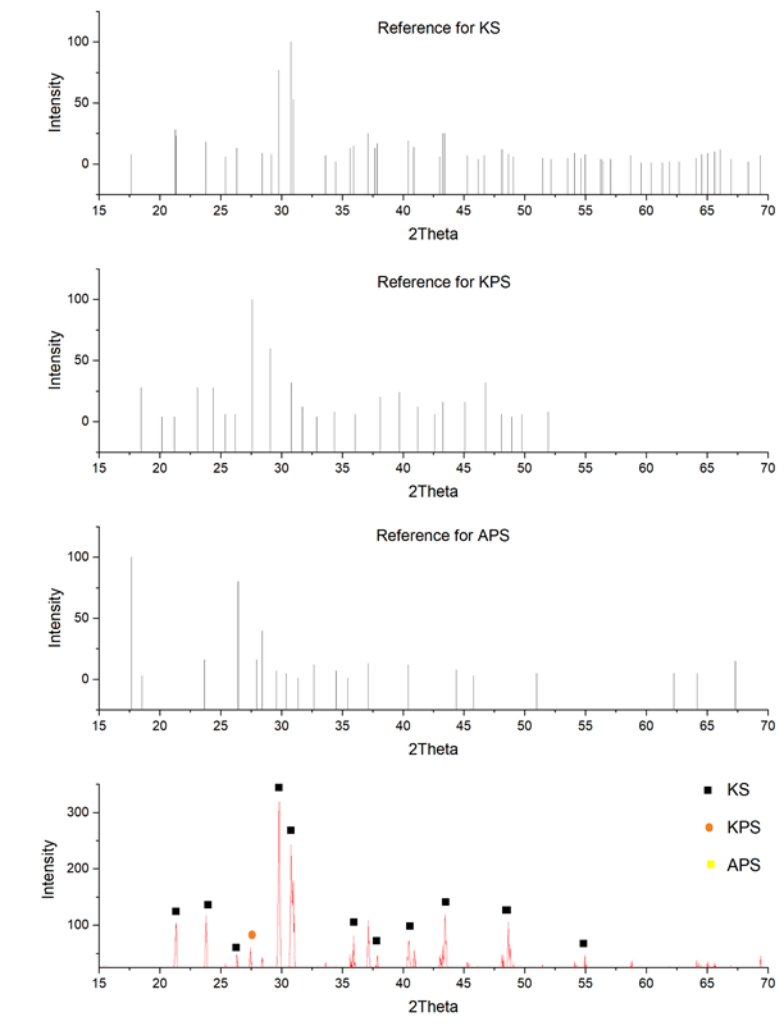

Figure 33: XRD Analysis for TGA2_38

Figure 32 showed that the decomposition of KPS produces KS as the end product with traces of KPS left behind. This spectrum was compared to spectrum obtained in Figure 31 and Figure 33. It was seen that as the ratio of KS increased in the initial reactant the amount of APS in the final product decreased. Moreover, the sample completely converted to KS with traces of KPS left as the ratio of KS was increased in the reactant.

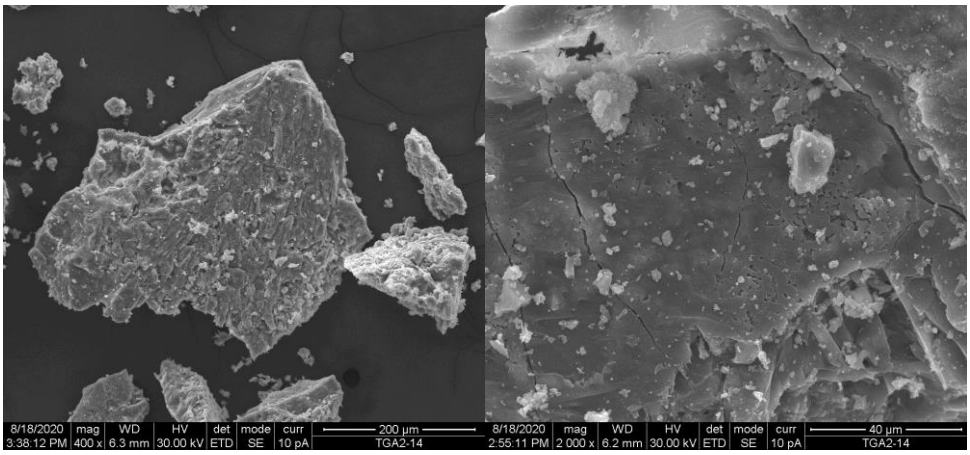

Figure 34: SEM Image for TGA2_14

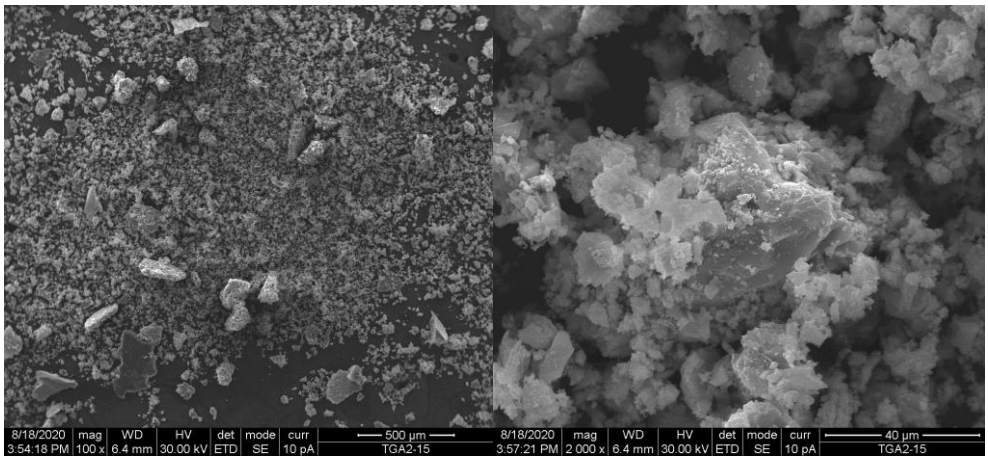

Figure 35: SEM Image for TGA2_15

Figure 34, Figure 35 and showed SEM of the sample after treatment under 2 ºC/min and 8 ºC/min. At lower heating rate, larger particles were formed with prominent cracks due to the heat treatment. At higher heating rates, the cracks break down the sample leading to smaller particles being formed as compared to the ones with lower heating rate. Higher heating rates showed smaller particles with more grains while slower heating rates show larger particles with less grains.

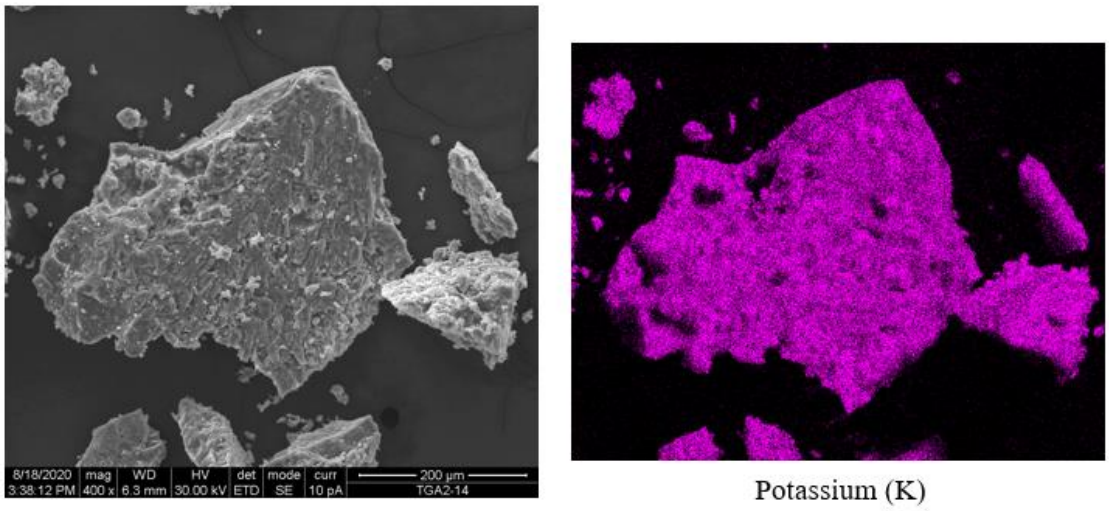

Figure 36: EDS for TGA2_14

Figure 36 showed that after thermal decomposition, only the potassium based compounds were left and the nitrogen based compounds were completely consumed. This was confirmed by EDS performed on TGA2_15 and TGA2_30 as shown in Appendix.

IV.2 Kinetics determination

IV.2.1 Reaction determination

The main idea behind determining the actual reaction was to present the possible products in each step to ensure that the reaction carried out follows the desired path with maximum conversion. It was important to understand and deduce the intermediate products as well as by products for detailed explanation of the steps taking place. Studies presented in literature have conflicting assumptions of products formed. The literature was to be summarized to reach the conclusion of the proper steps to be used in our study. AS was the major reactant which should ideally completely convert to ammonia gas and sulfur oxides. The different possible routes that AS decomposition can take in the presence or

absence of another reactant, KS, was studied. First, reaction of AS in the absence of KS was studied. According to the peaks of DSC obtained from the TGA analysis the whole experiment was divided into different steps. The gases produced in each step were studied using the MS and FT-IR gas analyser. According to Halstead *et al.* (Halstead, 1970) and Kiyoura *et al.* (Urano, 1970), AS thermally decomposes to form AHS and further decomposes to form APS according to the following reactions:

$$(NH_4)_2SO_4\ (s) \rightarrow NH_3\ (g) + NH_4HSO_4\ (s) \quad (20)$$

$$2NH_4HSO_4\ (s)\ \rightarrow (NH_4)_2S_2O_7\ (s) + H_2O\ (g) \quad (21)$$

According to the thesis presented, Wang (Wang, 2012) showed that AS decomposes as follows:

$$(NH_4)_2SO_4\ (s) \rightarrow 2NH_3\ (g) + H_2SO_4\ (g) \quad (22)$$

From the MS and FTIR, the gases produced in the first region showed that there was a presence of NH_3 and H_2O. The presence of H_2O in the first stage confirmed the conversion of AS to APS. Halstead *et al.* (Halstead, 1970) summarized the reactions as a set of one reaction. This was confirmed by the experiments that have been performed. The ratio of water to reactant was assumed to be 0.5 mol based on the literature and is confirmed by the experiments. The presence of half mol of H_2O in comparison to the starting reactant showed that the amount of sample converted, has been converted to APS. Moreover, the absence of H_2SO_4 from the MS results, confirmed that the reaction does not take the route proposed by Wang, (Wang, 2012).

Albert (Albert B. Welty, 1970), and Jariawala (Maheshwari Jariwala, 2007) confirmed the presence of APS as the by product instead of AHS. The studies further

suggest that production of AHS instead of APS was possible under conditions of excess moisture. However, due to the gases being removed from the system continuously, it was concluded that APS was formed.

APS was produced by an alternative method as well.

$$(NH_4)_2SO_4\ (s) + SO_3(g) \rightarrow (NH_4)_2S_2O_7\ (s) \quad (23)$$

However, SO_3 was absent in the first stage according to MS and FTIR. Therefore, it can be concluded that all the pyrosulfate produced in this reaction was due to the combination of equation 20 and 21. The two reactions can be combined as one to produce the process followed by the first step.

$$(NH_4)_2SO_4\ (s) \rightarrow NH_3\ (g) + 0.5\ (NH_4)_2S_2O_7\ (s) + 0.5\ H_2O\ (g) \quad (24)$$

The second step of the reaction was shown to be a sulfur oxide producing step. According to Halstead *et al.* (Halstead, 1970) the reaction taking place was

$$3(NH_4)_2S_2O_7\ (s) \rightarrow 2NH_3\ (g) + 6SO_2(g) + 2N_2(g) + 9H_2O(g)\ (g) \quad (25)$$

The presence of SOx, N_2, H_2O, and NH_3 in the second step confirms the reaction taking place. The reaction could alternatively be

$$(NH_4)_2S_2O_7\ (s) \rightarrow NH_3\ (g) + 2SO_3(g) + 0.5\ N_2(g) + H_2O(g) + \ 1.5\ H_2\ (g) \quad (26)$$

However, SO_3 was absent according to Kiyoura *et al.* (Urano, 1970) and Halsted *et al.* (Halstead, 1970) in the reactions taking place. The absence of SO_3 could only mean that an alternative product of sulfur was present, and it has been confirmed that SO_2 was the only next possible product that could be present. Bayer (G. Bayer, 1981) backed up the theory presented by Halstead *et al.* (Halstead, 1970) by mentioning the presence of SO_2 instead of SO_3. Tu *et al.* (Kanapilly, 1977a), confirmed the presence of SO_3 as a

product. Wentworth (Wentworth, 1992) conducted the decomposition of AHS which showed that APS was first formed and later SO_3 and SO_2 were released as the sulfur compounds. The combination of both were attributed to presence of platinum (Pt) which led to further investigation. On further investigation, it was seen that SO_3 decomposes to SO_2 at temperatures higher than 800ºC. However, presence of Pt in the system acted as a catalyst to drive the reaction and SO_3 decomposed to SO_2 at lower temperatures. As seen from the above experiments, all experiments were carried out in an environment consisting of Pt. Absence of Pt in large scale would keep the SO_3 from decomposing. In this study, SO_3 was considered as to account for the reaction taking place. Moreover, the tests showed lower amount of NH_3 than expected and presence of N_2 in the system from MS results. However, H_2 was not detected as a product from the MS. An increase in water production was seen in this stage attributing to the decomposition of ammonia partially and recombination of H_2 with free O_2 to produce H_2O. Song (Song *et al.*, 2013) confirmed that decomposition of products takes place which leads to incomplete recovery of the expected gases. The overall reaction of decomposition of APS produced SO_3 as the sulfur product which was present as a combination of SO_2 and O_2. Some of the SO_3 and NH_3 decomposed and recombine to form SO_2, H_2O and N_2. The presence of a catalyst leads to the decomposition of these products which would otherwise be impossible at temperatures below 800 ºC. Halstead (Halstead, 1970), used a Pt crucible for the experiment which could have acted as a catalyst for the product decomposition leading him to conclude equation 26 as the decomposition step for APS. Therefore, the ideal situation with SO_3 was considered as the reactions aimed at were to satisfy the reactions taking place at a

large scale where the decomposition of NH_3 would be negligible and SO_2 and 0.5 O_2 can be combined as SO_3. These ratios of products were tested to ensure agreement between the theory and experiments carried out.

$$(NH_4)_2S_2O_7\ (s) \rightarrow NH_3\ (g) + 2SO_3(g) + H_2O(g) \quad (27)$$

Similarly, the mixtures were divided into two steps containing mass losses as seen from the TGA. The behavior of AS in presence of different ratios of KS was studied. AS and KS reaction was divided into two steps based on the peaks obtained. The first step showed a production of NH_3, H_2O and SOx unlike AS without KS. The presence of SOx as one of the initial products suggested that either the SOx were released from AS or KS. According to Lau *et al.* (K. H. Lau, 1979), the decomposition of KS was given by:

$$K_2SO_4\ (s)\ \rightarrow 2K\ (g) + SO_2(g) + O_2(g) \quad (28)$$

However, the decomposition process takes place at temperatures higher than 900 ^oC while the temperatures aimed by the reactions were below 800 ^oC.

The only other option was the decomposition of APS after equation 20 and 21. The decomposition of APS takes place by reaction 22. The production of sulfur dioxide and oxygen as a byproduct of SO_3 dissociation leads to conversion of KS to potassium pyrosulfate (KPS) by equation 29.

$$K_2SO_4\ (s) + SO_3(g) \rightarrow K_2S_2O_7\ (s) \quad (29)$$

Wentworth *et al.* (W.E. Wentworth, 1979), showed the decomposition of AHS with KS and concluded the production of KPS which further decomposed to release a mixture of SO_2 and SO_3. Vries (Gellings, 1969), showed that in absence of Pt as well, the decomposition of $K_2S_2O_7$ follows equation 30 and 31.

$$K_2S_2O_7\ (s)\ \rightarrow K_2SO_5\ (s) + SO_2(g) \quad (30)$$

$$K_2SO_5\ \rightarrow K_2SO_4\ (s) + 0.5\ O_2(g) \quad (31)$$

The reactions took place at 400-600 ºC instead of directly decomposing to K_2SO_4 and SO_3. Therefore, the end products were K_2SO_4, SO_2 and O_2. Dearnaley *et al.* (R. I. Dearnaley, 1983), confirmed the above assumption in their study. The overall reaction was taken instead of the intermediate steps to summarize the reactions.

The interaction of AS with KS did not produce any intermediate products. This was confirmed by the absence of sulfuric acid, hydrogen sulfide and other possible products in the MS. The absence of these products as well as the agreement of the mass balance showed that no other products were formed.

The following reactions were considered for AS without KS:

Stage 1: $(NH_4)_2SO_4\ (s) \rightarrow NH_3\ (g) + 0.5\ (NH_4)_2S_2O_7\ (s) + 0.5\ H_2O\ (g)$ (32)

Stage 2: $(NH_4)_2S_2O_7\ (s) \rightarrow 2NH_3\ (g) + 2SO_3(g) + H_2O(g)$ (33)

The following reactions were considered for AS with KS:

Stage 1:

$$(NH_4)_2SO_4\ (s) + K_2SO_4\ (s) \rightarrow NH_3\ (g) + 0.5\ (NH_4)_2S_2O_7\ (s) + 0.5\ H_2O\ (g) + K_2SO_4\ (s) \quad (34)$$

$$(NH_4)_2S_2O_7\ (s) + 2K_2SO_4\ (s) \rightarrow 2NH_3\ (g) + 2SO_3(g) + H_2O(g)\ + 2K_2SO_4\ (s) \quad (35)$$

Stage 2:

$$(NH_4)_2S_2O_7\ (s) + 2K_2SO_4\ (s) \rightarrow 2NH_3\ (g) + 2SO_3(g) + H_2O(g)\ + 2K_2SO_4\ (s) \quad (36)$$

$$K_2SO_4\ (s) + SO_3(g) \rightarrow K_2S_2O_7\ (s) \quad (37)$$

Stage 3:

$$K_2S_2O_7\ (s)\ \rightarrow\ K_2SO_4\ (s) + SO_3(g) \quad (38)$$

The MS determined that the gaseous products in the first stage of 1AS:0KS were NH_3 and H_2O while the second stage consisted of NH_3, H_2O and SOx along with nitrogen and oxygen as seen in Figure 37.

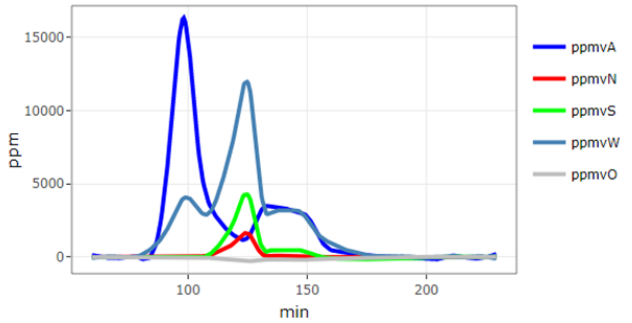

Figure 37: MS Result Sample for 1AS:0KS Experiments

The gaseous products for 1AS:1KS experiments were found to be NH_3, H_2O and SOx in all the steps. The presence of nitrogen and oxygen was detected as well from time to time as seen in Figure 38.

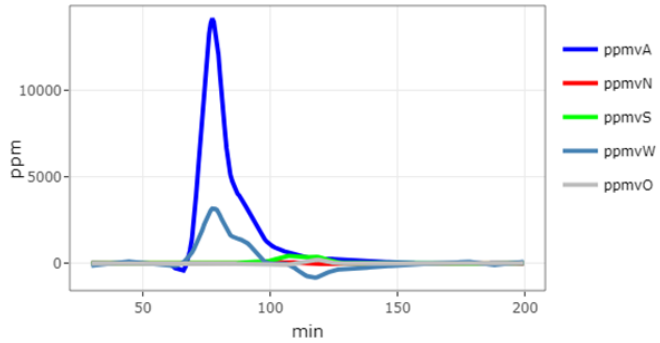

Figure 38: MS Results for 1AS:1KS Experiments

The reactions were modified depending on the MS results and above conclusions. The equations 31 to 37 were then tested in comparison with the theoretically calculated masses of gases and solids produced as a result of the reaction. The stoichiometric ratios of the reactions were used to calculate the theoretical mass loss in comparison to the

experimental mass loss. The negligible difference in values (less than 1%) showed the reliability of the reactions. Finally, the ratios of NH_3 (966 cm^{-1}), H_2O (1626 cm^{-1}) and SOx (1375 cm^{-1}) produced were tested using the FT-IR results. The FT-IR data obtained was as in Figure 39, Figure 40 and Figure 41.

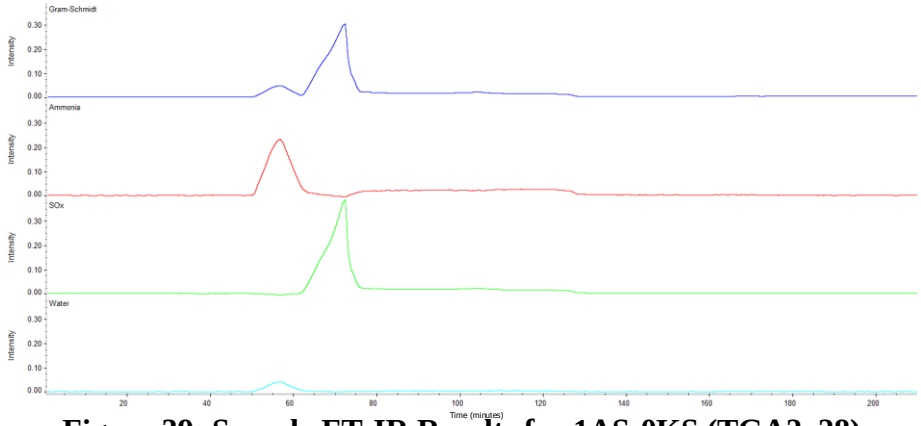

Figure 39: Sample FT-IR Results for 1AS:0KS (TGA2_28)

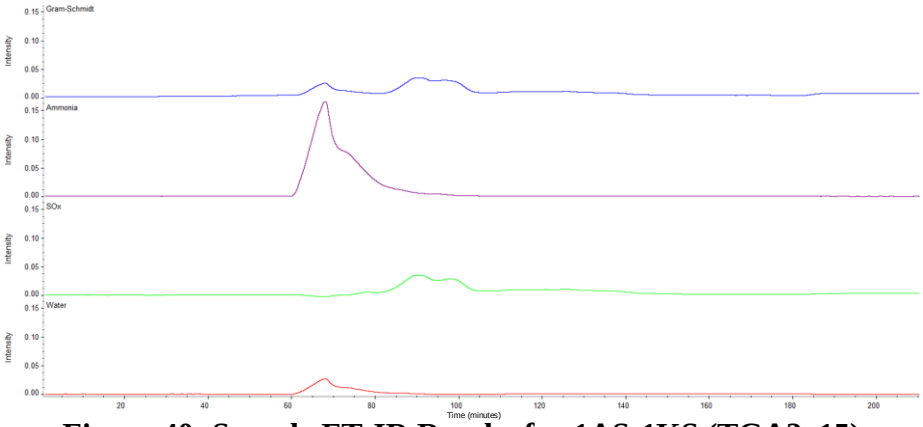

Figure 40: Sample FT-IR Results for 1AS:1KS (TGA2_15)

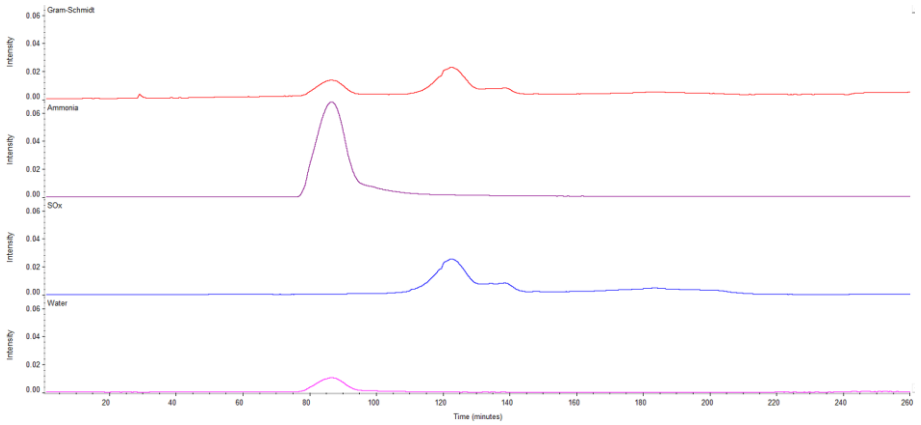

Figure 41: Sample FT-IR Results for 1AS:2KS (TGA2_38)

The thermal analysis and effect of different parameters on samples was discussed in the previous section. The FT-IR results for different ratios were as summarized in Table 6 and Table 7.

Table 6: Summary of FT-IR Results

		1AS:0KS	1AS:0KS	1AS:2KS
Step 1	Ammonia	1 mol	1.2 mol	1 mol
	Water	0.8 mol	0.75 mol	0.5 mol
	Sulfur Oxides	0 mol	0.01 mol	0.01 mol
Step 2	Ammonia	0.8 mol	0.2 mol	0.2 mol
	Water	0.2 mol	0.2 mol	0.75 mol
	Sulfur Oxides	0.8 mol	0.2 mol	0.2 mol
Step 3	Ammonia	0.2 mol	0.02 mol	0.05 mol
	Water	0.2 mol	0.5 mol	0.1 mol
	Sulfur Oxides	0.2 mol	0.2 mol	0.1 mol

Table 7: Table 6 Continued

		1AS:0KS	1AS:0KS	1AS:2KS
Total	Ammonia	2 mol	1.42 mol	1.25 mol
	Water	1.2 mol	1.45 mol	1.35 mol
	Sulfur Oxides	1 mol	0.41 mol	0.31 mol

It was seen that as ratio of KS to AS increased, the total amount of SOx decreased. This was attributed to capture of SOx by KS and incomplete release of SOx by the end of the experiment. Moreover, the amount of H_2O formed was more than expected (1 mol overall) and there was a significant decrease in NH_3 seen without any significant trend in water production seen which attributed to the dissociation of SOx or NH_3 and recombination to form water in presence of the catalyst (Pt rods in the TGA). This was further confirmed by seeing that in the first step where SOx were negligible for all three ratios, the expected amount of H_2O in the first step was produced. The conclusions drawn regarding the equations were used in further calculations of the kinetics.

IV.2.2 Miscellaneous thermal analysis

The thermal analysis conducted using different samples in the TGA were used to determine the effect of different conditions on the reaction in order to be incorporated in the model.

The change in mass of the sample (TGA2_22 compared with TGA2_11) showed that the change in mass by few milligrams did not affect the reaction mechanism. The FT-IR, MS and TGA results compared were similar for both the experiments.

The method of preparation of sample (TGA2_42 compared with TGA2_09) did not show any significant changes in the mechanism of reaction either.

Furthermore, tests were carried with different particle sizes (TGA2_43 compared with TGA2_42). It was seen that the results obtained using both experiments had comparable results in the TGA, FT-IR and MS. While the size of the particle might affect each particle, it does not affect the reaction taking place in the bulk.

The change in ratio of KS was tested (TGA2_38 compared with TGA2_15). It was seen that, as the ratio of KS increased, the amount of SOx decreased. Moreover, with increasing amount of KS, the NH_3 release peak and SOx release peak were seen to be more spread out in the FT-IR results (Figure 40 and Figure 41).

The decomposition of KS (KS_01) till 800 ºC showed no release of gases, attributing to the fact that KS does not undergo decomposition.

IV.2.3 Kinetics determination

The model-based method was used initially to determine the kinetics. The results obtained from the two methods showed that more than one model can be used to give the best fit for the equations above. Hence, starting the analysis with model-based methods led to misleading interpretations of the model that the reactions follow. It was seen that the data produced satisfying results with linear curves for different models and E_a values, hence confirming that model free methods should be used first to determine E_a values. An example of the linearity and similarity of results is as shown in Figure 42.

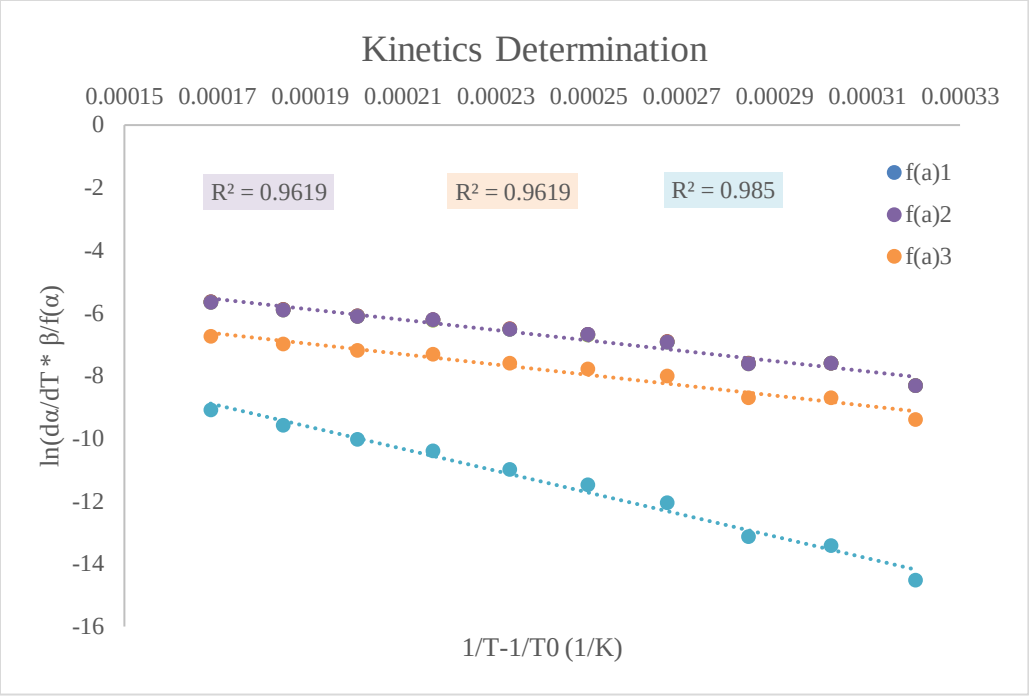

Figure 42: Sample Model Based Kinetics Plot (ASKS_01 Stage 1)

The model free method (iso-conversional) was used to calculate the kinetic parameters later. The kinetic parameters found were as summarized in Table 8.

Table 8: Summarized Kinetic Parameters

	AS				AS-KS			
	E_a (kJ/mol)	A (s^{-1})	n	D_e (m^2/s)	E_a (kJ/mol)	A (s^{-1})	n	D_e (m^2/s)
Stage 1	77.51	2.75×10^{4}	0.8	9.5×10^{-10}	77.4	1.51×10^{4}	0.8	3.8×10^{-10}
Stage 2	102.04	1.01×10^{5}	0.5		107	3.51×10^{4}	1	
Stage 3					110	3.17×10^{4}	0.4	

The two sets of experiments performed, 1AS:0KS and 1AS:1KS showed different results. The AS based experiments showed three distinct regions of TG drop and hence the experiments were divided into three regions. However, sub-regions were seen in AS-KS experiments since there were more than 1 reactions taking place. In step 1, the region was divided as stage 1 for ASKS experiments depending on the change in slope of A seen from the FT-IR results. Therefore, step 1 corresponded to the kinetics related to equation 32 for both AS and ASKS experiments. Stage 2 was seen as a combination of equation 33 and equation 37. Since step 2 is one region for AS experiments the order of reaction for equation 33 was found to be 0.5. The total order for equation 37 in ASKS experiments was 1, therefore, the order corresponding to just KS was found to be 0.5. Finally, the decomposition of potassium pyrosulfate was represented by stage 3. Therefore, the kinetics corresponding to equation 38 was given by the kinetics for stage 3. The order of the reaction was found to be 0.4. The reaction kinetics were summarized in Table 9.

Table 9: Summary of Kinetics for Each Reaction

Reaction	E_a (kJ/mol)	k_0 (s^{-1})	n
$(NH_4)_2SO_4\ (s) \rightarrow NH_3\ (g) + 0.5\ (NH_4)_2S_2O_7\ (s) + 0.5\ H_2O\ (g)$	77	1.51×10^4	0.8
$(NH_4)_2S_2O_7\ (s) + 2K_2SO_4\ (s) \rightarrow 2NH_3\ (g) + 2SO_3(g) + H_2O(g) + 2K_2SO_4\ (s)$	102	1.01×10^5	0.5
$(NH_4)_2S_2O_7\ (s) + 2K_2SO_4\ (s) \rightarrow 2NH_3\ (g) + 2SO_3(g) + H_2O(g) + 2K_2S_2O_7\ (s)$	107	3.51×10^4	1
$K_2S_2O_7\ (s) \rightarrow K_2SO_4\ (s) + SO_3(g)$	110	3.17×10^4	0.4

IV.3 Modelling of particle

IV.3.1 Description of the particle and its conditions

The model of the particle was designed by first describing the system and the particle. The particle under study (Figure 43) was a spherical, 53-125 µm diameter sized

AS particle which undergoes thermal decomposition in presence of KS. The AS particle was exposed to an inert gas with a constant flow to carry the gases formed continuously out of the system. As the heat flux was provided to the particle, the temperature of the particle increased steadily, converting AS to APS at around 260 ºC. APS further increased in temperature to release NH_3, H_2O and SOx at around 460 ºC. The SOx produced was entrapped by KS to form KPS and the rest of the gases were carried out of the system by Argon (carrier gas). Finally, KPS decomposes to KS and SOx at around 600 ºC. The rate of reactions taking place were summarized as equation 39, to equation 42.

$$-r_1 = k_1 \, {C_{AS}}^{0.8} \tag{39}$$

$$-r_2 = k_2 \, {C_{APS}}^{0.5} \tag{40}$$

$$-r_2 = k_3 \, {C_{APS}}^{0.5} {C_{KS}}^{0.5} \tag{41}$$

$$-r_4 = k_4 \, {C_{KPS}}^{0.4} \tag{42}$$

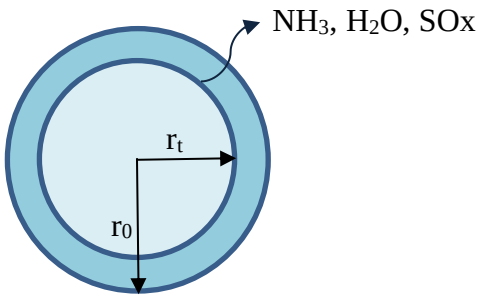

Figure 43: AS Particle Under Study

IV.3.2 Equations governing the system present

The general equations governing the system were derived from equation 18 and 19. They are given as equation 42 for heat transfer and equation 45 to 51 for mass transfer

where A=AS, B=KS, C=NH_3, D=H_2O, E=APS, F=KPS, G=SOx. The spherical particle is considered as a discretized space normalized from x=0 to x=1 with porosity ε.

$$\rho C_p \left(\frac{\partial T}{\partial x}\right) = k\left[\frac{1}{r^2}\frac{\partial}{\partial r}\left(r^2\frac{\partial T}{\partial x}\right)\right] + \Delta H\,(r_a) \quad \text{(Bird, 2007)} \tag{43}$$

$$\varepsilon C \left(\frac{\partial x_A}{\partial x}\right) = C\,D_{AB}\left[\frac{1}{r^2}\frac{\partial}{\partial r}\left(r^2\frac{\partial x_A}{\partial x}\right)\right] + ar_a \quad \text{(Bird, 2007)} \tag{44}$$

i) $$C_A(t) = -r_1 \tag{45}$$

ii) $$C_B(t) = -2r_3 + r_4 \tag{46}$$

iii) $$C_E(t) = 0.5r_1 - r_2 - r_3 \tag{47}$$

iv) $$C_F(t) = 2r_3 - r_4 \tag{48}$$

v) $$\varepsilon\left(\frac{\partial C_C}{\partial t}\right) = D_e\left[\frac{1}{r^2}\frac{\partial}{\partial r}\left(r^2\frac{\partial C_C}{\partial r}\right)\right] + r_1 + 2r_2 + 2r_3 \tag{49}$$

vi) $$\varepsilon\left(\frac{\partial C_D}{\partial t}\right) = D_e\left[\frac{1}{r^2}\frac{\partial}{\partial r}\left(r^2\frac{\partial C_D}{\partial r}\right)\right] + 0.5r_1 + r_2 + r_3 \tag{50}$$

vii) $$\varepsilon\left(\frac{\partial C_G}{\partial t}\right) = D_e\left[\frac{1}{r^2}\frac{\partial}{\partial r}\left(r^2\frac{\partial C_G}{\partial r}\right)\right] + 2r_3 + r_4 \tag{51}$$

$$r_t = ({r_0}^3 - \left(\frac{m_0 - m}{m_0}\right){r_0}^3)^{\frac{1}{3}} \tag{52}$$

$$m_0 = \frac{C_{A0} + C_{B0}}{0.5\,MW_A + 0.5\,MW_B} \times V \tag{53}$$

$$m = \left(\frac{C_A}{MW_A} + \frac{C_B}{MW_B} + \frac{C_E}{MW_E} + \frac{C_F}{MW_F}\right) \times V \tag{54}$$

$$X = \left(\frac{m_0 - m}{m_0}\right) \times 100 \tag{55}$$

$$Sh = 2 + 0.6\,Re^{1/2}Pr^{1/3} \quad \text{(Bird, 2007)} \tag{56}$$

$$h = \frac{Sh \times D_e}{D_p} \times C_p \times \rho \tag{57}$$

Boundary Conditions:

At r = 0,

$$\frac{\partial T}{\partial r} = 0 \tag{58}$$

At r = r_t

$$\frac{\partial T}{\partial r} = -\frac{h}{k}\,\Delta T \tag{59}$$

At r = 0,

$$\frac{\partial C_A}{\partial r} = 0 \tag{60}$$

$$\frac{\partial C_B}{\partial r} = 0 \tag{61}$$

$$\frac{\partial C_C}{\partial r} = 0 \tag{62}$$

$$\frac{\partial C_D}{\partial r} = 0 \tag{63}$$

$$\frac{\partial C_E}{\partial r} = 0 \tag{64}$$

$$\frac{\partial C_F}{\partial r} = 0 \tag{65}$$

$$\frac{\partial C_G}{\partial r} = 0 \tag{66}$$

At r = r_t

$$\frac{\partial C_A}{\partial r} = 0 \tag{67}$$

$$\frac{\partial C_B}{\partial r} = 0 \tag{68}$$

$$\frac{\partial C_C}{\partial r} = -\frac{K}{D_e}\,\Delta C_C \tag{69}$$

$$\frac{\partial C_D}{\partial r} = -\frac{K}{D_e}\,\Delta C_D \tag{70}$$

$$\frac{\partial C_E}{\partial r} = 0 \tag{71}$$

$$\frac{\partial C_F}{\partial r} = 0 \tag{72}$$

$$\frac{\partial C_G}{\partial r} = -\frac{K}{D_e}\,\Delta C_G \tag{73}$$

K is convective mass transfer coefficient in m/s. Sh is Sherwood's number, Re is Reynold's number, Pr is Prandlt's number. Re is 0 as the particle is stationary. ϑ is the flowrate of gas in m^3/s. The total convective mass transfer coefficient is calculated as

$$K = \frac{Sh \times D_e}{D_p} + \frac{\vartheta}{4\pi {r_t}^2} \tag{74}$$

$$\Delta H = \sum {H_f}^0(products) - \sum {H_f}^0(reactants) \tag{75}$$

Initial Conditions:

$$C_{A0} = \frac{\rho_A}{MM_A} \tag{76}$$

$$C_{B0} = C_{A0} \tag{77}$$

$$C_C = 0 \tag{78}$$

$$C_D = 0 \tag{79}$$

$$C_E = 0 \tag{80}$$

$$C_E = 0 \tag{81}$$

$$C_F = 0 \tag{82}$$

$$C_G = 0 \tag{83}$$

Final Condition:

$$C_{Bb} = C_{B0} \tag{84}$$

$$C_{Cb} = 2C_{A0} \tag{85}$$

$$C_{Db} = C_{A0} \tag{86}$$

$$C_{Gb} = C_{A0} \tag{87}$$

Table 10: Parameters for Modelling

Parameter	Values	Units
T_b	800	ºC
D_p	53-125	µm
Time	Varied	min
C_{A0}	1.34×10^4	mol/m^3
C_p	160 (Kalyva, 2017)	J/mol K
D_e	3.6×10^{-10}	m^2/s
E_{a1}	77	kJ/mol
E_{a2}	102	kJ/mol
E_{a3}	107	kJ/mol
E_{a4}	110	kJ/mol
k_{eff}	0.6224 (Song, 1994)	W/m K
ΔH_1	119 (Kalyva, 2017)	kJ/mol
ΔH_2	664 (Kalyva, 2017)	kJ/mol
ΔH_3	370 (Kalyva, 2017)	kJ/mol
ΔH_4	146 (Kalyva, 2017)	kJ/mol

Table 11: Parameters for Modelling Continued

Parameter	Values	Units
n_1	1.1, 0.8, 0.8, 0.8 (after trial error)	
n_2	0, 0, 0.6, 0 (after trial error)	
T_0	298	ºC
ε	0.3	
R	8.314	J/mol K
V	100	µL
C_{B0}	1.34×10^4	mol/m^3
k_{01}	1.23×10^4	
k_{02}	1.01×10^5	
k_{03}	3.51×10^4	
k_{04}	3.17×10^4	
ϑ	200	m^3/s

IV.3.3 Matlab solver

The Matlab Solver ode23s was used to solve the above equations with the given parameters and the results obtained were compared to the actual data. The partial differential equations were converted to ordinary differential equations using numerical method of lines using a discretized space. The results from the model were compared with the original data for ratios 1AS:0KS, 1AS:1KS and 1AS:2KS. The n values were varied

for better fitting of the data to the model and the n values for reaction 1, reaction 2, reaction 3 and reaction 4 were found to be 1.1, 0.8, 1.4 and 0.8 respectively.

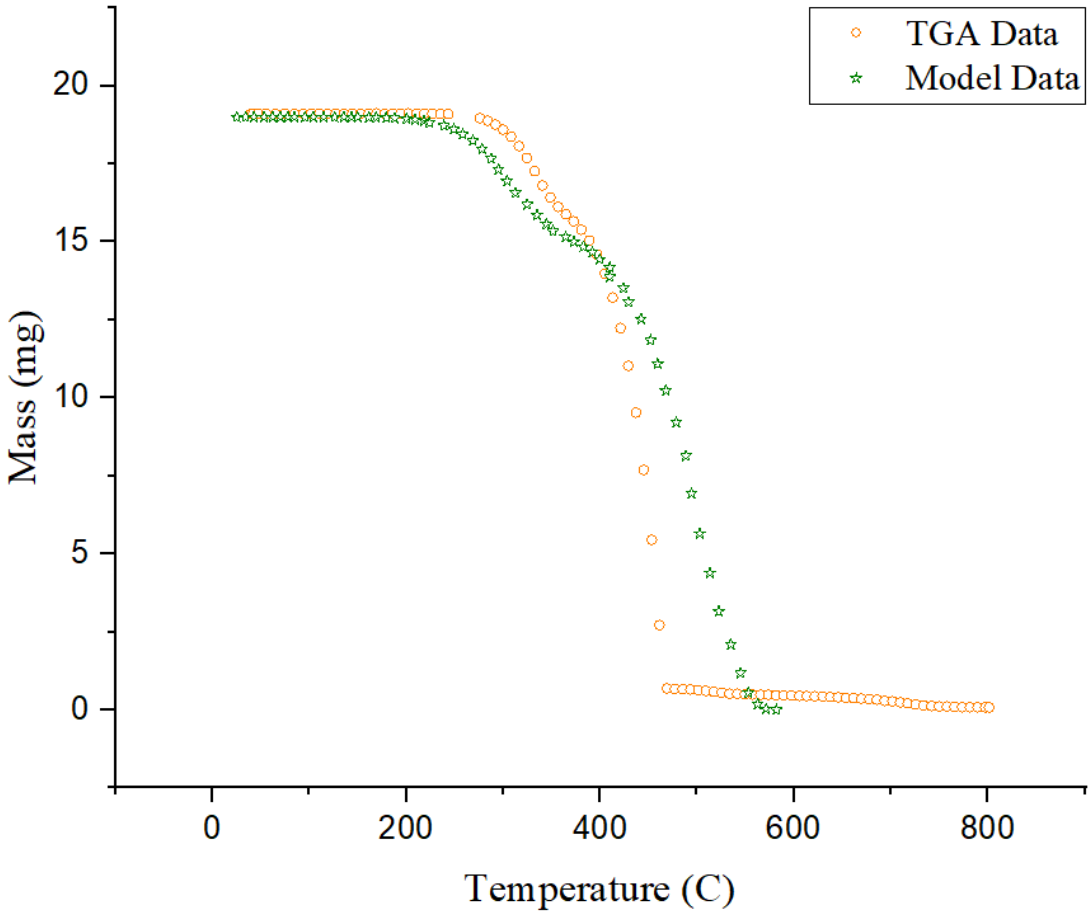

Figure 44: Mass Loss Comparison for Model Data with TGA Data for 1AS:0KS

As shown in Figure 44, the data obtained from the model with the above parameters was compared with the thermal analysis data for 1AS:0KS ratio. The graph showed that the results were comparable with normalized root mean square error 0.039. The results were compared for the ratios 1AS:1KS and 1AS:2KS as shown in Figure 45 and Figure 46 with normalized root mean square error 0.071 and 0.7 respectively.

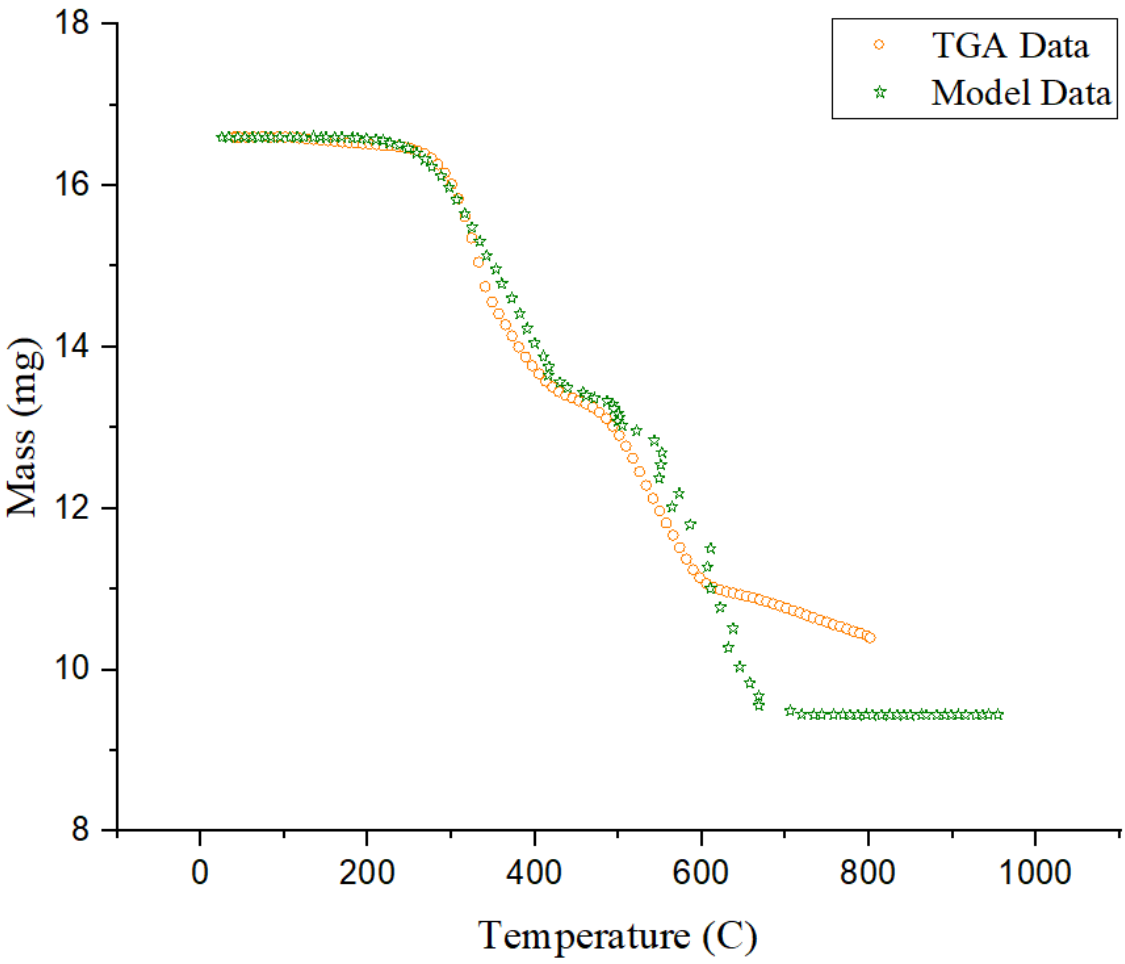

Figure 45: Mass Loss Comparison for Model Data with TGA Data for 1AS:1KS

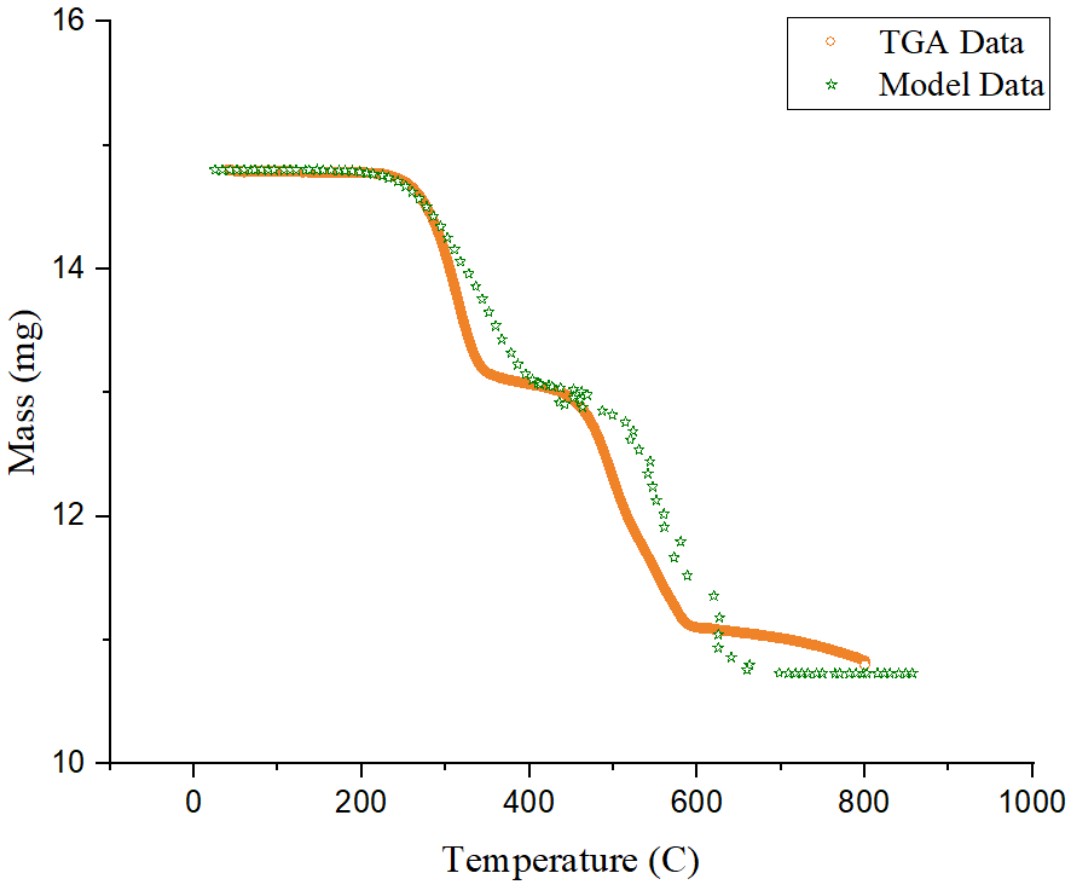

Figure 46: Mass Loss Comparison for Model Data with TGA Data for 1AS:2KS

The results obtained from the model were comparable with the TGA analysis data. Therefore, the reliability of the model was confirmed. The mass ratio change trend for the different ratios was seen from Figure 47, Figure 48 and Figure 49. The mass ratio changes closely relate to the trends that were suggested by the reactions.

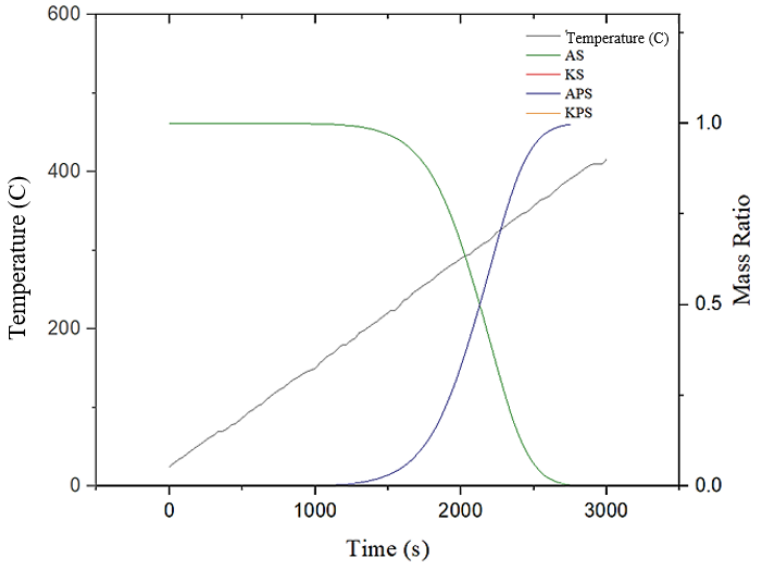

Figure 47: Change in Mass and Temperature with Time for 1AS:0KS

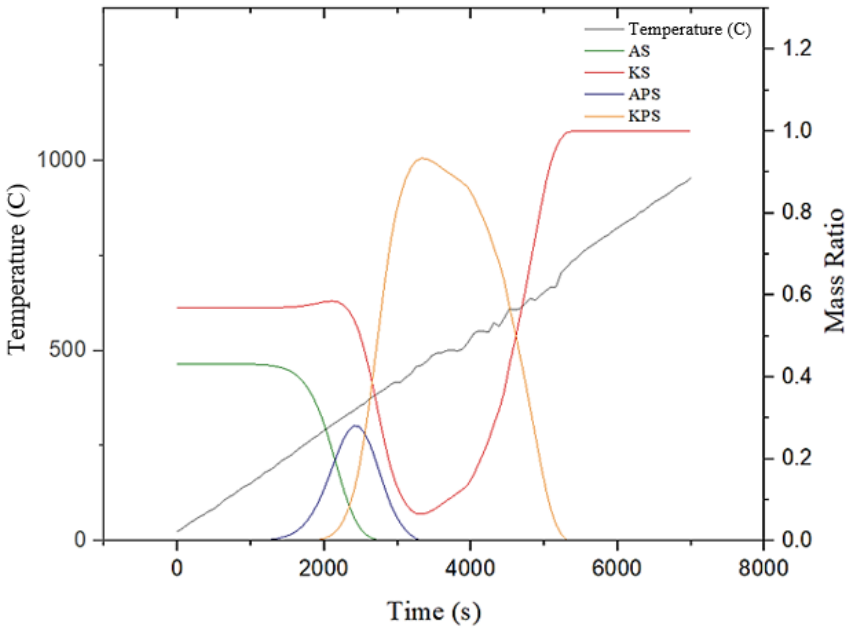

Figure 48: Change in Mass and Temperature with Time for 1AS:1KS

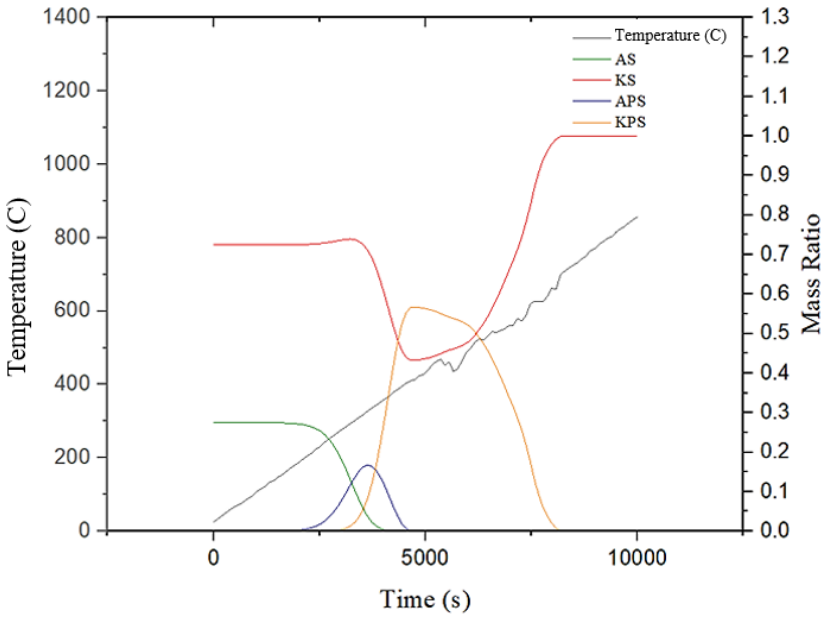

Figure 49: Change in Mass and Temperature with Time for 1AS:2KS

The sensitivity analysis based of KS ratio, heating rates and particle size was carried out.

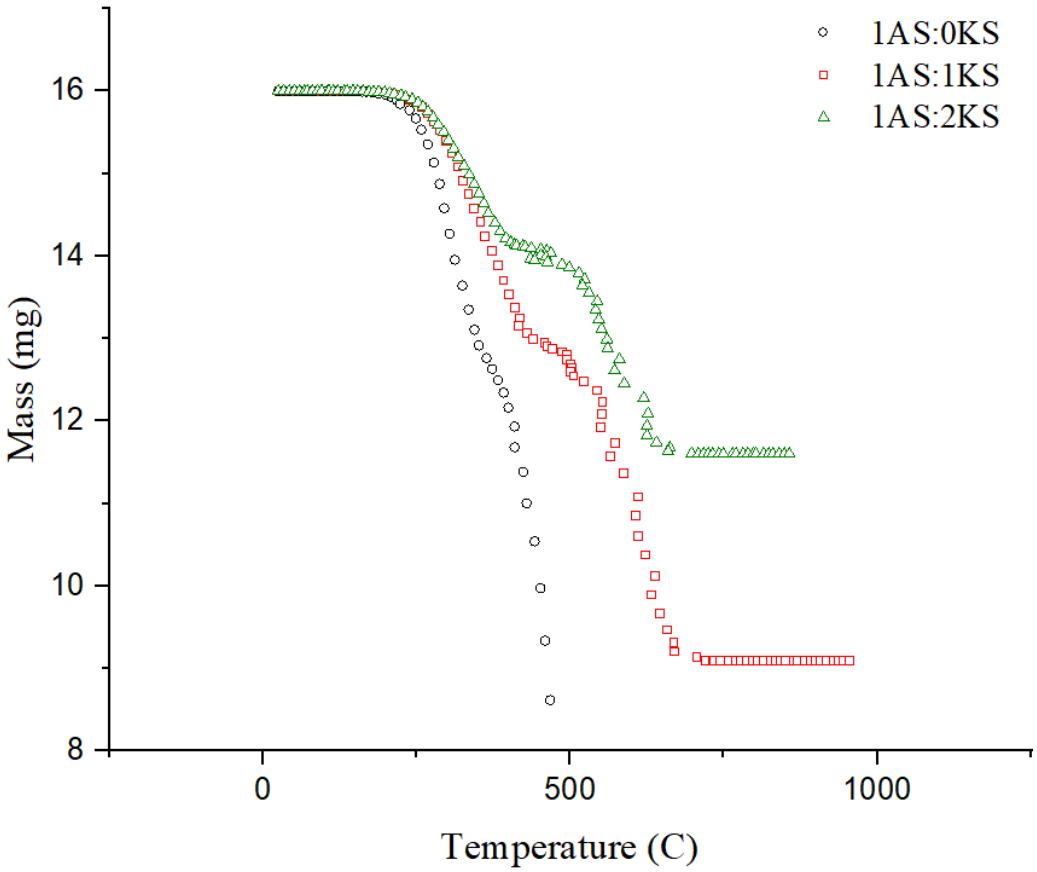

Figure 50: Mass Change with Temperature for Different AS:KS Ratios

Figure 50 showed that as the ratio of KS increased, the mass loss decreased as the initial reactant consisted more of KS, which does not decompose during the process. Moreover, the onset temperature of the KPS decomposition reaction increases as the excess amount of KS absorbs the SOx produced.

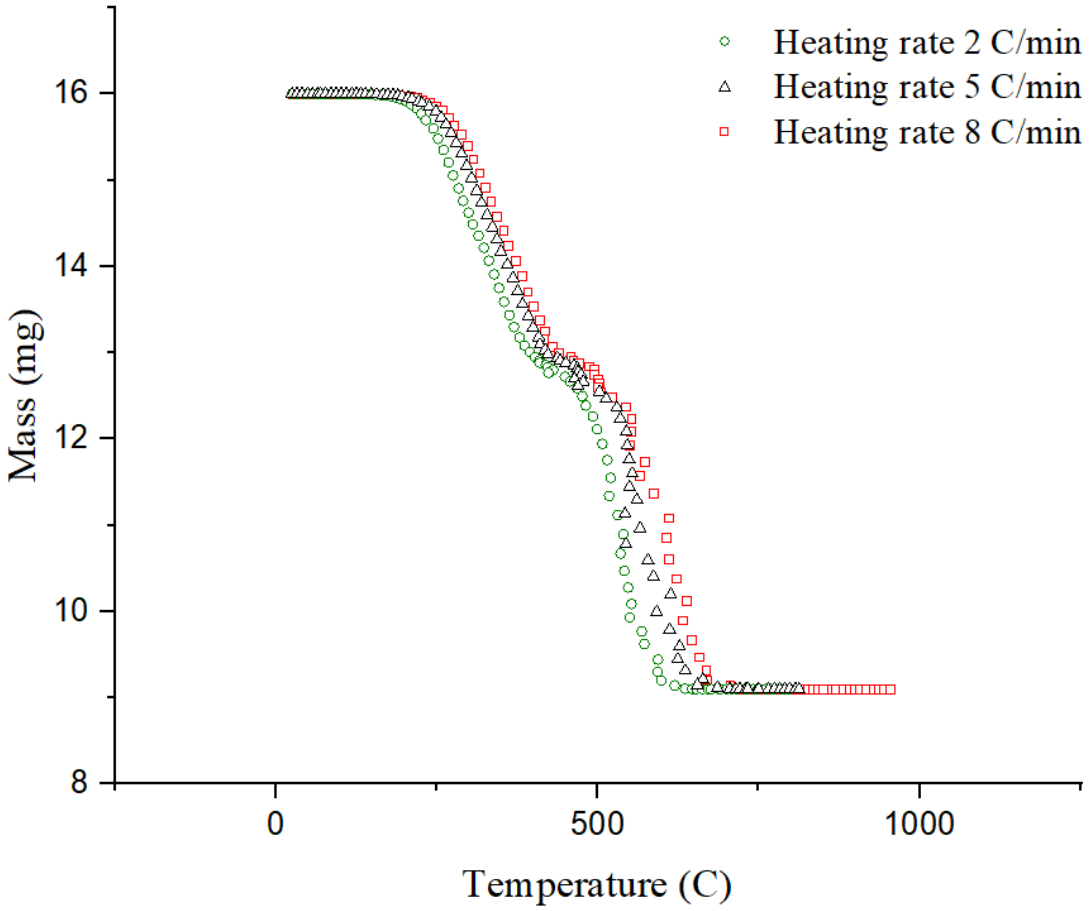

Figure 51: Mass Change with Temperature for Different Heating Rates

Figure 51 showed that as the heating rate increased the onset temperatures of the reactions increased.

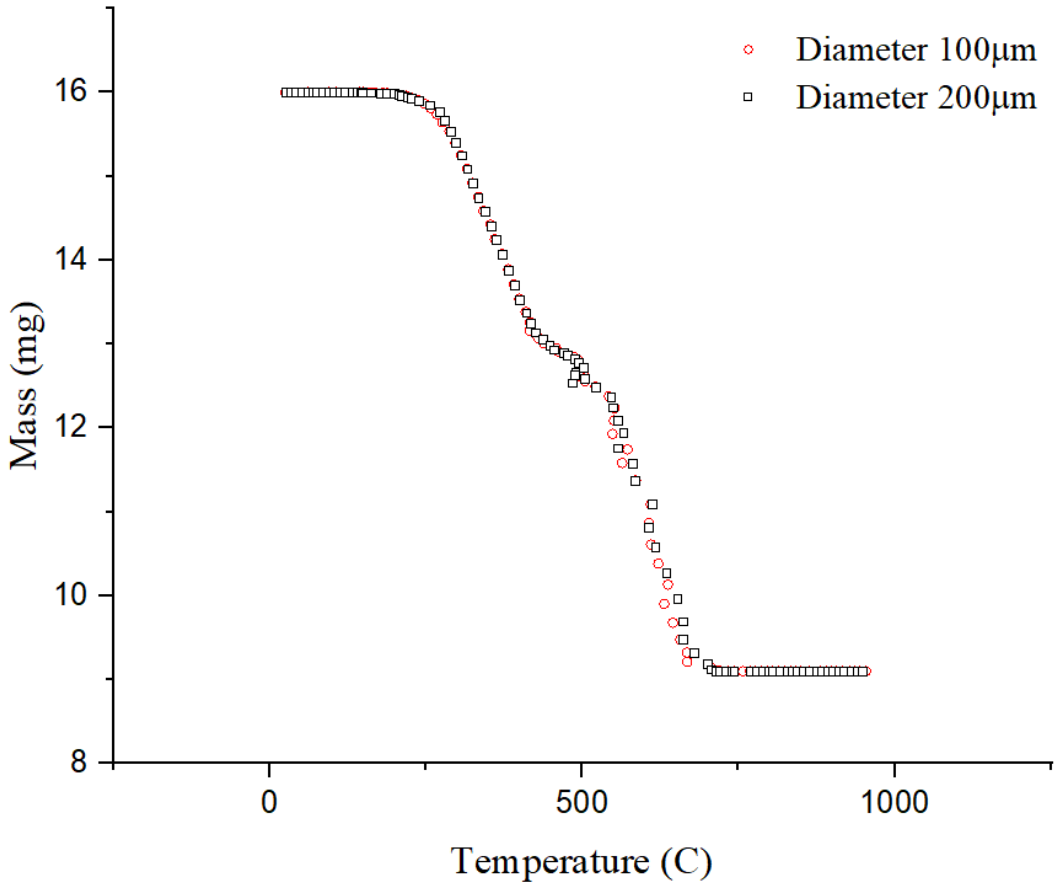

Figure 52: Mass Change with Temperature for Particles with Different Diameters

Figure 52 showed that as the particle diameter was changed from 100 to 200 µm, no significant changes were seen. However, further studies are required for conclusive results.

IV.4 Preliminary solar reactor results

The results obtained from the solar reactor were to determine if the response of the gases could be detected.

A sample of 12 mg pure AS was introduced in a capillary to replicate an aerosol phase. The sample was set to reach the set temperature of 600 ºC for 1 minute. Argon, the carrier gas was flowing at a flowrate of 142 mL/minute.

The number of particles in the capillary were calculated. The particles around the circumference, directly exposed were given by,

$$\text{Number of particles on the circumference} = \frac{\text{Circumference of capillary}}{\text{Diameter of particle}} \quad (88)$$

$$\text{Number of particles on the circumference} = \frac{2\pi\ (0.25\ \text{mm})}{125\ \mu\text{m}} = 12\ \text{particles}$$

$$\text{Total particles in a cross section} = \frac{\text{Cross sectional area of capillary}}{\text{Cross sectional area of particle}} \quad (89)$$

$$\text{Total particles in a cross section} = \frac{\pi\ (0.25\ \text{mm})^2}{\pi\ (62.5\ \mu\text{m})^2} = 16\ \text{particles}$$

Therefore, there were 16 particles of which 6 (Half of 12 since only the front half is directly radiated) were directly radiated and the rest were casted by another particle in front in each cross section. The bed was 1mm long. Therefore,

$$\text{Number of cross} - \text{sections} = \frac{\text{Length of bed}}{\text{Diameter of each particle}} \quad (90)$$

$$\text{Number of cross} - \text{sections} = \frac{1\text{mm}}{125\ \mu\text{m}} = 8\ \text{cross} - \text{sections}$$

Total particles were therefore, 128 particles (8×16).

The results obtained from the MS for reaction of the sample showed a release of major gases that were expected to be released. Ammonia and water increase in concentration while oxygen decreases due to purging of oxygen and other gases out of the system. However, sulfur dioxide was seen to be absent in this situation due to lack of catalyst to break down sulfur tri-oxide. In the next experiments, sulfur di-oxide will be replaced by sulfur tri-oxide to confirm the presence of sulfur tri-oxide. Hence, it was concluded that the desired gases can be detected using MS.

The gas analyzer connected detects NH_3. NH_3 peak was seen at two distinct time steps, first corresponded to the NH_3 release while the second corresponded to purge of system while releasing the gases as seen from Figure 53. The results obtained were converted to moles of NH_3. It was seen that 1.5 mol of NH_3 was produced during the experiment. Further investigation will be carried out to quantitatively determine the amount of NH_3 produced. Therefore, the gas analyzer showed promising results for detection of NH_3 which can be used to quantitatively determine the amount of NH_3 in the system.

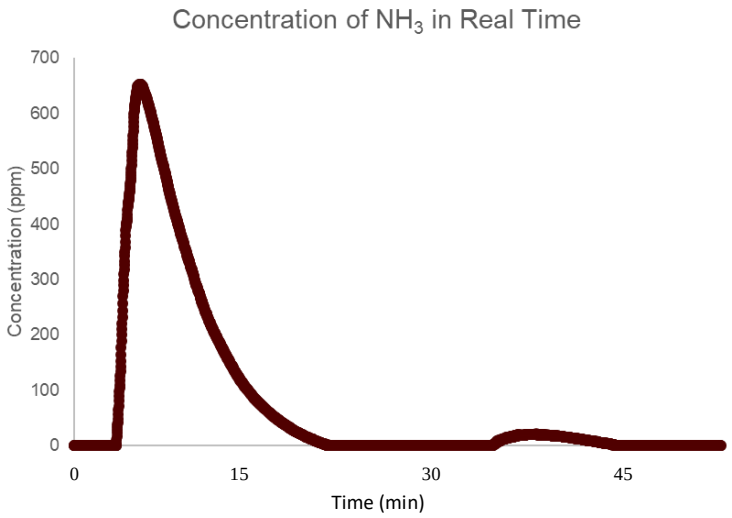

Figure 53: Gas Analyzer Results for Solar Experiment

The remaining sample was tested on ATR and compared with pure solids to determine the solid remaining as seen in Figure 54. This was confirmed by the software already calibrated. Figure 54 showed pure AS, KS, AHS and KPS peak compared with the sample peaks. It was seen that the sample consisted of peaks relative to AHS at 800,

1000, 1200, 3000 cm^{-1}. The peak at 1400 cm^{-1} was a characteristic feature of AS. Moreover, the other peaks seemed to be a combination of both AS and AHS.

From the analysis done automatically by comparing the sample to calibration standards, it was seen that most of the AS was converted to AHS. However, an error of 45% in reading KPS was seen due to the overlap of few peaks of APS and hence it was concluded that the software required more calibration standards to accurately differentiate KPS from the other peaks. The calibration standards for APS have to be included in the software.

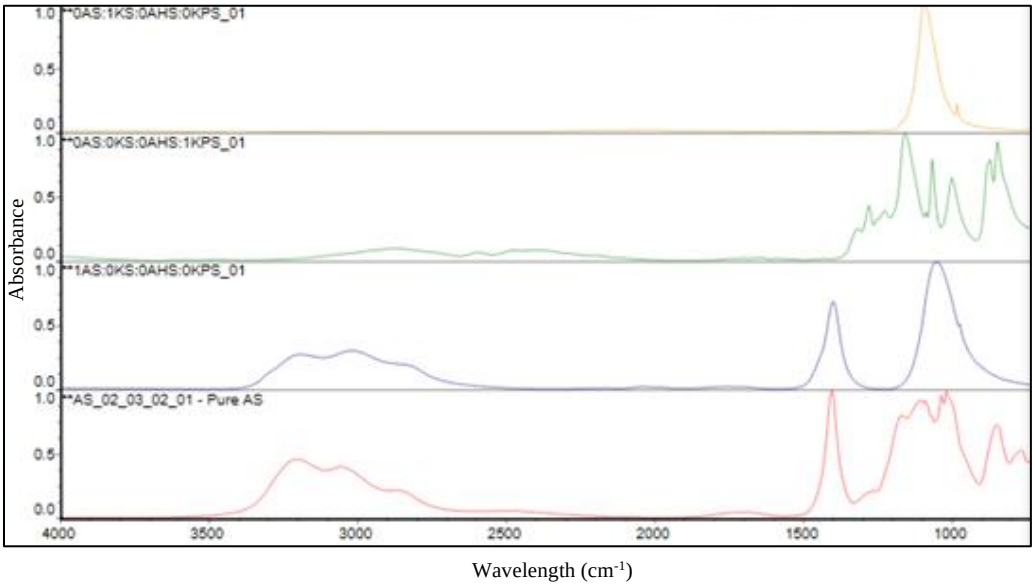

Figure 54: ATR Results Compared to Standards

The further tests for the aerosol reactor could not be carried out due to the restrictions placed by the pandemic. However, the tests in the aerosol reactor and results requiring verification will be carried forward by the team in future. The model developed and the kinetic parameters identified will act as the basis of further research.

CHAPTER V

CONCLUSIONS AND FUTURE RECOMMENDATIONS

In conclusion, the behavior of HySA thermochemical water splitting cycle was tested for its kinetics and model in aerosol phase.

The model of the particle was prepared as a result of heat transfer, mass transfer and reaction effects in the particle. The SEM and PSA results showed that the particles present were in micrometer scale. Therefore, samples with sizes 53-125 µm diameter were chosen. The model considered a particle of AS undergoing thermal decomposition in the presence of KS using shrinking core model. The differential equations formed were solved on MATLAB using numerical methods of lines to convert partial differential equations to ordinary differential equations. The ordinary differential equations were solved using ode23 solver and the results were presented.

The kinetic parameters of the reactions participating were calculated to incorporate in the model. The TGA alongside the MS and FT-IR were used to determine the kinetics. The MS qualitatively determined the gases present in each step of the reaction, the TGA results were used to confirm the mass balance between theoretical and experimental values and the FT-IR results were used to determine the realistic values of the gases produced. First, the reactions taking place were confirmed. It was seen that the first reaction yields APS, W and A on decomposition of AS in presence of KS at around 265 ºC. This reaction was of order 1.1 and had activation energy of 77 kJ/mol and pre-exponential factor 1.51×10^4 s^{-1}. APS further decomposed to NH_3, SOx and H_2O in absence of KS. This reaction was of order 0.8 and had activation energy of 102 kJ/mol and pre-exponential factor 1.01

$\times 10^5$ s^{-1}. APS further decomposed to NH_3 and H_2O in presence of KS which converts to KPS at around 430 ºC. This reaction was of order 1.4 and had activation energy of 107 kJ/mol and pre-exponential factor 3.51×10^4 s^{-1}. Finally, KPS decomposed to KS and SOx at around 600 ºC. This reaction was of order 0.8 and had activation energy of 110 kJ/mol and pre-exponential factor 3.17×10^4 s^{-1}.

The effects of different parameters were studied on the sample. It was seen that the slight change in sample mass, heating rate and particle size did not change the reaction steps taking place. The crystallized samples were compared to directly crushed samples. The samples showed new peaks after recrystallization. However, further tests are required for proper conclusions. The variation in ratio of KS in the sample showed that as the mass of KS increased compared to mass of AS, the NH_3 and SOx producing steps were more distinctly seen. Moreover, SOx was produced with a delay as a result of addition of more KS.

The setup prepared for solar reactor experiments with a capillary mimicking the aerosol phase could be used to study the behavior of the reaction in aerosol phase. The number of particles in the system were approximated as 128 particles of which $1/3^{rd}$ were directly exposed to radiation while $2/3^{rd}$ were shadowed by other particles. The MS could be used to provide qualitative results about the gases present in the system while the gas analyzer could be used to quantitatively determine the amount of ammonia produced during the reaction. The solid that was left behind was tested under ATR to determine the solids left. However, the ATR software requires more calibration standards to accurately determine the solids present. Therefore, the combination of MS, gas analyzer and ATR

would be sufficient to determine the outcome of the reaction at every step in the aerosol reactor.

In future work, the kinetics determined, and the model created will be used to better understand the reactions taking place in aerosol phase. The tests will be carried out in a capillary setup as shown in this study and the results will be verified with the results obtained from thermal analysis. Further analysis on sample will be carried out to determine the quantities of new compounds present on recrystallization of the particles. The hypothesis of the process working efficiently in the aerosol phase will be verified.

REFERENCES

Albert B. Welty, J., Westfield, N.J. (1970). United States Patent No. 3674427

Amiri, A., Bekker, A. V., Ingram, G. D., Livk, I., & Maynard, N. E. (2013). A 1-D non-isothermal dynamic model for the thermal decomposition of a gibbsite particle. *Chemical Engineering Research and Design, 91*(3), 485-496. doi:10.1016/j.cherd.2012.10.002

Amiri, A., Ingram, G. D., Bekker, A. V., Livk, I., & Maynard, N. E. (2013). A multi-stage, multi-reaction shrinking core model for self-inhibiting gas–solid reactions. *Advanced Powder Technology, 24*(4), 728-736. doi:10.1016/j.apt.2013.01.016

Amiri, A., Ingram, G. D., Maynard, N. E., Livk, I., & Bekker, A. V. (2014). An Unreacted Shrinking Core Model for Calcination and Similar Solid-to-Gas Reactions. *Chemical Engineering Communications, 202*(9), 1161-1175. doi:10.1080/00986445.2014.910771

Ammar Khawam, D. R. F. (2006). Solid-State Kinetic Models Basics and Mathematical Fundamentals. *J. Phys. Chem. B, 110*(35), 17315-17328.

Anabel, F., Celia, R., Germán, M., & Rosa, R. (2018). Determination of effective moisture diffusivity and thermodynamic properties variation of regional wastes under different atmospheres. *Case Studies in Thermal Engineering, 12*, 248-257. doi:10.1016/j.csite.2018.04.015

Angelopoulos, P. M., Balomenos, E., & Taxiarchou, M. (2016). Thin-Layer Modeling and Determination of Effective Moisture Diffusivity and Activation Energy for Drying of Red Mud from Filter Presses. *Journal of Sustainable Metallurgy, 2*(4), 344-352. doi:10.1007/s40831-016-0055-7

Babinski, P., Sciazko, M., & Ksepko, E. (2017). Limitation of thermogravimetry for oxy-combustion analysis of coal chars. *Journal of Thermal Analysis and Calorimetry, 133*(1), 713-725. doi:10.1007/s10973-017-6782-6

Bird, R. B., Stewart, W. E., & Lightfoot, E. N. (2007). *Transport phenomena. Rev. 2nd ed. R. Byron Bird, Warren E. Stewart, Edwin N. Lightfoot* (Rev. 2nd ed. ed.): J. Wiley.

Brown, M. E. (1998). *Handbook of Thermal Analysis and Calorimetry* (Vol. 1): ELSEVIER.

Brown, M. E. (2004). *Introduction To Thermal Analysis* (Vol. 1): Kluwer Academic Publisher.

Dahl, J., Buechler, K., Finley, R., Stanislaus, T., Weimer, A., Lewandowski, A., . . . Schneider, A. (2004). Rapid solar-thermal dissociation of natural gas in an aerosol flow reactor. *Energy, 29*, 715-725. doi:10.1016/S0360-5442(03)00179-8

Ding, Y., & Riediker, M. (2016). A System to Create Stable Nanoparticle Aerosols from Nanopowders. *J Vis Exp*(113). doi:10.3791/54414

Fedunik-Hofman, L., Bayon, A., & Donne, S. W. (2019). Kinetics of Solid-Gas Reactions and Their Application to Carbonate Looping Systems. *Energies, 12*(15). doi:10.3390/en12152981

Felix Trombe, L. G. I. C. R. a. J. F. R. (1971). FIRST RESULTS OBTAINED WITH THE 1000 KW SOLAR FURNACE. *Solar Energy, 15*, 63-66.

Funke, H. H., Diaz, H., Liang, X., Carney, C. S., Weimer, A. W., & Li, P. (2008). Hydrogen generation by hydrolysis of zinc powder aerosol. *International Journal of Hydrogen Energy, 33*(4), 1127-1134. doi:10.1016/j.ijhydene.2007.12.061

G. Bayer, G. K. a. M. M. V. (1981). Reactions of Ammonium Sulfates with Kaolinite and Other Silicate and Oxide Minerals. *Clay Minerals, 17*, 271-283.

G. Samdani, S. M., A. Ganesh, P. Aghalayam, R. K. Sapru, D. K. Mathur. (2012). *Diffusion Modeling in TGA in Context of CO2 Gasification of Char.* Paper presented at the COMSOL Conference, Bangalore.

Gellings, K. J. D. V. a. P. J. (1969). The thermal Decomposition of Potassium and Sodium Pyrosulfate. *J, inorg, nucl. Chem, 31*, 1307 to 1131.

Halstead, W. D. (1970). Thermal Decomposition of Ammonium Sulphate. *J. appl. Chem.,, 20*, 129-132.

Jiang, L., Yang, X. R., Gao, X., Xu, Q., Das, O., Sun, J. H., & Kuzman, M. K. (2020). Pyrolytic Kinetics of Polystyrene Particle in Nitrogen Atmosphere: Particle Size Effects and Application of Distributed Activation Energy Method. *Polymers (Basel), 12*(2). doi:10.3390/polym12020421

K. H. Lau, D. C., and D. L. Hildenbrand (1979). Effusion Studies of the Vaporization Decomposition of Potassium Sulfate. *Journal of The Electrochemical Society, 126*, 490-495.

Kalyva, A. E., Vagia, E. C., Konstandopoulos, A. G., Srinivasa, A. R., T-Raissi, A., Muradov, N., & Kakosimos, K. E. (2017). Particle model investigation for the

thermochemical steps of the sulfur–ammonia water splitting cycle. *International Journal of Hydrogen Energy, 42*(6), 3621-3629. doi:10.1016/j.ijhydene.2016.09.003

Kanapilly, K. W. T. a. G. M. (1977a). Generation and Characterization of Submicron Ammonium Sulfate and Ammonium Hydrogen Sulfate Aerosols. *Atmospheric Environment, 12*, 1623-1629.

Kanapilly, K. W. T. a. G. M. (1977b). Generation and Characterization of Submicron Ammonium Sulfate and Ammonium Hydrogen Sulfate Aerosols *Atmospheric Environment, 12*, 1623-1629.

Levenspiel, O. (1999). *Chemical Reaction Engineering* (3 ed.): John Wiley & Sons.

Maheshwari Jariwala, J. C., and Dale J. Le Captain. (2007). In Situ Raman Spectroscopic Analysis of the Regeneration of Ammonium Hydrogen Sulfate from Ammonium Sulfate. *Ind. Eng. Chem. Res., 46*, 4900-4905.

Marin, G. D., Wang, Z., Naterer, G. F., & Gabriel, K. (2012a). Coupled multiphase heat and mass transfer of a solid particle decomposition reaction with phase change. *International Journal of Heat and Mass Transfer, 55*(15-16), 4323-4333. doi:10.1016/j.ijheatmasstransfer.2012.03.081

Marin, G. D., Wang, Z., Naterer, G. F., & Gabriel, K. (2012b). Immersed particles of a multiphase reacting flow with chemical decomposition in the stokes flow regime. *International Journal of Heat and Mass Transfer, 55*(25-26), 8139-8148. doi:10.1016/j.ijheatmasstransfer.2012.08.053

Mazloomi, K., & Gomes, C. (2012). Hydrogen as an energy carrier: Prospects and challenges. *Renewable and Sustainable Energy Reviews, 16*(5), 3024-3033. doi:10.1016/j.rser.2012.02.028

Nakhaei, M., Wu, H., Grévain, D., Jensen, L. S., Glarborg, P., Clausen, S., & Dam–Johansen, K. (2018). Experiments and modeling of single plastic particle conversion in suspension. *Fuel Processing Technology, 178*, 213-225. doi:10.1016/j.fuproc.2018.05.003

Perkins, C., Lichty, P., & Weimer, A. W. (2007). Determination of aerosol kinetics of thermal ZnO dissociation by thermogravimetry. *Chemical Engineering Science, 62*(21), 5952-5962. doi:10.1016/j.ces.2007.06.039

R. I. Dearnaley, D. H. K., and D. J. Rogers. (1983). Molten Lithium Sulfate-Sodium Sulfate-Potassium Sulfate Eutectic Reactions of Some Sulfur Compounds by R. I. DEARNALEY, D. H. KERRIDGE, and D. J. ROGERS, 1983.pdf>. *Inorgancic Chemistry, 22*, 3242-3247.

Sánchez, S., Méndez, F., & Bautista, O. (2014). Critical Damkhöler number for the thermal decomposition of methane gas in a fluid-wall aerosol flow reactor. *Energy Conversion and Management, 77*, 152-162. doi:10.1016/j.enconman.2013.09.025

Saxena, A. R. a. S. C. (1976). Single Nonisothermal Noncatalytic Solid-Gas Reaction Effect of Changing Particle Size. *Ind. Eng. Chem., Process Des. Dev., 15*, 343-350.

Scheffe, J. R., Welte, M., & Steinfeld, A. (2014). Thermal Reduction of Ceria within an Aerosol Reactor for H2O and CO2Splitting. *Industrial & Engineering Chemistry Research, 53*(6), 2175-2182. doi:10.1021/ie402620k

SEGAL, E. (2011). RATE EQUATIONS OF SOLID STATE REACTIONS. EUCLIDEAN AND FRACTAL MODELS *Revue Roumaine de Chimie, 57*, 491-493.

Sinnott, R. K. (2017). *Coulson and Richardson Chemical Engineering* (R. V. a. S. N. G. R. Ravi Ed. 4 ed. Vol. 3A): John Fedor.

Song, X., Zhao, J., Li, Y., Sun, Z., & Yu, J. (2013). Thermal decomposition mechanism of ammonium sulfate catalyzed by ferric oxide. *Frontiers of Chemical Science and Engineering, 7*(2), 210-217. doi:10.1007/s11705-013-1320-y

Steinfeld, P. H. M. P. (1999). THE PRODUCTION OF ZINC BY THERMAL DISSOCIATION OF ZINCOXIDE—SOLAR CHEMICAL REACTOR DESIGN. *Solar Energy, 67*, 161–167.

T-Raissi, A., Muradov, N., Huang, C., & Adebiyi, O. (2007). Hydrogen From Solar Via Light-Assisted High-Temperature Water Splitting Cycles. *Journal of Solar Energy Engineering, 129*(2), 184-189. doi:10.1115/1.2710493

Timilsina, G. R., Kurdgelashvili, L., & Narbel, P. A. (2012). Solar energy: Markets, economics and policies. *Renewable and Sustainable Energy Reviews, 16*(1), 449-465. doi:10.1016/j.rser.2011.08.009

Urano, R. K. a. K. (1970). Mechanism, Kinetics, and Equilibrium of Thermal Decomposition of Ammonium Sulfate. *Ind. Eng. Chem. Process Des. Develop, 9*(4), 489-494.

W.E. Wentworth, C. J. C., C.F. Batten, E.C.M. Ch. (1979). The Storage and Regeneration of High Temperature Thermal Energy by Means of Reversible Chemical Reactions—The Ammonium Hydrogen Sulfate System. *THE AMERICAN SOCIETY OF MECHANICAL ENGINEERS*.

Wang, M. K. W. (2012). *Study of the Thermochemistry for Oxygen Production for a Solar Sulfur-Ammonia Water-Splitting Process* (Master of Science in Chemical Engineering). University of California, San Diego.

Welte, M., Barhoumi, R., Zbinden, A., Scheffe, J. R., & Steinfeld, A. (2016). Experimental Demonstration of the Thermochemical Reduction of Ceria in a Solar Aerosol Reactor. *Ind Eng Chem Res*, *55*(40), 10618-10625. doi:10.1021/acs.iecr.6b02853

Wentworth, W. E. (1992). *Thermochemical Cycles for Energy Storage Thermal Decomposition of ZnCO4 Systems*. Retrieved from

APPENDIX

No.	Function name	Mechanism	Integral function G(α)	Differential function f(α)
1	Parabolic line law	One-dimensional diffusion	α^2	$\frac{1}{2}\alpha^{-1}$
2	Valensi equation	Two-dimensional diffusion	$\alpha+(1-\alpha)\ln(1-\alpha)$	$[-\ln(1-\alpha)]^{-1}$
3	Ginstling-Brounstein equation	Three-dimensional diffusion (cylindrical symmetry)	$1-\frac{2}{3}\alpha-(1-\alpha)^{\frac{2}{3}}$	$\frac{3}{2}\left[(1-\alpha)^{-\frac{1}{3}}-1\right]^{-1}$
4	Jander equation	Three-dimensional diffusion (spherical symmetry)	$\left[1-(1-\alpha)^{\frac{1}{3}}\right]^2$	$\frac{3}{2}(1-\alpha)^{\frac{2}{3}}\left[1-(1-\alpha)^{\frac{1}{3}}\right]^{-1}$
5	Jander equation	Three-dimensional diffusion	$\left[1-(1-\alpha)^{\frac{1}{3}}\right]^{\frac{1}{2}}$	$6(1-\alpha)^{\frac{2}{3}}\left[1-(1-\alpha)^{\frac{1}{3}}\right]^{\frac{1}{2}}$
6	Jander equation	Three-dimensional diffusion	$\left[1-(1-\alpha)^{\frac{1}{3}}\right]^{\frac{1}{2}}$	$4(1-\alpha)^{\frac{1}{3}}\left[1-(1-\alpha)^{\frac{1}{3}}\right]^{\frac{1}{2}}$
7	Inverse Jander equation	Three-dimensional diffusion	$\left[(1+\alpha)^{\frac{1}{3}}-1\right]^2$	$\frac{3}{2}(1+\alpha)^{\frac{2}{3}}\left[(1+\alpha)^{\frac{1}{3}}-1\right]^{-1}$
8	Zhuralev-Lesokin-Tempelman equation	Three-dimensional diffusion	$\left[(1-\alpha)^{-\frac{1}{3}}-1\right]^2$	$\frac{3}{2}(1-\alpha)^{\frac{4}{3}}\left[(1-\alpha)^{-\frac{1}{3}}-1\right]^{-1}$
9	Mample power theorem	Nuclei growth ($n=1$)	$-\ln(1-\alpha)$	$1-\alpha$
10	Avrami-Erofee equation	Random nucleation and nuclei growth ($n=2/3$)	$[-\ln(1-\alpha)]^{\frac{2}{3}}$	$\frac{3}{2}(1-\alpha)[-\ln(1-\alpha)]^{\frac{1}{2}}$
11	Avrami-Erofee equation	Random nucleation and nuclei growth ($n=1/2$)	$[-\ln(1-\alpha)]^{\frac{1}{2}}$	$2(1-\alpha)[-\ln(1-\alpha)]^{\frac{1}{2}}$
12	Avrami-Erofee equation	Random nucleation and nuclei growth ($n=1/3$)	$[-\ln(1-\alpha)]^{\frac{1}{3}}$	$3(1-\alpha)[-\ln(1-\alpha)]^{\frac{2}{3}}$
13	Avrami-Erofee equation	Random nucleation and nuclei growth ($n=4$)	$[-\ln(1-\alpha)]^4$	$\frac{1}{4}(1-\alpha)[-\ln(1-\alpha)]^{-3}$
14	Avrami-Erofee equation	Random nucleation and nuclei growth ($n=1/4$)	$[-\ln(1-\alpha)]^{\frac{1}{4}}$	$4(1-\alpha)[-\ln(1-\alpha)]^{\frac{3}{4}}$
15	Avrami-Erofee equation	Random nucleation and nuclei growth ($n=2$)	$[-\ln(1-\alpha)]^2$	$\frac{1}{2}(1-\alpha)[-\ln(1-\alpha)]^{-1}$
16	Avrami-Erofee equation	Random nucleation and nuclei growth ($n=3$)	$[-\ln(1-\alpha)]^3$	$\frac{1}{3}(1-\alpha)[-\ln(1-\alpha)]^{-2}$
17	Contracting cylinder (area)	Phase boundary reaction, (cylindrical symmetry)	$1-(1-\alpha)^{\frac{1}{2}}$	$2(1-\alpha)^{\frac{1}{2}}$
18	Reaction order	Chemical reaction	$1-(1-\alpha)^3$	$\frac{1}{3}(1-\alpha)^{-2}$
19	Reaction order	Chemical reaction	$1-(1-\alpha)^2$	$\frac{1}{2}(1-\alpha)^{-1}$
20	Reaction order	Chemical reaction	$1-(1-\alpha)^4$	$\frac{1}{4}(1-\alpha)^{-3}$
21	Contracting sphere (volume)	Phase boundary reaction, (spherical symmetry)	$1-(1-\alpha)^3$	$3(1-\alpha)^{\frac{2}{3}}$
22	Reaction order	Chemical reaction	$1-(1-\alpha)^{\frac{1}{2}}$	$4(1-\alpha)^{\frac{3}{4}}$
23	Mampel Power theorem	Phase boundary reaction, (One-dimension) $n=1$	$1-(1-\alpha)^1=\alpha$	1
24	Mampel Power theorem	Exponential nucleation ($n=3/2$)	$\alpha^{\frac{3}{2}}$	$\frac{2}{3}\alpha^{-\frac{1}{2}}$
25	Mampel Power theorem	Exponential nucleation ($n=1/2$)	$\alpha^{\frac{1}{2}}$	$2\alpha^{\frac{1}{2}}$
26	Mampel Power theorem	Exponential nucleation ($n=1/3$)	$\alpha^{\frac{1}{3}}$	$3\alpha^{\frac{2}{3}}$
27	Mampel Power theorem	Exponential nucleation ($n=1/4$)	$\alpha^{\frac{1}{4}}$	$4\alpha^{\frac{3}{4}}$
28	Second order	Chemical reaction	$(1-\alpha)^{-1}$	$(1-\alpha)^2$
29	Reaction order	Chemical reaction	$(1-\alpha)^{-1}-1$	$(1-\alpha)^2$
30	2/3 order	Chemical reaction	$(1-\alpha)^{-\frac{1}{2}}$	$2(1-\alpha)^{\frac{3}{2}}$

Figure 55: Reactions models (Song, 2013)

Reaction Model	Code	$f(\alpha)$	$g(\alpha)$
Zero-order	F0	1	α
First-order	F1	$(1-\alpha)$	$-\ln(1-\alpha)$
Second-order	F2	$(1-\alpha)^2$	$\frac{1}{(1-\alpha)}-1$
Third-order	F3	$(1-\alpha)^3$	$\frac{1}{2}\left[(1-\alpha)^{-2}-1\right]$
Avrami-Erofeyev	A2	$2(1-\alpha)[-\ln(1-\alpha)]^{1/2}$	$[-\ln(1-\alpha)]^{1/2}$
Avrami-Erofeyev	A3	$3(1-\alpha)[-\ln(1-\alpha)]^{2/3}$	$[-\ln(1-\alpha)]^{1/3}$
Avrami-Erofeyev	A4	$4(1-\alpha)[-\ln(1-\alpha)]^{3/4}$	$[-\ln(1-\alpha)]^{1/4}$
Prout-Tompkins	B1	$\alpha(1-\alpha)$	$\ln[\alpha(1-\alpha)]+c^{\alpha}$
Power law	P2	$2\alpha^{1/2}$	$\alpha^{1/2}$
Contracting area	R2	$2(1-\alpha)^{1/2}$	$1-(1-\alpha)^{1/2}$
Contracting volume	R3	$3(1-\alpha)^{2/3}$	$1-(1-\alpha)^{1/3}$
1-D diffusion	D1	$1/(2\alpha)$	α^2
2-D diffusion	D2	$-\ln(1-\alpha)$	$((1-\alpha)\ln(1-\alpha))+\alpha$
3-D diffusion	D3	$\frac{3(1-\alpha)^{2/3}}{2-(1-\alpha)^{1/3}}$	$(1-(1-\alpha)^{1/3})^2$
Ginstling-Brounshtein	D4	$\frac{3}{2}\frac{1}{(1-\alpha)^{-1/3}-1}$	$1-(2/3)\alpha-(1-\alpha)^{2/3})$

Figure 56: Reaction models continued (Fedunik-Hofman, 2019)

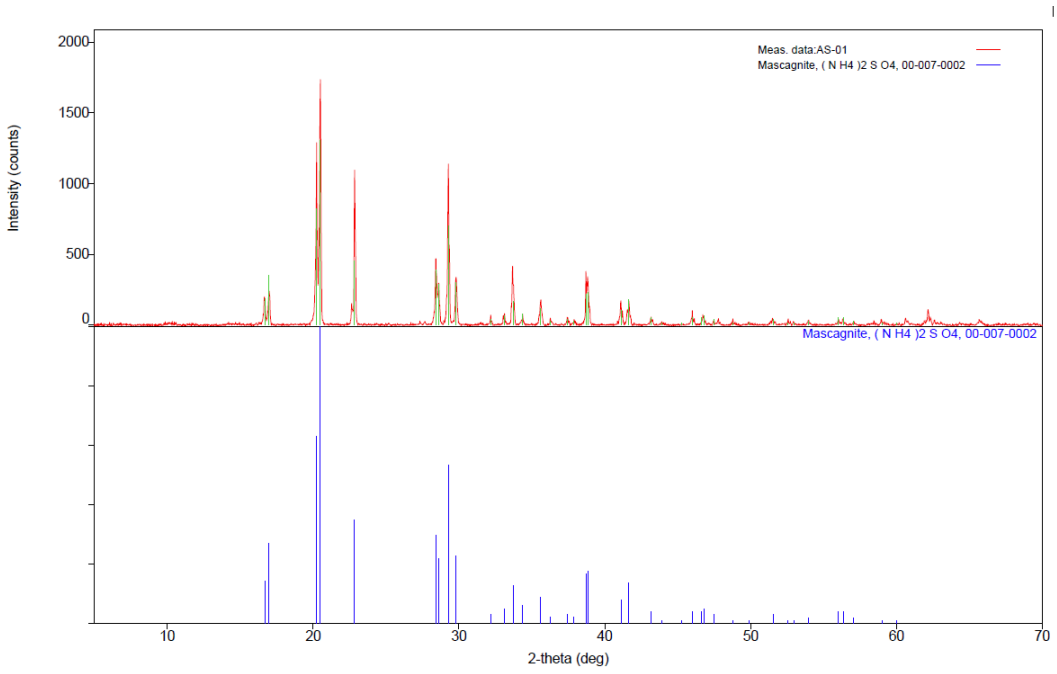

Figure 57: AS_01 compared with pure AS-XRD peaks

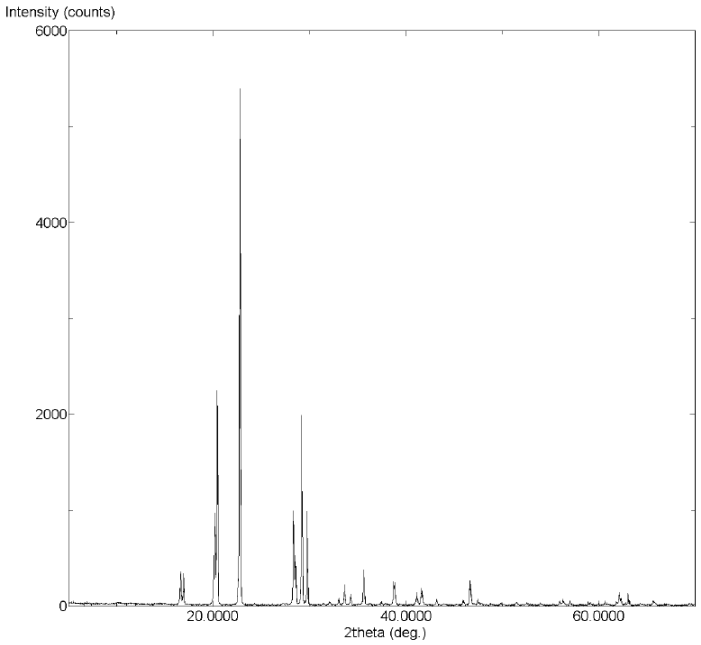

Figure 58: AS_03 XRD peaks similar to AS_01

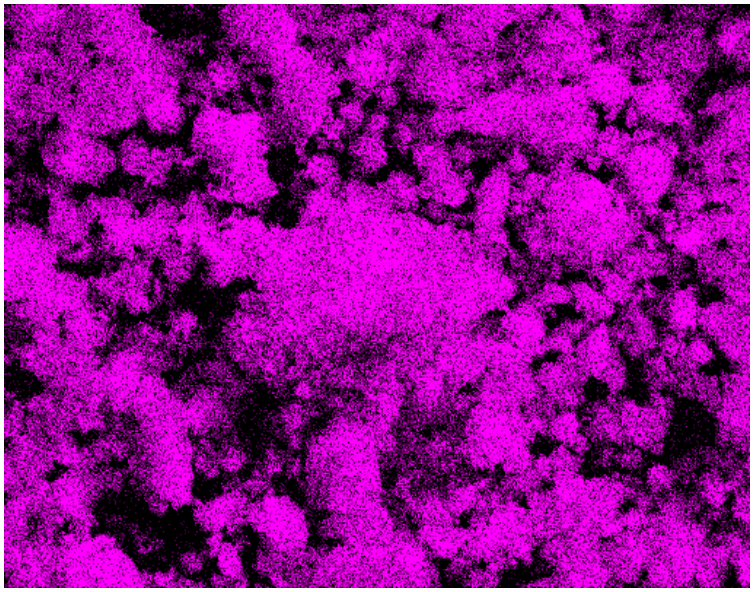

Figure 59: EDS results for TGA2_15 (Only K present)

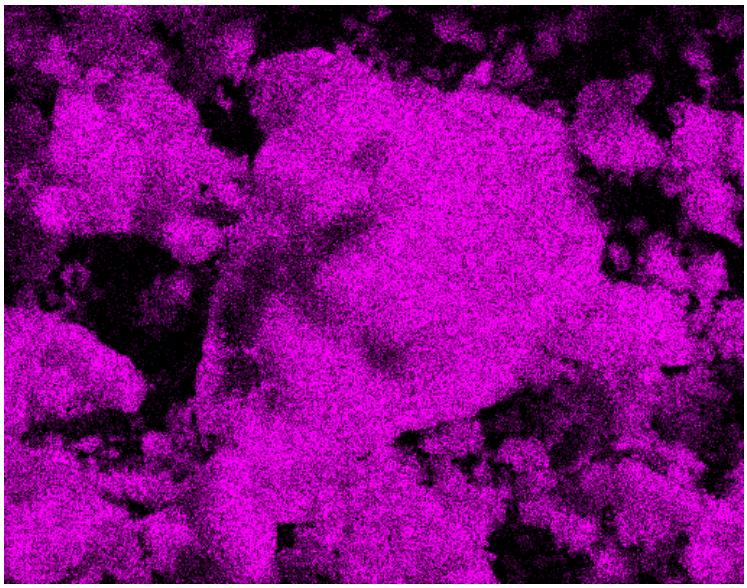

Figure 60: EDS results for TGA2_30 (Only K present)

Main Matlab Code:

```
function res= Model_pde_main(HR,Dp,epsilon,ASratio,time)
%parameters shared with the ODE routine
   global xl xu nx ncall ndss ncase C xg neq m
neq=5;

%Constants
%ASratio=1; %molar ratio of AS in mixture (AS+KS)
C.MW=[132.14,174.259,17.031,18.0153,212.21,254.32,80.066]; %g/mol
[AS=A,KS=B,A=C,W=D,APS=E,KPS=F,S=G]
C.T0=298; %Initial Temperature
T=C.T0;

C.epsilon=epsilon; %particle porosity
C.Dp=Dp; %m
C.Vol=4/3*(Dp/2)^3; %C.VAS+C.VKS; %m3 particle volume
C.rhoGAS=1.770*(10^6);%g/m3
C.rhoGKS=2.66*(10^6);%g/m3
C.rhoGAPS=1.98*(10^6);%g/m3
C.rhoGKPS=2.28*(10^6);%g/m3
C.rhoGA=730;%g/m3
C.rhoGW=36 ;%g/m3
C.rhoGS=3269 ;%g/m3
```

```
totalMol=(1-epsilon)*C.Vol/(ASratio*C.MW(1)/C.rhoGAS+(1-
ASratio)*C.MW(2)/C.rhoGKS);
%ParticleMW=(ASratio*C.MW(1)+(1-ASratio)*C.MW(2));

C.mAS=totalMol*ASratio*C.MW(1); %m0 in mg mAS in g
C.mKS=totalMol*(1-ASratio)*C.MW(2);

C.VAS=C.mAS/C.rhoGAS; %m3
C.VKS=C.mKS/C.rhoGKS; %m3

C.CA0= totalMol*ASratio/C.Vol; %initial concentration of AS mol/m3
C.CB0= totalMol*(1-ASratio)/C.Vol;

C.CpAS=102.36+0.2849*T;
C.CpKS=114.3634+0.08125*T;
C.CpAPS=102.36+0.2849*T;
C.CpKPS=260; %J/mol K
C.CpA=37.4;
C.CpW=35.928; %J/mol K
C.CpS=24.02+119.4607*T/1000-94.38686*((T/1000)^2);

C.Cp=(ASratio*C.CpAS+(1-ASratio)*C.CpKS); %Cp mix of AS+KS J/mol K
C.rho=totalMol/C.Vol; %1.3409*(10^4);%mol/m3

C.De=3.6*(10^-10); %m2/s
C.K=200/60*(10^-6)/(4*3.14*((Dp/2)^2))+2*C.De/Dp; %m/s (flowrate in m3/s/surface
area to account for heat transfer coefficient due to flow of gas+heat transfer coefficient
of the particle without gas flow)
C.Ea=[77,102,107,110]*1000; %J/mol
C.h=2*C.De/Dp*C.Cp*C.rho; %W/m2 K
C.DH=[119,664,370,146]*1000; %J/mol
C.k0=[1.23*(10^4),1.01*(10^5),3.51*(10^4),3.17*(10^4)];%s-1)
C.n1=[1.1,0.8,0.8,0.8];%main solid
C.n2=[0,0,0.6,0];%secondary solid
C.HR=HR; %heating rate
C.Tb=300+C.HR; %Temperature of bulk

C.lamdae= 0.6224; %W/m K
C.R=8.314; %J/mol K
%C.CBb=C.CB0; % Concentration of K2SO4 comes back to original
C.CCb=0;%C.CA0*2;
C.CDb=0;%C.CA0*1;
C.CGb=0;%C.CA0*1;
```

```
C.m0=(C.CA0*C.MW(1)+C.CB0*C.MW(2))*C.Vol; %mass of particle initially in g

% Grid in x, initial condition
  xl=0;xu=1;nx=50;

  for ix=1:nx
    xg(ix)=(xu-xl)*(ix)/(nx);
    T0(ix)=C.T0;
    CA0(ix)=C.CA0;
    CB0(ix)=C.CB0;
    CC0(ix)=0;
    CD0(ix)=0;
    CE0(ix)=0;
    CF0(ix)=0;
    CG0(ix)=0;
  end

  u0=[T0 CA0 CB0 CC0 CD0 CE0 CF0 CG0];

if size(time,1)==1
    t0=1;tf=time;nout=100;
    tout=linspace(t0,tf,nout);
else
    tout=time;
end
ncall=0;
%ODE integration
ncase=1;ndss=2;
m=C.m0;
clear textprogressbar;
option=odeset('NonNegative',1,'RelTol',1e-
2,'MaxStep',1,'InitialStep',0.1,'OutputFcn',@odetpbar);
[t,u]=ode23s(@Model_pde_1,tout,u0,option);

% Split Matrix

T=u(:,1:nx);
CA=u(:,nx+1:nx*2);
CB=u(:,nx*2+1:nx*3);
CC=u(:,nx*3+1:nx*4);
CD=u(:,nx*4+1:nx*5);
CE=u(:,nx*5+1:nx*6);
CF=u(:,nx*6+1:nx*7);
```

```
CG=u(:,nx*7+1:nx*8);

x=xg*C.Dp/2;

%conversion efficiency
%XA=(m-C.m0)/C.m0;

C.Vol=4/3*(Dp/2)^3;
%Mass fraction
MA=CA(:,1)*C.Vol*C.MW(1); %AS mass
MB=CB(:,1)*C.Vol*C.MW(2); %KS mass
ME=CE(:,1)*C.Vol*C.MW(5); %AHS mass
MF=CF(:,1)*C.Vol*C.MW(6); %KPS mass
W(:,1)=MA./(MA+MB+ME+MF);
W(:,2)=MB./(MA+MB+ME+MF);
W(:,3)=ME./(MA+MB+ME+MF);
W(:,4)=MF./(MA+MB+ME+MF);

M(:,1)=MA+MB+ME+MF; %mass left
%save('Export.mat',res);

 Tt=mean(T,2);
  %plot(x,T);
  xlabel('t');ylabel('u(x,t)');
  title('Time Evolution of Temp and Wfraction');
  yyaxis left
  plot(t,Tt);
  yyaxis right
  plot(t,W);
  xlabel('t (s)');ylabel('Weight% or T (K)');
  ylim([0,1.1]);
  legend('T','AS','KS','APS','KPS')

  figure;
  Tx=T(size(T,1),:);
  plot(x,Tx);

  %For 1AS:1KS at heating rate 8
  TC=T-273.15; %Temperature in C
  cx=16.599901/M(1,1); %factor for normalizing mass to mass initially in TGA. Total
mass initially in TGA/ Mass initially in model
  Mtot=M*cx;
  figure;
  plot(TC,Mtot,'x');
```

```
xlabel('T (C)');ylabel('Mass Loss (mg)');
legend('Model mass')

%TGA=importdata('TGA_15_Heating Rate 8.txt');
%nx=100;
%x1=(TGA(:,1));
%y=zeros(nx,1);
%for ix=1:nx
   %[r,c]=min(abs(x1-TC(ix,1)));
   %n=TGA(c,2);
   %y(ix)=n;
%end
%yq2=y;
%hold on
  %plot(TC(:,1),yq2,'o');
  %xlabel('T (C)');ylabel('Mass Loss (mg)');
  %hold off
  %drawnow;
  %legend('Model mass','TGA Mass')


%For 1AS:1KS at heating rate 2.5
%TC=T-273.15;
%cx=17.2/M(1,1);
%Mtot=M*cx;
%figure;
%plot(TC,Mtot,'x');
%legend('Model mass')

%TGA=importdata('TGA2_32_Heating Rate 2.5.txt');
%nx=100;
%x1=(TGA(:,1));
%y=zeros(nx,1);
%for ix=1:nx
   %[r,c]=min(abs(x1-TC(ix,1)));
   %n=TGA(c,2);
   %y(ix)=n;
%end
%yq2=y;
%hold on
  %plot(TC(:,1),yq2,'o');
  %xlabel('T (C)');ylabel('Mass Loss (mg)');
 % hold off
  %drawnow;
```

```
 %legend('Model mass','TGA Mass')


%For 1AS:0KS at heating rate 8
TC=T-273.15;
cx=19.100818/M(1,1);
Mtot=M*cx;
figure;
plot(TC,Mtot,'x');
legend('Model mass')

TGA=importdata('TGA2_28_Heating Rate 8.txt');
nx=100;
x1=(TGA(:,1));
y=zeros(nx,1);
for ix=1:nx
   [r,c]=min(abs(x1-TC(ix,1)));
   n=TGA(c,2);
   y(ix)=n;
end
yq2=y;
hold on
  plot(TC(:,1),yq2,'o');
  xlabel('T (C)');ylabel('Mass Loss (mg)');
  hold off
  drawnow;
  legend('Model mass','TGA Mass')

%For 1AS:0KS at heating rate 2
%TC=T-273.15;
%cx=17.2/M(1,1);
%Mtot=M*cx;
%figure;
%plot(TC,Mtot,'x');
%legend('Model mass')

%TGA=importdata('TGA2_22_Heating Rate 2.txt');
%nx=100;
%x1=(TGA(:,1));
%y=zeros(nx,1);
%for ix=1:nx
   %[r,c]=min(abs(x1-TC(ix,1)));
   %n=TGA(c,2);
   %y(ix)=n;
```

```
 %end
 %yq2=y;
 %hold on
  %plot(TC(:,1),yq2,'o');
  %xlabel('T (C)');ylabel('Mass Loss (mg)');
  %hold off
  %drawnow;
  %legend('Model mass','TGA Mass')


%For 1AS:2KS at heating rate 5
 %TC=T-273.15;
 %cx=14.799979/M(1,1);
 %Mtot=M*cx;
 %figure;
 %plot(TC,Mtot,'x');
 %legend('Model mass')

 %TGA=importdata('TGA2_38_Heating Rate 5.txt');
 %nx=100;
 %x1=(TGA(:,1));
 %y=zeros(nx,1);
 %for ix=1:nx
   %[r,c]=min(abs(x1-TC(ix,1)));
   %n=TGA(c,2);
   %y(ix)=n;
 %end
 %yq2=y;
 %hold on
  %plot(TC(:,1),yq2,'o');
  %xlabel('T (C)');ylabel('Mass Loss (mg)');
  %hold off
  %drawnow;
  %legend('Model mass','TGA Mass')


  dy=abs(yq2-Mtot)./yq2*100;
  RMSE=sqrt(mean((yq2-Mtot).^2));
  res={t,x',T,CA,CB,CC,CD,CE,CF,CG,W,M,dy,RMSE};
end
```

Function ode solver Model_pde_1 Code:

```
function ut=Model_pde_1(t,u)
```

```
% Parameters
global xl xu nx ncall ndss ncase C xg neq m

% Split Matrix
u(u<0)=0;
T=u(1:nx);
CA=u(nx+1:nx*2);
CB=u(nx*2+1:nx*3);
CC=u(nx*3+1:nx*4);
CD=u(nx*4+1:nx*5);
CE=u(nx*5+1:nx*6);
CF=u(nx*6+1:nx*7);
CG=u(nx*6+1:nx*7);

% ux
if    (ndss== 2)
   Tx=dss002(xl,xu,nx,T); % second order
   CAx=dss002(xl,xu,nx,CA); %
   CBx=dss002(xl,xu,nx,CB); %
   CDx=dss002(xl,xu,nx,CD); %
   CCx=dss002(xl,xu,nx,CC); %
   CEx=dss002(xl,xu,nx,CE); %
   CFx=dss002(xl,xu,nx,CF); %
   CGx=dss002(xl,xu,nx,CG); %
elseif(ndss== 4)
   Tx=dss004(xl,xu,nx,T); % fourth order
   CAx=dss004(xl,xu,nx,CA); % fourth order
   CBx=dss004(xl,xu,nx,CB); % fourth order
   CDx=dss004(xl,xu,nx,CD); % fourth order
   CCx=dss004(xl,xu,nx,CC); % fourth order
   CEx=dss004(xl,xu,nx,CE); % fourth order
   CFx=dss004(xl,xu,nx,CF); % fourth order
   CGx=dss004(xl,xu,nx,CG); % fourth order

elseif(ndss== 6) ux=dss006(xl,xu,nx,u); % sixth order
elseif(ndss== 8) ux=dss008(xl,xu,nx,u); % eighth order
elseif(ndss==10) ux=dss010(xl,xu,nx,u); % tenth order
end
C.Tb=300+C.HR*t/60;
rp=C.Dp/2;%((C.Dp/2)^3-(m-C.m0)/C.m0*((C.Dp/2)^3))^(1/3);
%C.Vol=4/3*3.14*rp^3;

% BC at x = 0 and 1 (Neumann)
```

```
nl=2;% Neumann
nu=1;% Dirichlet
Tx(1)=0;
Tx(nx)=-C.h*(T(nx)-C.Tb)*(rp)/C.lamdae; %heat equation
Txx=dss042(xl,xu,nx,T,Tx,nl,nu);

CCx(1)=0;
CCx(nx)=-C.K*(CC(nx)-C.CCb)*(rp)/C.De;
CCxx=dss042(xl,xu,nx,CC,CCx,nl,nu);
CDx(1)=0;
CDx(nx)=-C.K*(CD(nx)-C.CDb)*(rp)/C.De;
CDxx=dss042(xl,xu,nx,CD,CDx,nl,nu);
CGx(1)=0;
CGx(nx)=-C.K*(CG(nx)-C.CGb)*(rp)/C.De;
CGxx=dss042(xl,xu,nx,CG,CGx,nl,nu);


% nl=2;% Neumann
% nu=2;% Neumann
% CAx(1)=0;  %Boundary condition dCa/dT=0 since concentration change on surface
and in center is negligible
% CAx(nx)=0;
% CAxx=dss042(xl,xu,nx,CA,CAx,nl,nu);
% CBx(1)=0;
% CBx(nx)=0;
% CBxx=dss042(xl,xu,nx,CB,CBx,nl,nu);
% CEx(1)=0;
% CEx(nx)=0;
% CExx=dss042(xl,xu,nx,CE,CEx,nl,nu);
% CFx(1)=0;
% CFx(nx)=0;
% CFxx=dss042(xl,xu,nx,CF,CFx,nl,nu);



%    if   (ndss== 2)
%       Txx=dss002(xl,xu,nx,Tx); % second order
%       CAxx=dss002(xl,xu,nx,CAx);
%       CBxx=dss002(xl,xu,nx,CBx);
%       CDxx=dss002(xl,xu,nx,CDx);
%       CCxx=dss002(xl,xu,nx,CCx);
%       CExx=dss002(xl,xu,nx,CEx);
%       CFxx=dss002(xl,xu,nx,CFx);
%       CGxx=dss002(xl,xu,nx,CGx);
```

```
%    elseif(ndss== 4)
%       Txx=dss004(xl,xu,nx,Tx); % fourth order
%       CAxx=dss004(xl,xu,nx,CAx);
%       CBxx=dss004(xl,xu,nx,CBx);
%       CDxx=dss004(xl,xu,nx,CDx);
%       CCxx=dss004(xl,xu,nx,CCx);
%       CExx=dss004(xl,xu,nx,CEx);
%       CFxx=dss004(xl,xu,nx,CFx);
%       CGxx=dss004(xl,xu,nx,CGx);
%    elseif(ndss== 6) uxx=dss006(xl,xu,nx,ux); % sixth order
%    elseif(ndss== 8) uxx=dss008(xl,xu,nx,ux); % eighth order
%    elseif(ndss==10) uxx=dss010(xl,xu,nx,ux); % tenth order
%    end

% PDE
rR1=rG(T,CA,CB,C,1);
rR2=rG(T,CE,CB,C,2);
rR3=rG(T,CE,CB,C,3);
rR4=rG(T,CF,CB,C,4);
DH1=C.DH(1);
DH2=C.DH(2);
DH3=C.DH(3);
DH4=C.DH(4);

MolF=[CA(nx,1),CB(nx,1),CC(nx,1),CD(nx,1),CE(nx,1),CF(nx,1),CG(nx,1)]/(CA(nx,1)
+CB(nx,1)+CC(nx,1)+CD(nx,1)+CE(nx,1)+CF(nx,1)+CG(nx,1));
C.Cp=(MolF(1)*C.CpAS+MolF(2)*C.CpKS+MolF(3)*C.CpA+MolF(4)*C.CpW+MolF
(5)*C.CpAPS+MolF(6)*C.CpKPS+MolF(7)*C.CpS); %Cp mix of AS+KS J/mol K
C.rho=(MolF(1)*C.rhoGAS/C.MW(1)+MolF(2)*C.rhoGKS/C.MW(2)+MolF(3)*C.rho
GA/C.MW(3)+MolF(4)*C.rhoGW/C.MW(4)+MolF(5)*C.rhoGAPS/C.MW(5)+MolF(6)
*C.rhoGKPS/C.MW(6)+MolF(7)*C.rhoGS/C.MW(7)); %1.3409*(10^4);%mol/m3

TA=C.lamdae/(C.rho*C.Cp)/((rp)^2); %s-1 m-2
TB=1/C.rho/C.Cp; %1/(J/m3 K)
CCA=C.De/C.epsilon/((rp)^2); %s-1 m-2

Tt=TA.*(Txx'+(2./xg').*Tx')-TB*DH1.*rR1-TB*DH2.*rR2-TB*DH3.*rR3-
TB*DH4.*rR4;%
Tt(1)=3*TA*Txx(1)+TB*DH1(1)*rR1(1)+TB*DH2(1)*rR2(1)+TB*DH3(1)*rR3(1)+T
B*DH4(1)*rR4(1); %to address singularity at xg=0

CCt=CCA.*(CCxx'+(2./xg').*CCx')+1/C.epsilon.*rR1+2/C.epsilon.*rR2+2/C.epsilon.*r
R3;
```

```
CCt(1)=3*CCA*CCxx(1)-1/C.epsilon*rR1(1)-2/C.epsilon*rR2(1)-2/C.epsilon*rR3(1);
%to address singularity at xg=0

CDt=CCA.*(CDxx'+(2./xg').*CDx')+0.5/C.epsilon.*rR1+1/C.epsilon.*rR2+1/C.epsilon.
*rR3;
CDt(1)=3*CCA*CDxx(1)-0.5/C.epsilon*rR1(1)-1/C.epsilon*rR2(1)-
1/C.epsilon*rR3(1); %to address singularity at xg=0

CGt=CCA.*(CGxx'+(2./xg').*CGx')+2/C.epsilon.*rR3+1/C.epsilon.*rR4;
CGt(1)=3*CCA*CGxx(1)-2/C.epsilon.*rR3(1)-1/C.epsilon*rR4(1); %to address
singularity at xg=0

CAt=-1.*rR1;
CBt=-2.*rR3+1.*rR4;
CEt=0.5.*rR1-1.*rR2-1.*rR3;
CFt=2.*rR3-1.*rR4;

% Increment calls to pde_1
ncall=ncall+1;


%MA=CAt(1,:)*C.MW(1)*C.Vol; %AS
%MB=CBt(1,:)*C.MW(2)*C.Vol; %KS
%ME=CEt(1,:)*C.MW(5)*C.Vol; %AHS
%MF=CFt(1,:)*C.MW(6)*C.Vol; %KPS
%W(:,1)=MA./(MA+MB+ME+MF);
%W(:,2)=MB./(MA+MB+ME+MF);
%W(:,3)=ME./(MA+MB+ME+MF);
%W(:,4)=MF./(MA+MB+ME+MF);

% Concatenate
%m =  (MA+MB+ME+MF)*C.Vol;
ut=[Tt' CAt' CBt' CCt' CDt' CEt' CFt' CGt'];


end

function reactionG=rG(T,Csolid1,Csolid2,C,iR) % Kinetics Reaction
n1=C.n1(iR);
n2=C.n2(iR);
Ea=C.Ea(iR);
k0=C.k0(iR);
reactionG=k0*exp(-Ea./(C.R.*T)).*power(Csolid1,n1).*power(Csolid2,n2);
end
```